Medizinische Fakultät
der
Universität Duisburg-Essen

Aus dem Institut für Zellbiologie (Tumorforschung)

Die Bedeutung von Antioxidans-assoziierten mitochondrialen Transportsystemen als Ansatzpunkte für die Überwindung Hypoxie-vermittelter Strahlenresistenz von Krebszellen

I n a u g u r a l d i s s e r t a t i o n
zur
Erlangung des Doktorgrades der Medizin
durch die Medizinische Fakultät
der Universität Duisburg-Essen

Vorgelegt von

Julian Alexander Hlouschek

aus Bergisch Gladbach
2021

DOI: 10.17185/duepublico/75986
URN: urn:nbn:de:hbz:465-20220704-073433-8

Dekan: Univ.-Prof. Dr. med. J. Buer

1. Gutachter: Univ.-Prof. Dr. rer. nat. V. Jendrossek

2. Gutachter: Univ.-Prof. Dr. phil. nat. K. Lückerath

3. Gutachter: Prof. Dr. rer. nat. H. Zitzelsberger

Tag der mündlichen Prüfung: 11. Mai 2022

In der vorliegenden kumulativen Dissertation sind folgende Originalarbeiten enthalten:

Hlouschek, J., Hansel, C., Jendrossek, V., and Matschke, J. (2018). The Mitochondrial Citrate Carrier (SLC25A1) Sustains Redox Homeostasis and Mitochondrial Metabolism Supporting Radioresistance of Cancer Cells With Tolerance to Cycling Severe Hypoxia. Front Oncol 8, 170. (Doi: 10.3389/fonc.2018.00170)

Hlouschek, J., Ritter, V., Wirsdorfer, F., Klein, D., Jendrossek, V., and Matschke, J. (2018). Targeting SLC25A10 alleviates improved antioxidant capacity and associated radioresistance of cancer cells induced by chronic-cycling hypoxia. Cancer Lett 439, 24-38. (Doi: 10.1016/j.canlet.2018.09.002)

Inhaltsverzeichnis

Einleitung

Die Inzidenz von Krebserkrankungen verschiedener Entitäten steigt weltweit an (Torre et al., 2016). Während die Mortalität in Ländern mit höherem Einkommen tendenziell sinkt, steigt sie in Ländern mit niedrigerem Einkommen. Dennoch stellen Krebserkrankungen nach Herz-Kreislauferkrankungen in Industrienationen wie den USA die zweithäufigste Todesursache dar (Siegel et al., 2018). Auch in Deutschland sind für das kommende Jahrzehnt weiterhin steigende Inzidenzen von Krebserkrankungen prognostiziert (Quante et al., 2016). Einem Großteil von Krebserkrankungen in Europa und den USA könnte durch Verstärkung präventiver Maßnahmen vorgebeugt werden, aber auch die Entwicklung, Durchführung und kontinuierliche Verbesserung effektiver Therapien können zu einer zukünftigen Reduktion der Mortalität beitragen (Ferlay et al., 2018; Siegel et al., 2018; Torre et al., 2016).

Die Strahlentherapie ist eine bedeutende Säule der Krebstherapie. In der Behandlung von Tumorerkrankungen kann sie sowohl allein als auch in Kombination mit Chemotherapien, zielgerichteten Therapien und operativem Vorgehen im Rahmen multimodaler Therapiekonzepte angewendet werden. In Anbetracht der gesteigerten Überlebensraten von Tumorerkrankungen durch verbesserte Therapien liegt der heutige Fokus der Strahlenonkologie neben der Erzielung einer Heilung auch bei der Reduktion von akuten und langfristigen Nebenwirkungen, um die Lebensqualität der Patienten weiter zu verbessern (Citrin, 2017). Bei der individuellen Abwägung zwischen bestmöglicher Tumorkontrolle und gleichzeitig optimaler Normalgewebsschonung in der Bestrahlungsplanung konnten durch zahlreiche neuartige technische Entwicklungen, wie etwa intensitätsmodulierte Radiotherapie, in den vergangenen Jahren die Raten bestimmter Spätnebenwirkungen verringert werden (Hoeller et al., 2021).

Auch auf biologischer Ebene werden Konzepte entwickelt und Ansatzpunkte gesucht, um eine tumorspezifische Sensitivierung gegenüber Strahlentherapie bei gleichzeitiger Reduktion der Normalgewebstoxizität zur erreichen (Begg et al., 2011). Daher wird die Suche nach Wirkstoffen fortgesetzt, die eine ähnliche oder größere strahleninduzierte Abtötung von Tumorzellen mit reduzierter Toxizität bewirken können. Ionisierende Strahlung (IR) schädigt durch das Freisetzen reaktiver Sekundärelektronen nicht nur die

DNA von Krebszellen, sondern initiiert auch eine Reihe von überlebenswichtigen Signaltransduktionswegen in der Tumorzelle. Mit der Entwicklung einer wachsenden Anzahl von Inhibitoren der Signaltransduktion und der DNA-Reparatur hat sich beispielsweise eine Chance ergeben, Tumore durch gezielte Beeinflussung dieser Wege selektiv für die Bestrahlung zu sensibilisieren. Ziel derartiger Bemühungen ist es, Wirkstoffe zu entwickeln, mit denen die Wirksamkeit der an den Tumor abgegebenen Strahlung verbessert und gleichzeitig die zusätzliche Toxizität minimiert werden kann (Citrin, 2017).

Tumorzellen und -gewebe weisen verschiedene biologische Kennzeichen auf, die sie von Zellen normaler Gewebe unterscheiden. Hierzu gehören unter anderem die Entwicklung von Apoptoseresistenz und der Unabhängigkeit von Wachstumsfaktoren sowie die Induktion von Angiogenese, invasivem Wachstum und Metastasierung (Hanahan and Weinberg, 2011). Hierdurch bieten sich auch Vulnerabilitäten zur Entwicklung neuer therapeutischer Ansätze. Ein weiteres Kennzeichen ist ein deregulierter Energiehaushalt durch metabolische Umprogrammierung. Ein veränderter Zellmetabolismus ist im Rahmen der Entstehung und Entwicklung solider Tumoren mit schlechten Prognosen assoziiert (van der Mijn et al., 2016). Metabolische Anpassungsreaktionen werden durch Veränderungen im Tumor-Mikromillieu gefördert. Zu diesen Veränderungen gehören beispielsweise reduzierte Verfügbarkeiten von Sauerstoff (Tumor-Hypoxie), Nährstoffen sowie verringerte pH-Werte (Abrego et al., 2017; Zeng et al., 2015).

Zahlreiche präklinische und klinische Arbeiten haben gezeigt, dass das erhöhte Auftreten von Tumor-Hypoxie mit maligner Progression, Resistenz von Tumorzellen gegenüber Chemo- und Radiotherapie, sowie folglich schlechteren klinischen Therapieergebnissen assoziiert ist (Harris, 2002; Kim et al., 2018; Salem et al., 2018; Vaupel, 2004). Die zytotoxischen Effekte von Radiotherapie und verschiedenen DNA-schädigenden Krebsmedikamenten beruhen unter anderem auf der Entstehung reaktiver Sauerstoffspezies (ROS) auf zellulärer Ebene und sind somit abhängig von der lokalen Verfügbarkeit von Sauerstoff im Tumorgewebe (Bristow and Hill, 2008). Ein akut niedriger Sauerstoffgehalt im Tumorgewebe vermittelt somit direkte Therapieresistenz (Horsman et al., 2012; Liauw et al., 2013). Allerdings unterliegt Tumor-Hypoxie hinsichtlich Dauer und Dynamik (akut, intermittierend und chronisch) ausgeprägten und komplexen Schwankungen. Diese werden unter anderem durch mangelhaften

Sauerstofftransport aufgrund chaotischer Gefäßarchitektur und Fluktuationen des Blutflusses innerhalb solider Tumoren verursacht (Dewhirst et al., 2008; Lee et al., 2014; Matsumoto et al., 2010; Vaupel and Harrison, 2004). Je nach Dauer und Ausprägung der Hypoxie kommt es also zu unterschiedlichen Anpassungsreaktionen. Insbesondere der chronische Wechsel zwischen starker Hypoxie und intermittierendem Reoxygenierungs-Stress (chronisch-zyklische Hypoxie) führt zu zellulären Adaptationsprozessen mit Erhöhung der Tumorheterogenität und Selektion therapieresistenter Zellen (Bader et al., 2020; Matschke et al., 2016; Span and Bussink, 2015; Weinmann et al., 2005; Weinmann et al., 2004).

Die erhöhte Flexibilität therapieresistenter Tumorzellen, verursacht durch metabolische Umprogrammierung in Bezug auf Veränderungen im Tumor-Mikromillieu, umfasst unter anderem eine verbesserte Antioxidanskapazität. Diese ermöglicht eine Aufrechterhaltung der Redox-Homöostase bei der vermehrten Detoxifizierung von ROS (Cairns et al., 2011; DeBerardinis and Chandel, 2016; Matschke et al., 2016).

Vorarbeiten der eigenen Arbeitsgruppe haben gezeigt, dass die verbesserte Antioxidanskapazität insbesondere eine Eigenschaft von Tumorzellen mit Toleranz gegenüber wiederholten Zyklen von starker Hypoxie und intermittierender Reoxygenierung (chronisch-zyklische Hypoxie) ist (Matschke et al., 2016). Die Glutamin-abhängige Erhöhung von reduziertem Glutathion (GSH), das quantitativ bedeutsamste antioxidative Molekül eukaryontischer Zellen, trug hier zu einer erhöhten Radioresistenz bei. Andere Arbeiten beschreiben weitere Resistenzmechanismen Hypoxie-toleranter Tumorzellen, die entweder zur Erhöhung der Synthese von GSH oder der verstärkten Regeneration von GSH aus oxidiertem Glutathion (GSSG) mithilfe des vermehrt vorhandenen Reduktionsäquivalents NADPH führen (Nakashima et al., 2017; Rouschop et al., 2013). Generell sind erhöhte GSH-Spiegel in Tumorzellen mit verstärkter maligner Progression und Therapieresistenz assoziiert. Durch ein zielgerichtetes Eingreifen in diese Mechanismen können durch eine Verringerung der GSH-assoziierten Antioxidanskapazität Therapieresistenzen überwunden werden, was potenziell eine vielversprechende therapeutische Strategie insbesondere für resistentere, hypoxische Tumorzellen darstellt (Hatem et al., 2017; Jiang et al., 2018; Wang et al., 2019).

Neben der Erhöhung der Antioxidanskapazität umfasst die metabolische Umprogrammierung von Tumorzellen Veränderungen der Glykolyse, der Glutaminolyse und anderer metabolischer Pfade im Zytosol. Ebenso wichtig sind insbesondere Veränderungen der mitochondrialen Funktionen (DeBerardinis and Chandel, 2016; Vasan et al., 2020). Mitochondrien von Tumorzellen spielen eine wichtige Rolle bei der Entwicklung von Therapieresistenzen durch Gewährleistung der Energieversorgung, Erhaltung der Redox-Balance, Aktivierung onkogener Signalwege und Unterdrückung intrinsischer Apoptosesignale (Bock and Tait, 2019; Chandel, 2015; Jendrossek, 2012; Missiroli et al., 2020; Zong et al., 2016). In diesem Zusammenhang stellt der mitochondriale GSH (mGSH) Pool eine kritische Komponente bei der Regulierung der mitochondrialen Redox-Homöostase dar und schützt beispielsweise vor Cardiolipin-Oxidation, anschließender Cytochrom-c Freisetzung und damit Initiation von intrinsischer Apoptose (Handy and Loscalzo, 2012; Hatem et al., 2017; Mari et al., 2013). Für die Regeneration von GSH oder mGSH von der oxidierten zurück in die reduzierte Form ist jedoch auch das Reduktionsäquivalent NADPH notwendig, was hauptsächlich durch den Pentosephosphatweg oder teilweise durch reduktive Carboxylierung gewonnen wird, und ebenfalls in die mitochondriale Matrix transportiert werden muss (Jiang et al., 2016).

Da GSH exklusiv im Zytosol synthetisiert wird, bedarf es mitochondrialer Transportsysteme zur Aufrechterhaltung des mGSH-Pools. Für den mGSH-Import wurden insbesondere der Dicarboxylat-Carrier SLC25A10 sowie der 2-Oxoglutarat-Carrier SLC25A11, beide lokalisiert in der inneren mitochondrialen Membran, in verschiedenen präklinischen Modellen diskutiert und validiert (Baulies et al., 2018; Kamga et al., 2010; Ribas et al., 2014; Torres et al., 2017; von Montfort et al., 2012; Wilkins et al., 2013). Für den Transport von NADPH, gewonnen durch reduktive Carboxylierung, über die innere mitochondriale Membran, wird ein Zusammenspiel des mitochondrialen Citrat-Carrier SLC25A1 in der inneren mitochondrialen Membran, der zytosolischen Isocitrat-Dehydrogenase (IDH)1 und der mitochondrialen IDH2 postuliert (Jiang et al., 2016).

Die genannten Mitglieder der SLC25-Transporterfamilie beeinflussen neben ihren Funktionen zur Erhaltung der Redox-Homöstase ebenfalls den Transport von Carboxylaten zwischen der mitochondrialen Matrix und dem Intermembranraum bzw.

Zytosol. Sie unterstützen dadurch ebenfalls den deregulierten Energiehaushalt von Tumorzellen. Daher stellen sie einen potenziellen therapeutischen Ansatzpunkt mit mehreren Wirkungsebenen dar (Palmieri, 2014; Rochette et al., 2020). Darüber hinaus wurde Ihre Überexpression in Tumorzellen mit maligner Progression und Zunahme von Therapieresistenzen assoziiert (Catalina-Rodriguez et al., 2012; Kolukula et al., 2014; Lytovchenko and Kunji, 2017; Zhou et al., 2015).

Fragestellungen

Die Adaptation von Tumorzellen an akute oder schwere chronisch-zyklische Hypoxie und intermittierende Reoxygenierung führt zu zahlreichen Anpassungsreaktionen im Metabolismus von Tumorzellen, die die Sensitivität von Tumorzellen gegenüber einer Bestrahlung herabsetzen und somit zu einem Therapieversagen beitragen können. Metabolische Anpassungsreaktionen an solche ungünstigen Bedingungen im Tumormikromilieu stellen somit ein klinisch relevantes Problem dar. Nur ein detailliertes Verständnis dieser Adaptationsprozesse und der zugrundeliegenden Mechanismen bietet die Möglichkeit zur Identifizierung und Untersuchung neuer potenzieller therapeutischer Ansatzpunkte, um entstandene Resistenzen zu modulieren oder gänzlich zu überwinden.

Basierend auf Vorarbeiten der Arbeitsgruppe sollte im Rahmen der vorliegenden Arbeit untersucht werden, ob die Inhibition der Antioxidans-assoziierten mitochondrialen Transportsysteme SLC25A1, SLC25A10 und SLC25A11 eine durch Anpassung an Hypoxie induzierte gesteigerte Resistenz von Tumorzellen gegenüber einer Strahlentherapie überwinden kann. Dabei standen Untersuchungen zu den Auswirkungen einer zeitgleichen Beeinflussung der Redox-Homöostase und des Energiemetabolismus durch genetische oder pharmakologische Modulation dieser mitochondrialen Transportsysteme für die Modulation der Strahlenwirkung im Vordergrund. Die Bedeutung dieser Transportsysteme für die Entstehung einer Hypoxie-vermittelten Therapieresistenz und für die zelluläre Strahlenantwort wurden zuvor noch nicht untersucht.

Originalarbeit 1: Hlouschek et al. (2018) Front Oncol 8, 170.

frontiers in Oncology

ORIGINAL RESEARCH
published: 25 May 2018
doi: 10.3389/fonc.2018.00170

The Mitochondrial Citrate Carrier (SLC25A1) Sustains Redox Homeostasis and Mitochondrial Metabolism Supporting Radioresistance of Cancer Cells With Tolerance to Cycling Severe Hypoxia

*Julian Hlouschek, Christine Hansel, Verena Jendrossek and Johann Matschke**

Institute of Cell Biology (Cancer Research), University Hospital Essen, University of Duisburg-Essen, Essen, Germany

OPEN ACCESS

Edited by:
Andrea Rasola, Università degli Studi di Padova, Italy

Reviewed by:
Alessandra Castegna, University of Bari Medical School, Italy
Margaret Ashcroft, University of Cambridge, United Kingdom

***Correspondence:**
Johann Matschke
johann.matschke@uk-essen.de

Specialty section:
This article was submitted to Molecular and Cellular Oncology, a section of the journal Frontiers in Oncology

Received: *22 February 2018*
Accepted: *01 May 2018*
Published: *25 May 2018*

Citation:
Hlouschek J, Hansel C, Jendrossek V and Matschke J (2018) The Mitochondrial Citrate Carrier (SLC25A1) Sustains Redox Homeostasis and Mitochondrial Metabolism Supporting Radioresistance of Cancer Cells With Tolerance to Cycling Severe Hypoxia. Front. Oncol. 8:170. doi: 10.3389/fonc.2018.00170

Pronounced resistance of lung cancer cells to radiotherapy and chemotherapy is a major barrier to successful treatment. Herein, both tumor hypoxia and the upregulation of the cellular antioxidant defense systems observed during malignant progression can contribute to radioresistance. We recently found that exposure to chronic cycling severe hypoxia/reoxygenation stress results in glutamine-dependent upregulation of cellular glutathione (GSH) levels and associated radiation resistance opening novel routes for tumor cell-specific radiosensitization. Here, we explored the role of the mitochondrial citrate carrier (SLC25A1) for the improved antioxidant defense of cancer cells with tolerance to acute and chronic severe hypoxia/reoxygenation stress and the use of pharmacologic SLC25A1 inhibition for tumor cell radiosensitization. Exposure to acute or chronic cycling severe hypoxia/reoxygenation stress triggered upregulated expression of SLC25A1 in lung cancer, prostate cancer, and glioblastoma cells *in vitro*. Interestingly, exposure to ionizing radiation (IR) further promoted SLC25A1 expression. Inhibition of SLC25A1 by 1,2,3-benzene-tricarboxylic acid (BTA) disturbed cellular and mitochondrial redox homeostasis, lowered mitochondrial metabolism, and reduced metabolic flexibility of cancer cells. Even more important, combining IR with BTA was able to overcome increased radioresistance induced by adaptation to chronic cycling severe hypoxia/reoxygenation stress. This radiosensitizing effect of BTA-treated cells was linked to increased reactive oxygen species and reduced DNA repair capacity. Of note, key findings could be reproduced when using the SLC25A1-inhibitor 4-Chloro-3-[[(3-nitrophenyl)amino]sulfonyl]-benzoic acid (CNASB). Moreover, *in silico* analysis of publically available databases applying the Kaplan–Meier plotter tool (kmplot.com) revealed that overexpression of SLC25A1 was associated with reduced survival of lung cancer patients suggesting a potential link to aggressive cancers. We show that SLC25A1 can contribute to the increased antioxidant defense of cancer cells allowing them to escape the cytotoxic effects of IR. Since upregulation of SLC25A1 is induced by adverse conditions in the tumor environment, exposure to IR, or both pharmacologic inhibition of SLC25A1 might be an effective strategy for radiosensitization of cancer cells particularly in chronically hypoxic tumor fractions.

Keywords: redox homeostasis, SLC25A1, radiation resistance, chronic hypoxia, cell metabolism, mitochondria, DNA repair

INTRODUCTION

More than 50% of NSCLC patients receive radiotherapy (RT) or radiochemotherapy (RCT) as part of their treatment. Recent meta-analysis revealed that tumor hypoxia is major biological barrier to successful chemotherapy, RT, and potentially some targeted therapies, promoting treatment failure and poor prognosis of patients suffering from non-small cell lung cancer (NSCLC) (1). Though targeting hypoxia-mediated therapy resistance is considered as an attractive approach to improve therapy outcome in solid human tumors including NSCLC, so far clinical trials evaluating the use of hypoxia-targeting agents did not meet the expectations as they failed to reveal a benefit for the patients (1). This might at least be partially due to the lack of appropriate predictive biomarkers for patient selection but emphasizes the need for the definition of mechanism-based more effective novel therapeutic strategies to overcome hypoxia-induced therapy resistance and the co-development of predictive biomarkers and improved imaging of heterogeneous tumor hypoxia to guide RT protocols (1).

Tumors form a complex microenvironment by co-opting various normal tissue cells and immune cells to support their growth and survival (2). However, the imbalance between cell growth and tumor vascularization limits not only the availability of nutrients and oxygen (O_2) but also the removal of secreted potentially toxic metabolites such as lactic acid. As a consequence of rapid proliferation, poor blood supply and altered metabolism tumor hypoxia is frequently linked to lactic acidosis and thus a low pH in the tumor (3, 4). The resulting O_2-deprived and nutrient-deprived acidic microenvironment exerts a selection pressure on the tumor cells thereby directing the acquisition of genetic and epigenetic alterations that allow the cancer cells to survive and to adapt to these adverse conditions during multistep carcinogenesis thereby promoting tumor growth and even metastasis (5–8). Moreover, accumulating evidence indicates that the adverse microenvironment also impacts the therapy response at multiple levels and promotes the resistance of solid tumors to chemotherapy and RT (9, 10).

Herein limited availability of O_2 known as "tumor hypoxia" is considered as a major environmental factor driving genomic instability, malignant progression, and resistance of solid tumors to RT and chemotherapy (9–11). The cytotoxic efficacy of RT and certain DNA-damaging anticancer drugs relies on the formation of reactive oxygen species (ROS) and thus on local availability of molecular O_2 in the tumor tissue during treatment delivery; therefore, an acute decrease in O_2 levels as a consequence of insufficient O_2 supply confers direct resistance by decreasing oxidative stress and therapy-induced cell killing, the so-called "oxygen-effect" (10, 12, 13). Moreover, cancer cells dispose of multiple survival pathways that allow them to adapt to acute hypoxia and survive these adverse conditions [for a review, see Ref. (14)].

But tumor hypoxia is highly dynamic with respect to its duration (short term to long term) and schedule (transient, chronic, or intermittent), and also fluctuates regionally presumably as a result of the instability and chaotic organization of the tumor vasculature (15–18). Thus, considerable fractions of human vascularized solid tumors are exposed to dynamic changes between hypoxia and intermittent reoxygenation. Chronic changes between hypoxia and intermittent reoxygenation ("cycling hypoxia") constitute a major driving force in the development of malignant progression, tumor heterogeneity, and clonal evolution of therapy-resistant cells (15, 19–24). Acute hypoxia/reoxygenation stress and tumor cell adaptation to chronic cycling severe hypoxia/reoxygenation stress also impact the outcome of cancer RT (23–26). A detailed understanding of the processes that allow cancer cells to escape the cytotoxic effects of RT in the adverse tumor microenvironment is required if we aim to develop effective therapeutic strategies to improve therapy outcome.

In this context, others and we demonstrated that adaptation to chronic hypoxia/reoxygenation stress drives upregulation of cellular GSH levels to avoid excessive ROS damage and promote death resistance (24, 27, 28). Altered nutrient and energy metabolism is one of the emerging hallmarks of cancer cells (29, 30). Moreover, a progressive upregulation of cellular antioxidant systems has been associated with malignant progression (31), suggesting a broader relevance of the above findings for understanding tumor progression and clonal evolution of therapy-resistant cells in tumors with heterogeneous environments. Importantly, as a proof of principle others and we demonstrated that targeting metabolic reprogramming associated with increased GSH levels is a promising strategy for radiosensitization (24, 32).

However, the above studies also demonstrated that cancer cells use different metabolic adaptation strategies to increase their cellular GSH levels, avoid ROS-dependent damage, and escape genotoxic therapies, presumably depending on the genetic background (24, 28, 31–33). Thus, targeting altered glutamine usage will be a viable therapeutic strategy to reduce glutathione levels in some but not all cancer models (24). We therefore reasoned that targeting the increased GSH-based antioxidant capacity and thus the common phenotype of aggressive cancer cells with increased stress tolerance, might be an effective strategy for therapeutic intervention with broader relevance.

Generally, increased GSH levels can be targeted by using drugs interfering with the regeneration of glutathione, the provision of reduction equivalents, increased glutathione synthesis, or glutathione transport and uptake (24, 34, 35). In an effort to define novel ways to specifically target increased GSH levels in aggressive cancer cells the observation about a link between the mitochondrial citrate carrier (CIC, also known as mitochondrial citrate transport protein, CTP) and the maintenance of cytosolic and mitochondrial NADPH pools and the mitochondrial redox homeostasis attracted our attention (36, 37).

The CIC is encoded by the *SLC25A1* gene located on chromosome 22q11.2. Besides citrate, SLC25A1 is also responsible for the electroneutral transport of isocitrate, malate, and phosphoenolpyruvate (38). Furthermore, SLC25A1—together with cytosolic isocitrate dehydrogenase 1 (IDH1) and mitochondrial isocitrate dehydrogenase 2 (IDH2)—takes part in the transport of NADPH derived from reductive carboxylation over the mitochondrial membrane (36) and might thus play a role in GSH regeneration. Overall, SLC25A1 is important for the maintenance of mitochondrial homeostasis and its overexpression was shown to drive tumorigenesis in various types of cancer (39).

Though the authors linked SLC25A1 expression to anchorage-independent growth of NCI-H460 cancer cells (36), it was tempting to speculate that the function of SLC25A1 regarding maintenance of redox homeostasis and mitochondrial function might contribute to the increased radioresistance of lung cancer cells with tolerance to chronic hypoxia/reoxygenation stress. However, the role of SLC25A1 for the cellular radiation response has not yet been investigated. Therefore, in the present study we aimed to explore the role of SLC25A1 for the increased antioxidant capacity of cancer cells adapted to chronic cycling severe hypoxia/reoxygenation stress and the use of SLC25A1 inhibition as novel strategy for radiosensitization of NCI-H460 lung adenocarcinoma cells exposed to acute or chronic cycling severe hypoxia.

RESULTS

Acute and Chronic-Cycling Hypoxia Increase Expression of *SLC25A1* and *IDH2*

To gain insight into a potential relevance of SLC25A1 for tolerance of lung cancer cells to chronic cycling severe hypoxia, we used our established cell model of so-called "anoxia-tolerant" NCI-H460 lung cancer cells and the respective control cells termed "oxic" NCI-H460 cells. These cells had been exposed to 25 cycles of severe hypoxia (48 h) and reoxygenation stress (120 h) as described earlier (24). Quantitative real-time PCR (qRT-PCR) analysis revealed a significant upregulation of *SLC25A1* in the anoxia-tolerant NCI-H460 cells as compared with the oxic control cells under standard culturing conditions, suggesting that basal upregulation of *SLC25A1* might be a consequence of adaptation to chronic cycling severe hypoxia (**Figure 1A**). *SLC25A1* upregulation was associated with upregulation of *IDH2*, whereas *IDH1* expression was not altered (**Figure 1A**). To test a more general relevance of these findings, we additionally examined the expression of the respective genes in similarly generated anoxia-tolerant DU145 and T98G cells and again observed an upregulated basal *SLC25A1* and *IDH2* expression in the anoxia-tolerant cells as compared to the respective oxic control cells (**Figures 1B,C**), whereas *IDH1* expression was not altered. Interestingly, exposure to acute severe hypoxia (0.2% O_2) was also able to trigger increased expression of *SLC25A1* and *IDH2* in the lung cancer cells and this effect was observed in both, oxic and anoxia-tolerant NCI-H460 cancer cells, compared to the oxic NCI-H460 control cells under normoxic (Nx) conditions (**Figures 1D,E**). However, the apparent upregulation of *SLC25A1* and *IDH2* expression induced by acute hypoxia was not significant for anoxia-tolerant NCI-H460 cells as the major increase over the levels of oxic NCI-H460 control cells in normoxia was already caused by the adaptation to chronic cycling severe hypoxia, whereas exposure to acute hypoxia had only a minor addition effect (Figures S1D,E in Supplementary Material). Similar observations about a significant upregulation of SLC25A1 expression upon exposure of NCI-H460 cells to acute or chronic cycling severe hypoxia were made using Western blot analysis (Figures S1A,B in Supplementary Material).

Overexpression of SLC25A1 in Lung Cancer Is Associated With Reduced Overall Survival of Lung Cancer Patients

To investigate whether upregulation of SLC25A1 in an adverse microenvironment *in vitro* might be relevant for the clinical situation, we searched for and analyzed the data of Kaplan–Meier plotter tool (kmplot.com) (40–42), about SLC25A1 expression in lung cancer patients (**Figures 2A,C**) and normal lung tissue by an *in silico* analysis, respectively (**Figure 2B**). The patient cohort has been described in detail in Ref. (40), whereas the parameters used for our *in silico* analysis are given in Tables S1 and S2 in Supplementary Material. We split the lung cancer patient cohort by median of SLC25A1 expression into "High" and "Low," respectively. Our *in silico* analysis revealed that SLC25A1 overexpression was associated with significantly reduced overall survival and median survival in lung cancer patients. Interestingly, this effect regarding overall and median survival was enhanced in the cohort of patients with successful surgery with tumor-free margins (R0-resection) (**Figure 2C**). Of note, SLC25A1 displayed a higher expression in lung cancer patients compared to normal lung tissue (**Figure 2B**) suggesting that SLC25A1 might be a relevant target in lung cancer.

Pharmacologic Inhibition of SLC25A1 Sensitizes Cancer Cells to the Cytotoxic Action of Ionizing Radiation (IR) and Overcomes Increased Radioresistance Induced by Chronic Cycling Severe Hypoxia

So far, our data demonstrated that acute and chronic cycling severe hypoxia alter the expression levels of SLC25A1. Moreover, our earlier data revealed that anoxia-tolerant NCI-H460 cells are more resistant to IR and chemotherapeutic agents compared to non-selected oxic control cells and this increased radioresistance could be linked to improved antioxidant defense of anoxia-tolerant cancer cells (22–24). Since SLC25A1 has recently been linked to cellular redox homeostasis (36) we wondered whether SLC25A1 might contribute to increased radioresistance of cancer cells in acute or chronic cycling severe hypoxia. To test a potential influence of SLC25A1 on radiosensitivity, we treated the anoxia-tolerant NCI-H460 cells and the oxic control cells with the pharmacological SLC25A1-inhibitor 1,2,3-benzene-tricarboxylic acid (BTA) (38, 39) 2 h before irradiation with 0–5 Gy under standard Nx conditions (20% O_2) and determined the effects of single and combined treatment on cell survival in standard long-term colony survival assays upon removal of BTA 24 h after treatment (delayed plating) (experimental timeline, **Figure 3A**). To test the impact of drug-treatment in acute hypoxia, we additionally performed similar experiments in cells that had been adapted to acute severe hypoxia (0.2% O_2) for 2 h prior to inhibitor treatment (**Figure 3A**).

Our results revealed that treatment with the SLC25A1-inhibitor BTA sensitized both oxic and anoxia-tolerant NCI-H460 cancer cells to the cytotoxic action of IR when treatment was performed under Nx conditions (**Figures 3B,D**). As expected, the effect was more pronounced in the anoxia-tolerant cells with increased

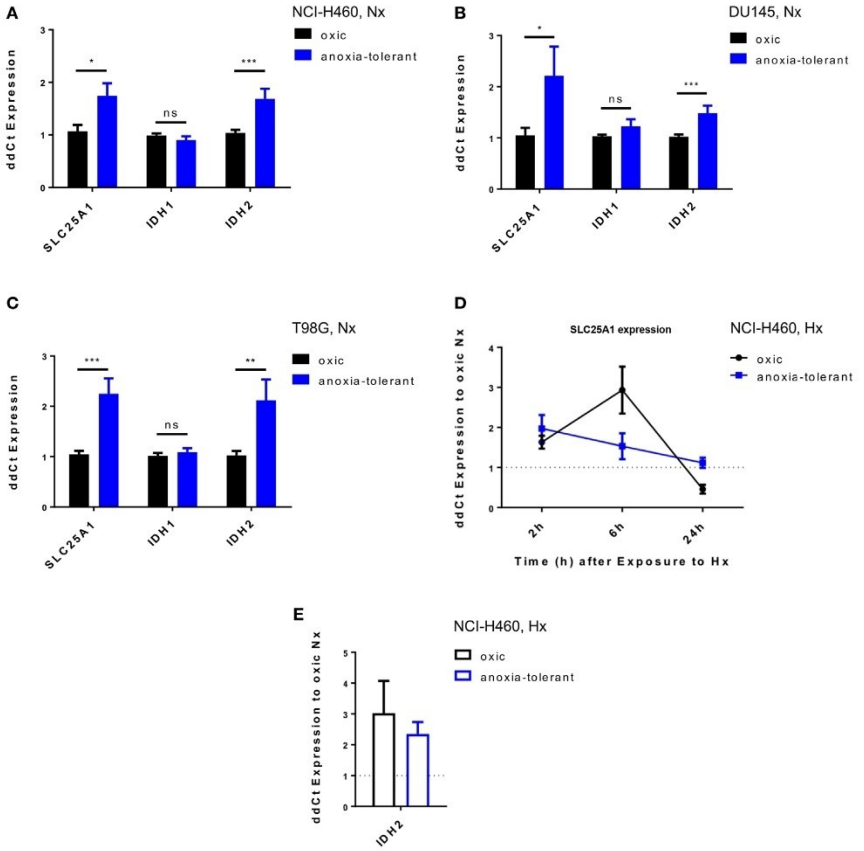

FIGURE 1 | Exposure of cancer cells to acute or chronic cycling severe hypoxia leads to upregulated expression of *SLC25A1* and *IDH2*. Expression of *SLC25A1*, isocitrate dehydrogenase 1 (*IDH1*; cytosolic), and isocitrate dehydrogenase 2 (*IDH2*; mitochondrial) was determined in anoxia-tolerant cancer cells generated by exposure to 16 cycles (T98G) or 25 cycles (NCI-H460, DU145) of severe hypoxia (48 h, <0.1% O_2) and reoxygenation (120 h air plus 5% CO_2 referred as 20% O_2) and the respective oxic control cells (24) by quantitative real-time PCR analysis. Data show basal expression of *SLC25A1*, *IDH1*, and *IDH2* in **(A)** NCI-H460, **(B)** DU145, and **(C)** T98G oxic and anoxia-tolerant cells under normoxic (Nx) conditions (20% O_2). Changes in *SLC25A1* [2–24 h, **(D)**] and *IDH2* [24 h, **(E)**] expression in oxic and anoxia-tolerant NCI-H460 cells in response to acute severe hypoxia (Hx, 0.2% O_2). Data were always normalized to the respective oxic control cells under basal Nx conditions. Mean values ± SEM are shown, $n = 3$ (*$p \leq 0.05$, **$p < 0.01$, and ***$p \leq 0.001$; *t*-test).

SLC25A1 expression and higher radioresistance. Interestingly, radiosensitization was also observed when treatment was performed in acute severe hypoxia (**Figures 3C,E**). BTA treatment was even able to partially compensate the reduced efficacy of IR in acute hypoxia (**Figure 3E**). Remarkably, we observed these effects even though BTA was already removed 24 h after IR so that long-term incubation was performed in inhibitor-free media. To confirm the relevance of SLC25A1 inhibition for the radiorsensitizing effects of BTA, we performed additional experiments with a chemically distinct SLC25A1-inhibitor 4-Chloro-3-[[(3-nitrophenyl)amino]sulfonyl]-benzoic acid (CNASB), with higher specificity for SLC25A1 (43). These experiments revealed that combined treatment of CNASB and IR similarly sensitized both, oxic and anoxia-tolerant NCI-H460 cancer cells, to the cytotoxic action of IR under Nx and hypoxic (Hx) conditions in short-term proliferation (Figure S4A in Supplementary Material) and long-term survival assays (Figure S4C in Supplementary Material) corroborating the radisensitizing action of BTA at the level of SLC25A1.

Cellular and Mitochondrial Redox Homeostasis Is Impaired After Inhibition of SLC25A1

As demonstrated in NCI-H460 cells IDH1, IDH2, and SCL25A1 are all part of a pathway responsible for the bidirectional

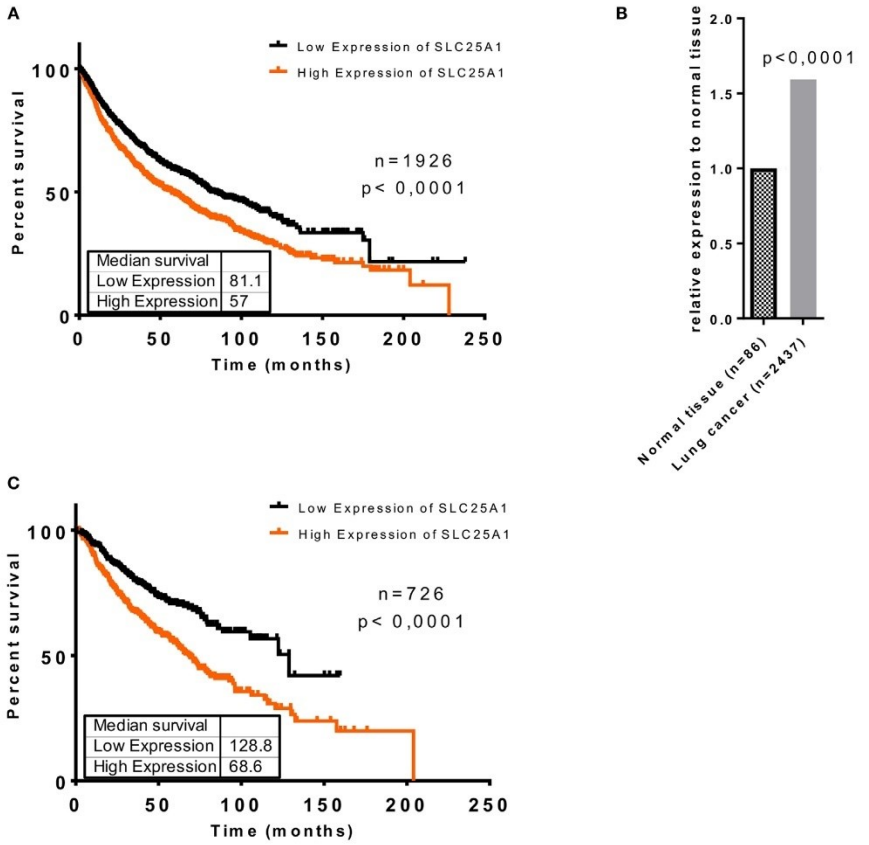

FIGURE 2 | Elevated expression of SLC25A1 is associated with worse clinical outcome of lung cancer patients, particularly upon tumor resection with negative margins (R0). Clinical relevance of the SLC25A1 expression was obtained by searching and analyzing available patient array data by the Kaplan–Meier plotter tool (kmplot.com). Data show **(A)** overall survival in lung cancer patients, **(B)** relative expression of SLC25A1 in normal tissue and lung cancer, and **(C)** overall survival in lung cancer patients upon surgery with negative tumor margins (R0). For the analysis, the cohort was split by median of SLC25A1 expression ("High" and "Low," respectively). Median survival (in months) is indicated for each survival curve.

transport of NADPH over the mitochondrial inner membrane (36). We therefore investigated whether the cytotoxic and radiosensitizing effects of the acute BTA treatment might be linked to alteration of cellular redox homeostasis. To this end, we measured total NADPH level (NADPH + $NADP^+$) by using a luciferase-coupled enzymatic reaction. As shown in **Figure 4A,** anoxia-tolerant NCI-H460 cells were characterized by a significant increase of total NADPH, presumably as a consequence of adaptation to chronic cycling severe hypoxia, whereas treatment with BTA for 2 h reduced the total NADPH level to the levels of the untreated oxic control cells (**Figure 4A**). In contrast, BTA had no significant effect on total NADPH levels in the oxic control cells (**Figure 4A**). We observed less pronounced effects regarding the BTA-mediated depletion of total NADPH levels in acute hypoxia (**Figure 4B**). Interestingly, the $NADP^+$/NADPH ratios were slightly increased after BTA treatment especially in anoxia-tolerant NCI-H460 cancer cells compared to respective controls in normoxia and hypoxia (**Figures 4C,D**).

NADPH is required amongst others for the regeneration of the reduced form of glutathione (GSH). We therefore next examined the effect of BTA treatment on cellular glutathione levels (**Figures 4E,F**). In line with our previous findings (24), anoxia-tolerant NCI-H460 cancer cells had elevated GSH levels compared to oxic control cells (**Figure 4E**). As expected, BTA treatment significantly reduced GSH levels in oxic and anoxia-tolerant NCI-H460 cancer cells when BTA treatment was performed under Nx conditions (**Figure 4E**). Similar observations were made when cells were treated with BTA in acute severe hypoxia (**Figure 4F**). Of note, BTA decreased the GSH levels of

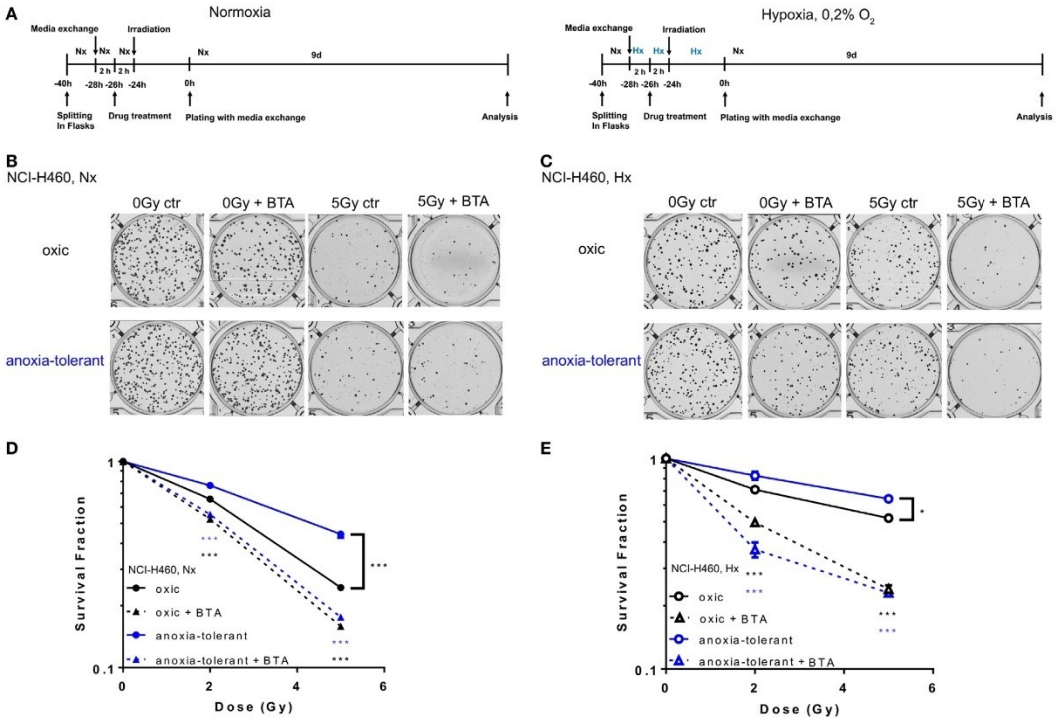

FIGURE 3 | Pharmacologic inhibition of SLC25A1 overcomes chronic cycling hypoxia-induced radioresistance. Anoxia-tolerant NCI-H460 cells and the oxic NCI-H460 control cells were pretreated with 5-mM BTA (2 h prior to IR) under normoxic (Nx) conditions (20% O_2) or upon 2-h preincubation in severe hypoxia (Hx, 0.2% O_2). Twenty-four hours after treatment cells were collected, plated at different cell numbers (200–3,200) in full medium without the inhibitor and grown under Nx for 9 days. **(A)** Schematic representation of the experimental timeline in normoxia (Nx, left panel) or severe Hx (right panel). Photomicrographs in **(B)** and **(C)** show representative pictures of colony formation upon treatment with IR without or with prior BTA treatment for Nx **(B)** or severely hypoxic conditions **(C)**. Survival curves shown in **(D,E)** depict quantification of colony formation upon treatment in normoxia **(D)** and severe hypoxia **(E)**. Colonies were scanned and counted using GelCount. Survival fractions were calculated to the plating efficiency of unirradiated cells under Nx or Hx conditions. Mean values ± SEM are shown, $n = 3$ ($^*p \leq 0.05$, $^{**}p < 0.01$, and $^{***}p \leq 0.001$; two-way ANOVA with Tukey post-test.) Comparisons between treatment and corresponding controls at the same dose are indicated.

the anoxia-tolerant cancer cells to the levels of the oxic control cells (**Figures 4E,F**).

To further specify the impact of the SLC25A1-inhibitor BTA on cellular antioxidant capacity, particularly mitochondrial and cellular redox homeostasis, we measured mitochondrial and cellular ROS after BTA treatment in normoxia and acute severe hypoxia (**Figures 4G,H**; Figure S2 in Supplementary Material). Importantly, BTA treatment increased the levels of mitochondrial ROS in oxic and anoxia-tolerant NCI-H460 cancer cells under Nx conditions (**Figure 4G**). This effect was even enhanced when BTA treatment was performed in acute hypoxia (**Figure 4H**; Figure S2 in Supplementary Material). Additionally, cellular ROS-levels were increased in both, oxic and anoxia-tolerant cells, upon BTA treatment in normoxia and acute severe hypoxia (Figures S2E,F in Supplementary Material). Nevertheless, BTA-induced cellular ROS levels were lower compared to the mitochondrial ROS levels (Figures S2 in Supplementary Material).

Taken together, the SLC25A1-inhibitor BTA efficiently decreased cellular NADPH and GSH levels resulting in increased mitochondrial and cellular ROS. These findings point to a role of SLC25A1 in the regulation of cellular antioxidant capacity and mitochondrial redox homeostasis.

SLC25A1 Inhibition Lowers Mitochondrial Metabolism and Alters Metabolic Demand

So far, our data indicated that increased production of mitochondrial ROS upon SLC25A1 inhibition by BTA treatment might play a role in BTA-mediated radiosensitization. However, SLC25A1 is of broader relevance for the transport of metabolites between mitochondrial intermembrane space and mitochondrial matrix as it shuttles isocitrate, malate and phosphoenolpyruvate, in addition to citrate (38, 44). We therefore wondered whether BTA

might have a more general effect on mitochondrial metabolism and therefore additionally measured the effects of BTA on mitochondrial metabolism by using extracellular flux measurements (**Figure 5**).

Pretreatment of cells with BTA for 24 h led to decreased basal mitochondrial respiration and lowered ATP-Production in both, oxic and anoxia-tolerant NCI-H460 cells, as determined by using the Mito Stress Test (**Figure 5A**). Additionally, we observed a decreased ability of cells treated with the SLC25A1 inhibitor to respond to forced mitochondrial respiration by uncoupling the electronic transport chain, an effect that is termed reduced spare respiratory capacity (**Figure 5A**, left panel). As shown in **Figure 5A,** the inhibitory effect was more pronounced in the anoxia-tolerant NCI-H460 cells as these cells were found to dispose of an increased spare respiratory capacity (**Figure 5A**, right panel) in comparison to oxic control cells (**Figure 5A**, middle

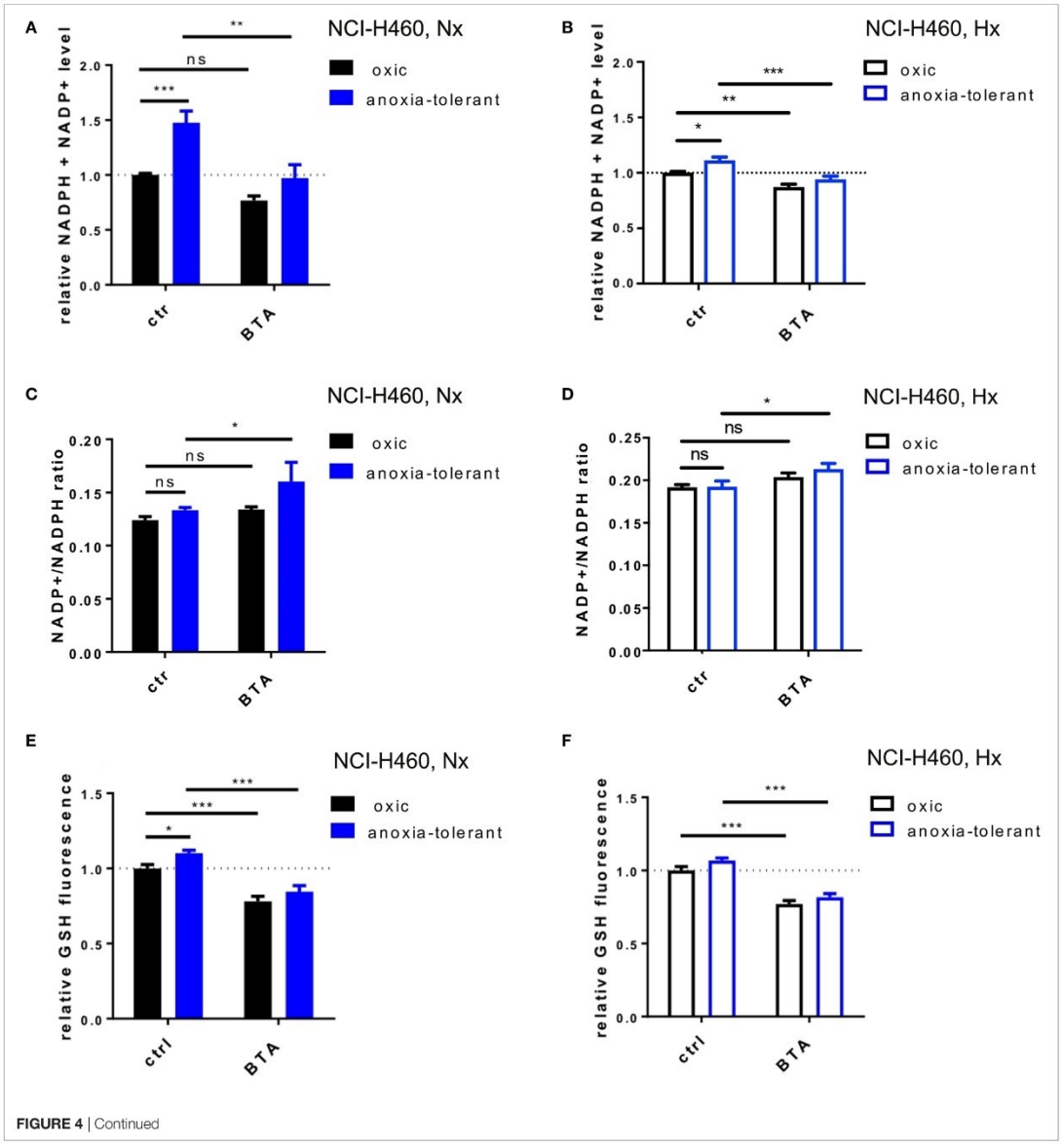

FIGURE 4 | Continued

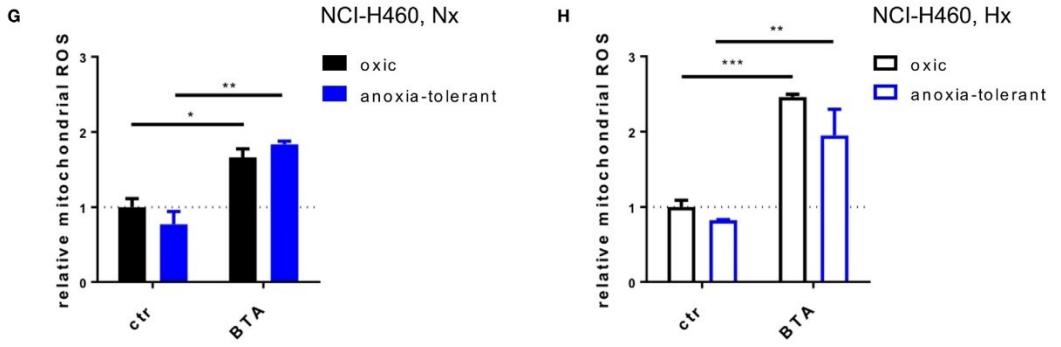

FIGURE 4 | Inhibition of SLC25A1 disturbs cellular and mitochondrial redox homeostasis. NCI-H460 oxic and anoxia-tolerant cells were treated with 5 mM BTA in normoxia (Nx, 20% O_2) or upon preincubation for 2 h in acute severe hypoxia (Hx, 0.2% O_2) and antioxidant capacity and ROS formation were determined 2 or 6 h after treatment in functional assays. **(A)** Impact of BTA treatment on total NADPH levels (NADPH + $NADP^+$) under normoxic (Nx) conditions as determined by using a luciferase-coupled enzymatic reaction 2 h after treatment. **(B)** Impact of BTA treatment on total NADPH levels (NADPH + $NADP^+$) under Hx conditions. **(C)** $NADP^+$/NADPH ratio upon 2 h of BTA treatment under Nx conditions. **(D)** $NADP^+$/NADPH ratio upon 2 h of BTA treatment under Hx conditions. **(E)** Influence of BTA treatment on GSH levels under Nx conditions as measured by fluorescence of monochlorobimane (MCB) 2 h after treatment. **(F)** Influence of BTA treatment on GSH levels under Hx conditions. **(G)** Mitochondrial superoxide reactive oxygen species (ROS) as determined in flow cytometry by staining with MitoSox 6 h after treatment under Nx conditions. Fold changes of gated positive cells are indicated. **(H)** Mitochondrial ROS as determined in flow cytometry by staining with MitoSox 6 h after treatment under Hx conditions. Mean values ± SEM are shown, $n = 3$. (ns $p > 0.05$, $^*p \leq 0.05$, $^{**}p < 0.01$, and $^{***}p \leq 0.001$; two-way ANOVA with Tukey post-test.)

panel). Similar effects on cell metabolism were observed when using CNASB, another more potent small molecule inhibitor of SLC25A1 (Figure S4B in Supplementary Material).

But inhibition of SLC25A1 might also impact the metabolic demands of oxic and anoxia-tolerant NCI-H460 cells to maintain mitochondrial function. To identify the metabolic pathways needed to maintain mitochondrial respiration under BTA treatment we performed the Fuel Flex Test. In this test the glucose/pyruvate pathway was inhibited by UK5099, the glutamine pathway by using BPTES and the fatty acid (FA) pathway by etomoxir treatment, respectively. Overall, BTA treatment induced a higher dependency of oxic and anoxia-tolerant NCI-H460 cells on the final glycolytic product pyruvate as well as glutamine to maintain mitochondrial respiration (**Figure 5B**). Furthermore, combined inhibition of two of these pathways reduced the capacity to maintain mitochondrial respiration only for glucose/pyruvate and FAs but not for glutamine when the other two pathways were inhibited (**Figure 5B**). This suggests that BTA reduces the capacity and flexibility of oxic and anoxia-tolerant cells to oxidize other fuels, when the pathway of interest is inhibited. Since BTA treatment lowered the flexibility of oxic and anoxia-tolerant cell to oxidize FAs, when glucose/pyruvate or glutamine pathways were inhibited, we measured FA uptake upon BTA treatment. We observed a reduction in the uptake of labeled FAs following BTA treatment (**Figure 5C**). Taken together, BTA treatment lowered the metabolic flexibility for all metabolic pathways examined in both oxic and anoxia-tolerant NCI-H460 cells, as defined by the difference between metabolic dependency and capacity (**Figure 5B**) and lead to reduced FA uptake (**Figure 5C**).

These findings revealed a role of SLC25A1 in conserving mitochondrial metabolism. Importantly, the enhanced flexibility of mitochondrial metabolism as a consequence of upregulated SLC25A1 expression might contribute to increased stress-tolerance of the NCI-H460 cancer cells.

Inhibition of SLC25A1 Affects the Repair of IR-Induced Double-Strand Breaks (DSB)

So far, our data indicated that pharmacologic inhibition of SLC25A1 by BTA or CNASB increases radiosensitivity of oxic and anoxia-tolerant NCI-H460 cancer cells and that disturbance of the redox homeostasis and of metabolic flexibility might participate in the radiosensitizing effects. Herein, one important aspect of radiosensitivity is the ability of the cells to repair IR-induced DNA DSB. Therefore, we finally examined if BTA treatment would affect the time-dependent induction and resolution of DNA-repair foci positive for Histone H2A.X phosphorylated at serine 139 (γH2AX), a marker for DNA DSB (45). BTA treatment alone (without IR) did not induce additional DSB, ruling out a direct effect of BTA on DNA-damage induction and repair (**Figures 6A,B**). Interestingly, the presence of BTA during exposure to IR slowed the resolution of IR-induced γH2AX-foci and led to higher residual amount of DNA lesions 24 h after IR-treatment in Nx (**Figures 6A,C**) and even in Hx conditions (**Figures 6B,D**). Surprisingly, despite the differences in SLC25A1 expression between oxic and anoxia-tolerant NCI-H460 cells, BTA treatment had similar effects on DSB repair in both cell lines. Even more important, despite the obvious differences in radiosensitivity, the kinetics of DSB repair as determined by the resolution of IR-induced γH2AX-foci were rather similar in oxic and anoxia-tolerant NCI-H460 cells. This suggests that other parameters of the DNA damage response might dictate the differences in radiosensitivity, presumably the differences in

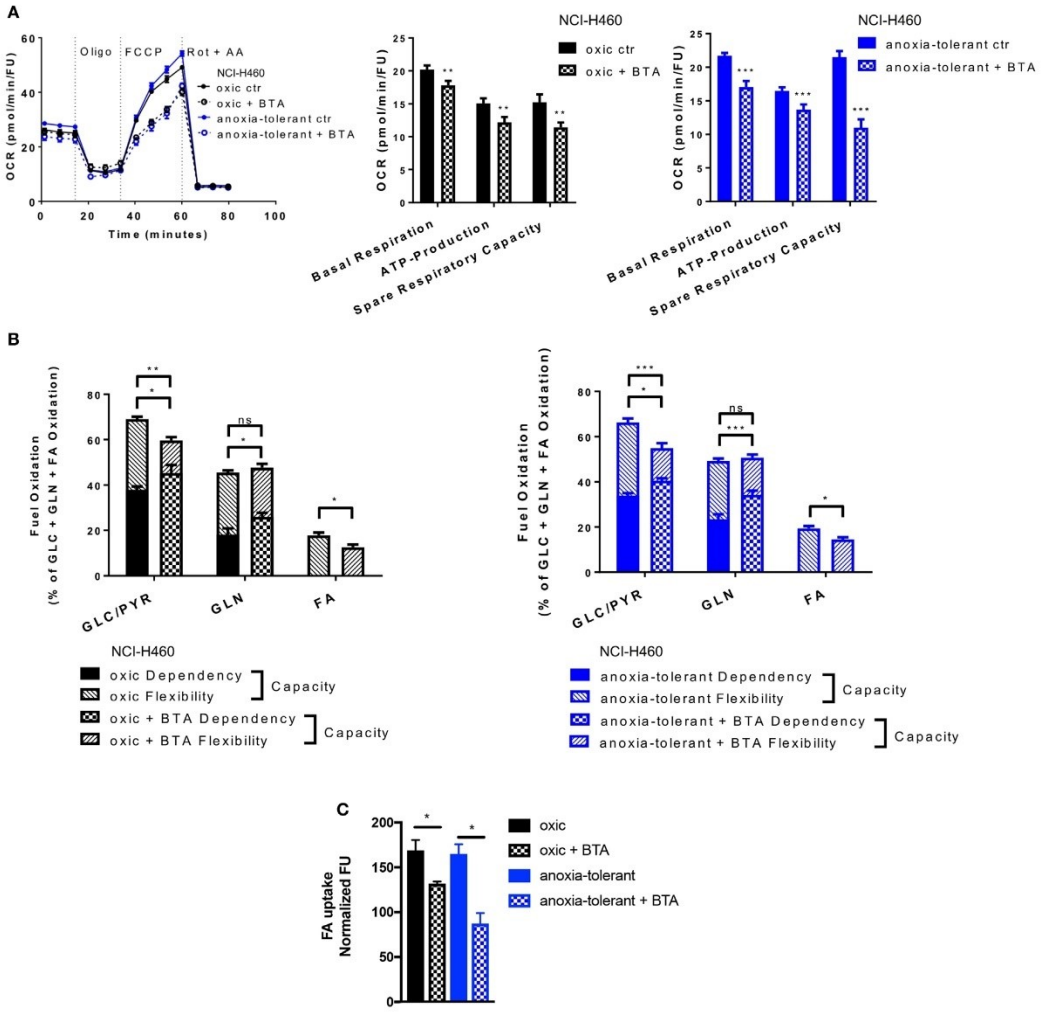

FIGURE 5 | Metabolic alterations upon SLC25A1 Inhibition in NCI-H460 oxic and anoxia-tolerant cells. NCI-H460 oxic and anoxia-tolerant cells were treated for 24 h with 5 mM 1,2,3-benzene-tricarboxylic acid (BTA) under standard ambient conditions and various parameters of cell metabolism were determined by using a Seahorse XFe 96 analyzer. Fatty-acid (FA) uptake was measured by using the fluorescent FA analog C1-BODIPY® 500/510 C12. **(A)** Oxygen consumption rate (OCR) was measured using Mito Stress Test Kit and normalized to Hoechst 33342 fluorescence units (FU) 24 h after treatment with BTA. Real-time Injection of oligomycin (Oligo, 1 μM), carbonyl cyanide-4-(trifluoromethoxy)phenylhydrazone (FCCP, 2 μM), Rotenone (Rot, 0.5 μM) and antimycin A (AA, 0.5 μM). Calculated parameters of the assay are indicated in bar graphs. **(B)** Percentage of total mitochondrial respiration for each fuel pathway measured with Seahorse XFe 96 analyzer using Fuel Flex Test Kit 24 h after treatment with BTA (fuel pathways: GLC/PYR: Glucose/Pyruvate, inhibition by UK5099; GLN, glutamine, inhibition by BPTES, FA: fatty acids, inhibition by etomoxir). **(C)** FA uptake measured after 24 h of BTA treatment. Mean values ± SEM are shown. Data in **(A)** and **(B)** from $n = 12$–18 wells from two independent experiments; Data in **(C)** $n = 3$ ($^*p \leq 0.05$, $^{**}p < 0.01$, and $^{***}p \leq 0.001$. **(A)** t-test; **(B)** and **(C)** two-way ANOVA with Tukey post-test).

the ability to cope with radiation-induced ROS. Nevertheless, it was an interesting observation that BTA was able to retard the resolution of IR-induced γH2AX-foci and cause a higher amount of residual DNA lesions 24 h after irradiation.

Interestingly, it had recently been shown that a knockout of SLC25A1 not only impairs mitochondrial function, resulting in higher glycolysis rate and the usage of glutamine for compensation of impaired FA synthesis, but also leads to the accumulation of

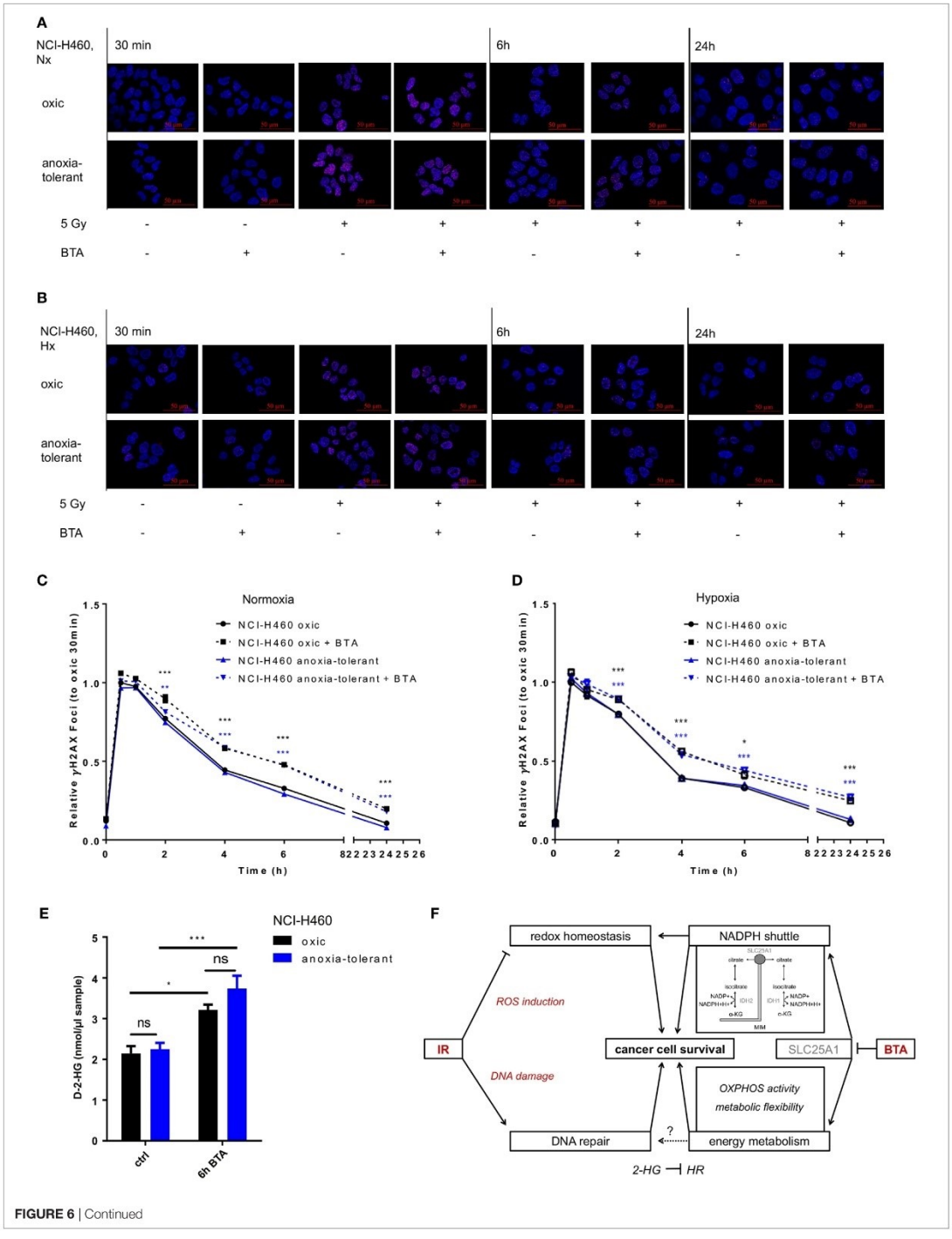

FIGURE 6 | Continued

FIGURE 6 | Inhibition of SLC25A1 affects the repair of radiation-induced DNA damage. NCI-H460 oxic and anoxia-tolerant cells were left untreated or exposed to ionizing radiation (IR) with a single dose of 5 Gy with or without prior preincubation of the cells for 2 h with 5 mM 1,2,3-benzene-tricarboxylic acid (BTA) under normoxic (Nx, 20% O_2) and hypoxic (Hx, 0,2% O_2) conditions. **(A)** Time-dependent accumulation of γH2AX foci in irradiated NCI-H460 oxic and anoxia-tolerant cells under Nx conditions was evaluated by fluorescence microscopy without and with additional treatment with 5 mM BTA at indicated time points after IR. **(B)** Time-dependent accumulation of γH2AX foci in irradiated NCI-H460 oxic and anoxia-tolerant cells under Hx conditions was evaluated by fluorescence microscopy without and with additional treatment with 5-mM BTA at indicated time points after IR. **(C)** Mean number of γH2AX foci per cell after IR without and with additional BTA treatment in Nx was calculated with the Focinator v2 software and normalized to oxic control cells 30 min after IR. **(D)** Mean number of γH2AX foci per cell after IR without and with additional BTA treatment in Hx was calculated with the Focinator v2 software and normalized to oxic control cells 30 min after IR. **(E)** D-2-hydroxyglutarate levels (D-2-HG) were determined in lysed cells 6 h after treatment with BTA in Nx. **(F)** Schematic representation of the suggested mechanisms of the actions of BTA and IR on cancer cell survival. Mean values ± SEM are shown, $n = 3$ ($^*p \leq 0.05$, $^{**}p < 0.01$, and $^{***}p \leq 0.001$; two-way ANOVA with Tukey post-test. Comparisons between treatment and corresponding controls at the same time point are indicated). MIM, mitochondrial inner membrane; α-KG, α-Ketoglutarate; HR, homologous recombination.

2-hyodroxyglutarate (2-HG) in NCI-H460 cells (44). Of note, accumulation of the oncometabolite 2-HG has been linked to DNA-repair defects (46). We therefore wondered whether BTA-mediated inhibition of SLC25A1 might have similar effects and measured the effects of BTA treatment on the level of D-2-HG. For this, we used an enzymatic reaction detecting a colored product photometrically at 450 nm. As shown in **Figure 6E**, BTA treatment indeed significantly increased the levels of D-2-Hydroxyglutarate (D-2-HG) 6 h after BTA treatment in both oxic and anoxia-tolerant NCI-H460 cells (**Figure 6E**). This increase in 2-HG might thus be responsible for the observed delay in the kinetics of the repair of radiation-induced DNA DSB observed in both cell lines (**Figures 6A–D**). The finding that there was no significant difference in the absolute D-2-HG levels upon BTA treatment between oxic control and anoxia-tolerant NCI-H460 might explain why the BTA-induced retardation in DNA repair was similar in both cell lines. Taken together our novel findings suggest that BTA exerts a dual effect on the cellular radiation response by targeting both DNA repair and metabolic escape mechanisms of aggressive cancers making it a promising radiosensitizer.

DISCUSSION

Tumor hypoxia is an important biological factor causing poor therapy outcome and worse prognosis in NSCLC patients. However, so far hypoxia-targeting strategies have not been translated into clinical practice highlighting the need for an improved understanding of the underlying mechanisms if we aim to develop more effective strategies for therapeutic intervention. In our work, we focus on mechanisms of radiation resistance caused by adaptation of cancer to an adverse Hx environment.

Our previous work identified enhanced antioxidant capacity based on glutamine-dependent glutathione-regeneration as a mechanism favoring stress tolerance and radioresistance of cancer cells with tolerance to chronic cycling severe hypoxia (23, 24). Here, we reveal important novel mechanistic aspects of increased antioxidant capacity in cancer cells and demonstrate a therapeutic potential for SLC25A1 inhibition to overcome radioresistance in chronically Hx lung cancer cells: (i) Exposure of cancer cells to acute or chronic cycling severe hypoxia was associated with upregulated expression of the citrate transporter SLC25A1. (ii) Pharmacologic inhibition of SLC25A1 by BTA reduced cellular antioxidant capacity, enhanced the generation of mitochondrial ROS and abrogated the increase in radioresistance of lung cancer cells induced by adaptation to chronic cycling severe hypoxia. (iii) BTA treatment was also associated with a pronounced disturbance of mitochondrial metabolism, accumulation of the oncometabolite 2-HG, and impaired repair of radiation-induced DNA DSB. These findings point to a yet unknown role of SLC25A1 in radioresistance that might be linked to regeneration of GSH for ROS-detoxification and metabolic regulation of DNA repair. Remarkably, we confirmed the metabolic and radiosensitizing effects of SLC25A1-inhibition also with CNASB, another potent small-molecule inhibitor with documented higher specificity to SLC25A1 (43). In line with our observations using BTA the radiosensitizing effects of CNASB were more prominent in the anoxia-tolerant cancer cells. This further corroborates our assumption that chronic cycling hypoxia/reoxygenation stress increases not only the expression but also the reliance of cancer cells on the SLC25A1 mediated redox-homeostasis for survival under stress conditions.

Interestingly, high SLC25A1 expression in lung cancer patients has already been linked with poorer overall survival compared to lung cancer patients with low SLC25A1 expression in an earlier report (42). However, here we expand these findings with respect to the importance of SLC25A1 in terms of recurrence and progression of lung cancer suggesting that SLC25A1 may be an attractive therapeutic target for tumor cell-specific radiosensitization at least in patients with high SLC25A1 expression. Of note, mutant p53 can promote transcriptional activation of SLC25A1 eventually by an interaction with the FOXO-1 transcription factor (42). This suggests that SLC25A1 might mediate some of the oncogenic activities of mutant p53—an important prognostic marker predictive for relapse and resistance to chemotherapy and RT (47).

In addition, upregulated expression of SLC25A1 was always associated with upregulation of IDH2. Thus, SLC25A1 and IDH2 might cooperate in adaptive metabolic processes that allow cancer cells to cope with the adverse conditions in the tumor microenvironment. Others have described a crucial role of the presence of active IDH2 for proliferation and survival of glioblastoma cancer cells in hypoxia (48).

However, our primary goal was to evaluate the use of SLC25A1 as a therapeutic target to overcome radioresistance in chronically Hx lung cancer cells. It has been shown earlier that inhibition of SLC25A1 by BTA reduces the growth of xenograft tumors

of breast, bladder or lung cancer cells without any evidence for additional normal tissue toxicity (39). But here we demonstrate for the first time that SLC25A1 has a role in lung cancer cell radiation resistance. For this we measured the effects of the SLC25A1-inhibitor BTA on radiation-induced eradication of clonogenic tumor cells in long-term colony formation assays (delayed plating) upon treatment in combination with IR. Our results revealed that treatment with BTA for 24 h was sufficient to significantly reduce the survival fraction of both, anoxia-tolerant NCI-H460 cells and the respective oxic NCI-H460 control cells. However, the radiosensitizing effect was more pronounced in the anoxia-tolerant NCI-H460 cells and could be further enhanced by treatment in acute severe hypoxia. Of note, we made similar observations when using a chemically distinct small molecule SLC25A1 inhibitor, CNASB, thereby corroborating the action of BTA at the level of SLC25A1. Moreover, the latter finding underlines the importance of SLC25A1-controlled metabolic and redox related alterations for adaptation to acute and chronic cycling hypoxia.

Mechanistically, we discovered that BTA exerts a dual effect on the cellular radiation response by targeting both, cell metabolism and DNA repair, making it a promising radiosensitizer. On the one hand, radiosensitizing effect of the SLC25A1-inhibitor BTA was associated with a reduction of the cellular antioxidant capacity: BTA treatment significantly reduced cellular total NADPH levels and increased $NADP^+$/NADPH ratios in the anoxia-tolerant NCI-H460 cells. Moreover, BTA reduced GSH levels in both oxic and anoxia-tolerant NCI-H460 cancer cells, even in acute severe hypoxia. The reduction in these major determinants of cellular antioxidant capacity resulted in increased production of mitochondrial ROS and this effect on cellular redox-balance was even more pronounced when treatment had been performed in acute severe hypoxia. Our findings strongly suggest that SLC25A1 plays a role for maintenance of the antioxidant defense of lung cancer cells with tolerance to acute or chronic cycling severe hypoxia with potential impact on the sensitivity of the cells to ROS-induced damage. Our findings are in line with a report about a role of SLC25A1 for redox homeostasis in NCI-H460 cancer cells obtained by a stable knockout of SLC25A1 (36). Thus, our pharmacologic approach reproduces the findings obtained by the genetic approach, but shows in addition that such effects can also be obtained under conditions of acute severe hypoxia and in cells with tolerance to chronic cycling severe hypoxia. Importantly, the above-mentioned effects were neither due to direct toxic effects of BTA neither under Nx nor under Hx conditions as shown by the lack of a relevant increase in apoptosis (Figure S3 in Supplementary Material) or total cell death (not shown) upon acute treatment up to 72 h, nor to BTA-induced alterations in *SLC25A1* expression (Figure S1F in Supplementary Material).

Though SLC25A1 inhibition by BTA led to a significant induction of mitochondrial ROS compared to the respective untreated control cells, the percentage of cells stained positive for mitochondrial ROS was below 20% (Figure S2 in Supplementary Material). We therefore assume that inhibition of SLC25A1 might have effects in addition to the alterations in the redox balance that contribute to the cytotoxic effects BTA.

SLC25A1 is responsible for the bidirectional shuttling of citrate between the mitochondria and cytosol thereby supporting redox homeostasis by delivery of isocitrate to IDH2, which in turn regenerates NADPH. But SLC25A1 also impacts biosynthetic processes such as lipid biosynthesis (42) and other cellular processes. For example, it has been demonstrated that SLC25A1 and its function in citrate export to cytosol is central for cytokine-induced inflammatory signals and maintenance of NADPH redox state in macrophage activation (37, 49). Moreover, knockout of SLC25A1 has been associated with dysregulation of mitochondrial metabolism in cancer cells (44). Therefore, we further tested the effects of adaptation to chronic cycling severe hypoxia and BTA treatment on energy metabolism. Interestingly, anoxia-tolerant NCI-H460 cells displayed enhanced basal respiration and increased ability to respond to forced mitochondrial respiration (spare respiratory capacity) when compared to oxic NCI-H460 control cells. These findings demonstrate that the mitochondrial changes caused by adaptation to chronic cycling severe hypoxia are not restricted to components of the mitochondrial apoptosis signaling cascade as described earlier (22) but extend to alterations in mitochondrial oxidative metabolism. We also found that pharmacologic inhibition of SLC25A1 by BTA or CNASB significantly decreased mitochondrial respiration and ATP production. Interestingly, treatment with BTA or CNASB particularly lowered the spare respiratory capacity of anoxia-tolerant NCI-H460 cancer cells, pointing to a possible involvement of SLC25A1 in adaptation of oxidative metabolism to metabolic stress induced by chronic cycling severe hypoxia.

In addition, BTA treatment rendered NCI-H460 oxic and anoxia-tolerant cells more dependent on glycolysis-derived pyruvate and glutamine. It has been discussed that enhanced glucose uptake and a shift toward the pentose phosphate pathway (PPP) to generate more NADPH might be a strategy of cancer cells to counteract increased ROS (50). However, cancer cells use diverse strategies to increase their antioxidant capacity (cellular GSH) (31). For example, serine catabolism can participate in mitochondrial redox control under Hx conditions (51) whereas in our hands, altered glutamine usage contributed to the regeneration of glutathione and improved ROS defense of cancer cells with tolerance to cycling severe hypoxia (24). Excessive ROS-production—caused for example by oncogene-induced proliferation—causes oxidative damage of cellular macromolecules such as nuclear and mitochondrial DNA, membranes and proteins, thereby affecting major cell functions and cell survival (52–55). Moreover, there is an intimate link between adaptive changes in cell metabolism, generation of ROS, and the death threshold at the mitochondria by interconnected metabolic and redox sensitive pathways (56, 57). Therefore, the ability of the SLC25A1-inhibitor BTA to disrupt redox homeostasis makes it an attractive approach to enhance the cytotoxic effects of ROS-dependent treatments such as IR.

Finally, pharmacologic inhibition of SLC25A1 reduced the flexibility of oxic and anoxia-tolerant NCI-H460 cells to oxidize major metabolic fuels, which could in turn reduce their capability to meet altered nutrient availability after hypoxia-induced microenvironmental changes. Furthermore, BTA treatment decreased the capacity of NCI-H460 cells to oxidize FAs and also reduced FA uptake, particularly in anoxia-tolerant cells. Thereby our findings

corroborate data obtained by genetic knockout of SLC25A1 in NCI-H460 cells revealing increased glycolysis and the usage of glutamine to compensate for the loss of FA synthesis as a consequence of reduced citrate transport (44). The same group further highlighted the complex functional role of SLC25A1 in glycolysis, redox homeostasis, and lipogenesis by quantitative metabolic flux analysis (44). Of note, dependency on the uptake of FAs has been recognized as a specific metabolic vulnerability of Hx cancer cells (58, 59).

Our metabolic investigations demonstrate that in addition to ensure the export of citrate from the mitochondria to the cytosol, e.g., for FA synthesis, SLC25A1 seems to be crucial for mitochondrial homeostasis and increased metabolic flexibility of the anoxia-tolerant NCI-H460 cells. Thereby our data confirm the assumption that SLC25A1 might be crucial for metabolic plasticity of cancer cells enabling adaptation and survival under adverse conditions such as nutrient starvation (glucose) or oxidative stress suggested by others (39, 47). But our data extend the stress conditions to acute and chronic cycling severe hypoxia. It appears that inhibition of SLC25A1 leads to a massive disturbance of mitochondrial metabolism and this might severely affect the ability of cancer cells to cope with the toxic effects of IR leading to radiosensitization and enhanced clonogenic cell death.

However, radiosensitivity is largely determined by the ability of the cells to repair radiation-induced DNA DSB. Analyzing the time-dependent formation and resolution of γH2AX –positive DNA repair foci as a mean of DNA-DSB we found that BTA treatment did not alter the initial amount of radiation-induced γH2AX -foci at 0.5–1 h after irradiation. However, BTA-mediated SLC25A1 inhibition slowed the kinetics of γH2AX-foci resolution, and this resulted in significantly higher levels of residual DNA damage in oxic and anoxia-tolerant NCI-H460 cells exposed to combined treatment when compared to irradiation alone at 2, 4, 6, and 24 h after irradiation.

Unexpectedly, we found that despite the obvious differences in radiosensitivity between anoxia-tolerant and oxic control NCI-H460 cells the kinetics in formation and resolution of γH2AX-foci indicative were rather similar in both cell lines. Therefore, it was not surprising that both cell lines responded similarly to combined treatment with BTA and IR with respect to the kinetics of the induction and repair of DNA DSB. From these data we conclude that other parameters of the DNA damage response such as their ability to cope with radiation-induced ROS might dictate the adaptation-induced differences in radiosensitivity and that the resulting differences in the extent of radiosensitization between oxic control and anoxia-tolerant cells might be due to drug-induced interference with redox homeostasis and disturbance of mitochondrial metabolism to meet cellular energy demands during the radiation response.

Nevertheless, these observations revealed that inhibition of SLC25A1 impacts DNA repair. Analyzing the underlying mechanisms we found that BTA-mediated inhibition of DSB repair correlated with an increase in D2-hydroxyglutarate levels induced by BTA treatment. In this context, BTA treatment led to elevated levels of D-2-HG in both NCI-H460 oxic and anoxia-tolerant cancer cells. Thereby, pharmacologic inhibition of SLC25A1 with BTA reproduces another metabolic effect of genetic inhibition of SLC25A1 where somatic loss of SLC25A1 induced a broad dysregulation of mitochondrial metabolism with accumulation of L- and D-enantiomers of 2-HG in NCI-H460 cells (44). Moreover, deletion of the SLC25A1 gene in humans causes the neurometabolic disorder D- and L-2-hydroxyglutaric aciduria, which is also characterized by increased accumulation of 2-HG (60, 61). These observations make it highly likely that elevated D-2-HG levels observed in response to BTA treatment are a direct and acute consequence of SLC25A1 inhibition.

Both enantiomers of 2-HG have been shown to promote malignant progression by their inhibitory action on α-ketoglutarate (αKG)-dependent dioxygenases; they are either synthesized as so-called "oncometabolite" as a result of gain-of-function mutations in IDH1/IDH2 (62, 63) or as pathologic metabolites in Hx cancer cells (64, 65).

Of note, accumulation of 2-HG has recently been linked to inhibition of DNA repair by inducing a homologous recombination repair defect thereby sensitizing cancer cells to poly (ADP-ribose) polymerase (PARP) inhibitors (46, 66). Furthermore, 2-HG was also shown to inhibit ALKBH DNA repair enzymes, leading to enhanced sensitivity to alkylating agents (67). Our new findings strongly suggest that BTA-induced accumulation of 2-HG might contribute to BTA-mediated radiosensitization and this finding could be exploited therapeutically in combination treatments.

Taken together, we identified a role of SLC25A1-regulated redox homeostasis in the tolerance of cancer cells to acute and chronic cycling hypoxia and increased radioresistance caused by adaptation to these stress conditions. In addition, our results clearly demonstrate that inhibition of SLC25A1 by the small molecule inhibitors BTA and CNASB is suited to increase radiosensitivity of NCI-H460 cancer cells exposed to acute or chronic cycling hypoxia. Mechanistically, treatment with the SLC25A1-inhibitor BTA disturbed cellular redox homeostasis by decreasing NADPH/GSH levels but also affected mitochondrial metabolism and cellular energy provision thereby reducing cancer cell survival (summarized in **Figure 6F**). Importantly, we demonstrate that BTA treatment impaired the repair of IR-induced DNA DSB and this was associated with elevation of D-2-HG levels. Since the method allowed us only to detect D-2-HG we cannot exclude that BTA treatment might also increase L-2-HG levels.

The pronounced effects of the SLC25A1-inhibitor BTA on cellular antioxidant capacity, cell metabolism and DNA repair make SLC25A1 inhibitors such as BTA interesting leads for the development of metabolic inhibitors of radioresistance. However, the development of small molecule inhibitors specifically targeting SLC25A1 at nanomolar drug concentrations is required for clinical translation of this approach.

Importantly, high expression of SLC25A1 in lung cancer patients was associated with a poor outcome, particularly after successful surgery (R0-resection), pointing to a potential clinical relevance of SLC25A1 particularly in terms of tumor recurrence. Moreover, exposure to IR, acute hypoxia, and chronic cycling severe hypoxia increased SLC25A1 expression in our *in vitro* models of anoxia-tolerant cancer cells. These findings suggest that SLC25A1 could be relevant as a potential biomarker of increased antioxidant capacity and metabolic flexibility and thus of a high potential for metabolic escape from radio (chemo)therapy.

We conclude that targeting the increased metabolic flexibility of cancer cells with tolerance to environmental stress, or of metabolic escape mechanisms ensuring DNA repair and cell survival under therapy, e.g., by pharmacologic inhibition of SLC25A1, represent attractive strategies to enhance vulnerability to genotoxic treatments and overcome microenvironment-mediated resistance to radio(chemo)therapy in advanced cancers.

MATERIALS AND METHODS

Reagents and Cell Lines

If not stated otherwise, all chemicals were purchased from Sigma Aldrich (St. Louis, MO, USA). NCI-H460 lung adenocarcinoma cells, DU145 prostate cancer cells and T98G glioblastoma cells were obtained from ATCC (Bethesda, MD, USA) and were routinely tested for mycoplasma. NCI-H460, DU145 or T98G cells with tolerance to cycling severe hypoxia/reoxygenation stress were generated by exposure to 16 cycles (T98G) or 25 cycles (NCI-H460, DU145) of severe hypoxia (48 h, <0.1% O_2) and reoxygenation (120-h air plus 5% CO_2 referred as 20% O_2) as described earlier (24). These cells hypoxia/reoxygenation-tolerant cells will be termed "anoxia-tolerant cells" throughout the manuscript. Control cells were cultured in parallel under standard ambient O_2 conditions (20% O_2 plus 5% CO_2; the control cells will be termed "oxic cells" throughout the manuscript) (24, 59). Upon selection, cancer cells were routinely grown in RPMI 1640 medium supplemented with 10% (v/v) fetal calf serum (Gibco/Life Technologies, Carlsbad, CA, USA) and maintained in a humidified incubator at 37°C and 5% CO_2 (referred to as "normoxia" or "Nx conditions,"). For severely Hx conditions cells were grown in a humidified hypoxia work station (*In vivo* 400, Ruskinn Technology Ltd., Bridgend, Great Britain) at 37°C, 0.2% O_2, and 5% CO_2 (referred to as "hypoxia" or "Hx conditions,").

Patient Survival Data

Patient array data were obtained from and analyzed by Kaplan–Meier plotter tool (kmplot.com) as described elsewhere (40, 41). The cohort was split by median of SLC25A1 expression ("High" and "Low," respectively). Analysis was performed in the cohort once without additional restrictions and once including only patients which had successful surgery (only surgical margins negative), as described in detail elsewhere (40). For further details of used settings please refer to Tables S1 and S2 in Supplementary Material.

qRT-PCR Analysis

cDNA was synthesized from 1 µg of total RNA using QuantiTect Reverse Transcription Kit (Qiagen, Hilden, Germany) according to the manufacturer's protocol. Specific primers were synthesized based on available sequences for each listened gene. Primer sets for qRT-PCR were designed with the Blast web tool (U.S. National Center for Biotechnology Information, Bethesda, MD, USA). To exclude cross-reaction of primers with the genes the sequence of interest was compared as well with the Blast database. PCR products were 150–200 bp in size. We used published β2-microglobulin (B2M) primer sequences as housekeeping gene (68). qRT-PCR and cycling conditions were performed using specific oligonucleotide primers (*B2M* forward: TGCTGTCTCCATGTTTGATGTATCT; reverse: TCTCTGCTCCCCACCTCTAAGT; *SLC25A1* forward: CAACGGGGTGAGGGCAT; reverse: CTCGGTGGGGAAGGT GATG; *IDH1* forward: CTCTGTGGCCCAAGGGTATG; reverse: GGATTGGTGGACGTCTCCTG; IDH2 forward: CCTGCTCG TTCGCTCTCC; reverse: GCTTCGCCACCTTGATCCT) and using qPCR kit for SYBR® Green I, 6-Carboxyl-X-Rhodamine (ROX) (Eurogentec, Cologne, Germany) according to the manufacturers protocol. Reactions were carried out on an ABI Prism 7900HT using MicroAmp Optical 384 well Reaction plate (Applied Biosystems by Life Technologies, Bleijswijk, Netherlands) and BIO-RAD PCR Sealers Microseal "B" Film Adhesive seal (optically clear; BIORAD, Munich, Germany). Melting curves were obtained after each PCR run and showed single PCR products. cDNAs were run in triplicate, without reverse transcriptase and no-template controls were run in duplicates. Expression levels for the genes of interest and for the housekeeping gene *B2M* were measured in three independent PCR runs. Expression ratios were calculated using the geometric mean expression of the housekeeping gene *B2M* to normalize the expression data for the genes of interest according to the $2^{-\Delta\Delta Ct}$—method as described by others (69).

Western Blot Analysis

Anti-rabbit SLC25A1 Polyclonal antibody (Thermo Fisher, Rockford, IL, USA) and anti-mouse β-actin from Sigma Aldrich (St. Louis, MO, USA) were used for Western blot analysis. After harvesting, cells were lysed in 75 µL of RIPA buffer containing 0,5% Sodiumdesoxycholate, 1% NP-40 (Nonidet), 0,1% Sodiumdodecylsulfate (SDS), 50-mM Tris-HCl, 150-mM NaCl, 5-µg/mL aprotinin, 5-µg/mL leupeptin, and 3-µg/mL pepstatin. Protein was separated by 12% sodium dodecyl sulfate-polyacrylamide gel electrophoresis (SDS-PAGE) under reducing conditions and transferred onto polyvinylidene fluoride (PVDF) membranes (Roth, Karlsruhe, Germany). Blots were blocked in RotiBlock (Roth, Karlsruhe, Germany) for 1 h at room temperature. The membranes were incubated overnight at 4°C with the respective primary antibodies. The secondary antibody was incubated for 1 h at room temperature. Detection of antibody binding was performed by enhanced chemiluminescence (ECL Western Blotting Analysis System; GE Healthcare/Amersham Biosciences, Freiburg, Germany). Equal loading was verified by antibodies against β-actin. Densitometry analysis was performed using ImageJ 2.00 (National Institutes of Health, Bethesda, MD, USA).

Determination of Redox Homeostasis

NADPH levels were measured using NADPH Glo Assay (Promega, Madison, WI, USA) according to manufacturer's protocol. Briefly, adherent cells in 96-well plates were lysed and heated under acidic and basic conditions to measure $NADP^+$ and NAPH individually using a luciferase-coupled enzymatic reaction. In parallel, technical replicates were fixed with 4% paraformaldehyde and stained with 10-µg/mL solution of fluorescent dye Hoechst 33342 (Thermo Scientific, Waltham, MA, USA) for normalization to DNA content. Luminescence and Flourescence were measured

in triplicates using a BioTek Synergy Microplate reader (BioTek, Winooski, NH, USA).

Levels of reduced Glutathione (GSH) were determined by using Monochlorobimane (MCB) which was described to be specific for GSH metabolized by Glutathione-S-Transferase, leading to a fluorescent adduct (70). The published protocol for measurement of GSH in a Microplate Reader (71) was adapted for using 10-µM MCB with 15 min of preincubation. To rule out alterations in the speed of dye metabolism instead of alterations in absolute cellular GSH levels, kinetic measurements of fluorescence were performed for 15 min at 37°C. Each assay contained cells treated with H_2O_2 to deplete GSH as a negative control.

To quantify mitochondrial ROS production, cells were stained for 30 min at 37°C with 5 µM of MitoSox (Molecular Probes/Invitrogen, Carlsbad, CA, USA). To quantify cellular ROS production, cells were stained for 30 min at 37°C with 5 µM of Dihydroethidium (DHE) (Molecular Probes/Invitrogen, Carlsbad, CA, USA). MitoSox- or DHE-positive cells were detected by flow cytometry (BD Accuri C6, Becton Dickinson, Heidelberg, Germany; FL-2). Fractions of gated positive cells (at least 10,000) with higher fluorescence were evaluated. Fold changes were quantified to the corresponding controls.

Extracellular Flux Analysis

NCI-H460 cells were plated at 7.500 cells/well in XF96 microplates (Seahorse Bioscience, Billerica, MA, USA) in RPMI Medium with 10% FCS according to manufacturer's recommendations 48 h prior to the assay. Treatment with 5 mM BTA was performed for 24 h. One hour prior to the assay, medium was exchanged to XF base medium (Seahorse Bioscience, Billerica, MA, USA) with 1-mM Pyruvate, 2-mM Glutamine and 10-mM Glucose and incubated at 37°C without CO_2. During assays, OCR was measured using a Seahorse XFe 96 analyzer. Mito Stress Test Kit containing 1-µM Oligomycin, 2-µM Carbonyl cyanide-*4*-(trifluoromethoxy)phenylhydrazone (FCCP), 0.5-µM Rotenone and 0.5-µM Antimycin A was perfomed according to manufacturer's protocol. For individual normalization to DNA content, fluorescence was measured after cells were fixed with 4% PFA and stained with 10-µg/mL Hoechst 33342 solution after each assay. Fuel Flex Test Kit containing 3-µM BPTES, an inhibitor of glutaminase (GLS1), 4-µM etomoxir, an inhibitor of carnitine palmitoyl-transferase 1 A (CPT1A) and 2-µM UK5099, an inhibitor of the mitochondrial pyruvate carrier (MPC), was also performed according to manufacturer's protocol. Data were analyzed using Wave 2.4 software (Seahorse Bioscience, Billerica, MA, USA).

Determination of Fatty-Acid Uptake

The uptake of FA was quantified by using fluorescent FA analog C1-BODIPY® 500/510 C12. In brief, fluorescent FA (5 µM) were added 24 h after treatment with 5-mM BTA to serum-free media. We quenched the fluorescence of FA in media by adding trypan blue (0.33 mM) to the media. The uptake of fluorescent FA was measured after 1 h, at 37°C spectrophotometrically at 485/528 nm (59). For individual normalization to DNA content, Hoechst 33342 fluorescence was measured after the assay. Cells were fixed with 4% PFA and stained with 10-µg/mL Hoechst 33342 solution.

Quantification of D-2-Hydroxyglutarate

Levels of D-2-HG were measured using colorimetric D-2-Hydroxyglutarate Assay Kit (BioVision, Milpitas, CA, USA) according to manufacturer's protocol. At a glance, 10^7 cells were lysed, spun down and supernatant was transferred into a 96-well plate to quantify the enzymatic conversion of D-2-Hydroxyglutarate to α-Ketoglutarate leading to colored product which is detected photometrically at 450 nm using a BioTek Synergy Microplate reader (BioTek, Winooski, NH, USA).

Irradiation and Treatment

1,2,3-benzene-tricarboxylic acid and CNASB were purchased from Sigma-Aldrich (St. Louis, MO, USA). Stock solutions of 200-mM BTA were made with phosphate-buffered aqua bidest and 14-mM CNASB was solved in DMSO. Irradiation was performed at room temperature with an X-ray machine (Precision X-Ray Inc., North Branford, CT, USA) operated at 320 kV, 12.5 mA with a 1.65-mm Al filter, at a distance of 50 cm and a dose rate of 3.71 Gy/min. For an irradiation dose of 2 Gy, the cells were irradiated approximately 32 s, for 5 Gy approximately 81 s. Cells were returned to the incubator immediately after exposure to IR. For irradiation under Hx conditions, Hx cell dishes were kept in BD GasPak EZ Pouch System (Becton Dickinson, Heidelberg, Germany). In terms of combined treatments, inhibitors were added 2 h prior to irradiation.

Immunofluorescence: γH2AX Assays

Cells were seeded on glass coverslips placed in 12-well plates and irradiated 24 h later with 5 Gy. Next, cells were fixed and permeabilized in 3% PFA/0.2% Triton-X100 for 15 min and incubated in blocking solution including 2% goat serum at room temperature for 1 h. γH2AX foci were stained for 1 h at room temperature (RT) with Alexa Fluor® 647 mouse anti-H2A.X (pS139) (BD Biosciences, San Jose, CA, USA) diluted 1:50 in blocking solution. DNA was stained with Hoechst33342 (3 µM in PBS) for 30 min at RT. Coverslips were mounted onto glass slides with DAKO mounting medium (Dako NA Inc., Carpinteria, CA, USA). Slides were analyzed with a Zeiss Axiovert 200 fluorescence microscope with ApoTome and ZEN imaging software (Carl Zeiss, Goettingen, Germany). γH2AX foci in at least 50 cells per slide were counted with the Focinator software developed in our laboratory (72, 73).

Colony Formation Assays

Clonogenic cell survival in response to the respective treatments was determined comparing the clonogenic survival of cells cultured under Nx and severely Hx conditions. For treatment in normoxia, exponentially growing cells were seeded in tissue culture flasks, incubated under standard culturing conditions (20% O_2, 5% CO_2, 37°C) and irradiated 24 h later (0 to 5 Gy) without or with prior BTA treatment (5 mM). BTA treatment was performed 2 h prior to irradiation. For treatment in hypoxia, tissue culture flasks of exponentially growing cells were exposed to severe hypoxia (0.2% O_2) 2 h prior to BTA treatment and 4 h prior to irradiation, respectively. After completion of the treatments, cells were incubated for 24 h under Nx or Hx conditions, respectively,

then washed, collected (0.05% Trypsin, 0.01% EDTA), and plated to 6-well plates at densities of 200–3,200 cells per well (delayed plating). The cell viability was checked before plating the cells by using CASY COUNT (Omni Life Science, Bremen, Germany) and only the number of viable cells was plated. Plates were subsequently incubated for 9 days under standard Nx conditions before quantification of colony formation. For this, cells were fixed in 3.7% formaldehyde and 70% ethanol, stained with 0.05% Coomassie blue, and colonies of at least 50 cells were counted by GelCount (Oxford Optronix, Oxfordshire, Great Britain). The plating efficiency and surviving fraction (SF) to corresponding Nx and Hx controls were calculated as described elsewhere (74).

Toxicity Testing

For quantification of apoptotic DNA-fragmentation (sub-G1 population), cells were incubated for 30 min at room temperature with a staining solution containing 50-µg/mL PI in a hypotonic citrate buffer 0.1% (w/v) sodium citrate and 0.05% (v/v) Triton X-100 and subsequently analyzed by flow cytometry (BD Accuri C6, Becton Dickinson, Heidelberg, Germany; FL-2) (75).

For determination of cell proliferation and viability, cells were washed with PBS (1x), fixed with Glutaraldehyde (0.1% in PBS), and stained with crystal violet (0.1% in PBS). The dye was released by TritonX-100 (0.2% in PBS) and measured spectrophotometrically at 540 nm as described elsewhere (76).

Statistics

Data represent mean values of at least three independent experiments ± SEM except for **Figures 5A,B** which show data from $n = 12–18$ wells from two independent experiments. Data analysis was performed either by two-way ANOVA test using parametric methods and employing Tukey multiple comparison post-test where appropriate or by unpaired Student's *t*-test using Prism6 software (Graph Pad Inc., La Jolla, CA, USA). The values of $P \leq 0.05$ were considered significant.

AUTHOR CONTRIBUTIONS

JM, JH, and VJ designed and conceptualized the research. JH, CH, and JM performed experiments, analyzed, validated, and visualized the results. JM, JH, and VJ wrote the original manuscript draft. JM and VJ supervised the work. VJ acquired the funding. All authors critically revised, edited, and approved the final version of the manuscript.

ACKNOWLEDGMENTS

We thank A. Warda for excellent technical support, K. Al-Refae and A. Krysztofiak for support with DNA DSB foci analysis, and the Focinator-Software and the Brigitte und Dr. Konstanze Wegener-Stiftung for funding of the Seahorse XFe 96 analyzer to VJ.

FUNDING

The work was supported by grants of the German Research Association (grant number DFG GRK1739/2) and the Deutsche Krebshilfe/Mildred-Scheel-Stiftung (grant numbers 110355 and 70112711) to VJ.

SUPPLEMENTARY MATERIAL

The Supplementary Material for this article can be found online at https://www.frontiersin.org/articles/10.3389/fonc.2018.00170/full#supplementary-material.

REFERENCES

1. Salem A, Asselin MC, Reymen B, Jackson A, Lambin P, West CML, et al. Targeting hypoxia to improve non-small cell lung cancer outcome. *J Natl Cancer Inst* (2018) 110(1):14–30. doi:10.1093/jnci/djx160
2. Barcellos-Hoff MH, Lyden D, Wang TC. The evolution of the cancer niche during multistage carcinogenesis. *Nat Rev Cancer* (2013) 13(7):511–8. doi:10.1038/nrc3536
3. Chiche J, Brahimi-Horn MC, Pouyssegur J. Tumour hypoxia induces a metabolic shift causing acidosis: a common feature in cancer. *J Cell Mol Med* (2010) 14(4):771–94. doi:10.1111/j.1582-4934.2009.00994.x
4. Chen JL, Merl D, Peterson CW, Wu J, Liu PY, Yin H, et al. Lactic acidosis triggers starvation response with paradoxical induction of TXNIP through MondoA. *PLoS Genet* (2010) 6(9):e1001093. doi:10.1371/journal.pgen.1001093
5. Gatenby RA, Gillies RJ. A microenvironmental model of carcinogenesis. *Nat Rev Cancer* (2008) 8(1):56–61. doi:10.1038/nrc2255
6. Flavahan WA, Gaskell E, Bernstein BE. Epigenetic plasticity and the hallmarks of cancer. *Science* (2017) 357(6348):eaal2380. doi:10.1126/science.aal2380
7. Macaluso M, Paggi MG, Giordano A. Genetic and epigenetic alterations as hallmarks of the intricate road to cancer. *Oncogene* (2003) 22(42):6472–8. doi:10.1038/sj.onc.1206955
8. Chan DA, Giaccia AJ. Hypoxia, gene expression, and metastasis. *Cancer Metastasis Rev* (2007) 26(2):333–9. doi:10.1007/s10555-007-9063-1
9. Harris AL. Hypoxia—a key regulatory factor in tumour growth. *Nat Rev Cancer* (2002) 2(1):38–47. doi:10.1038/nrc704
10. Vaupel P. Tumor microenvironmental physiology and its implications for radiation oncology. *Semin Radiat Oncol* (2004) 14(3):198–206. doi:10.1016/j.semradonc.2004.04.008
11. Rankin EB, Giaccia AJ. Hypoxic control of metastasis. *Science* (2016) 352(6282):175–80. doi:10.1126/science.aaf4405
12. Bristow RG, Hill RP. Hypoxia and metabolism. Hypoxia, DNA repair and genetic instability. *Nat Rev Cancer* (2008) 8(3):180–92. doi:10.1038/nrc2344
13. Liauw SL, Connell PP, Weichselbaum RR. New paradigms and future challenges in radiation oncology: an update of biological targets and technology. *Sci Transl Med* (2013) 5(173):173sr2. doi:10.1126/scitranslmed.3005148
14. Wouters BG, Koritzinsky M. Hypoxia signalling through mTOR and the unfolded protein response in cancer. *Nat Rev Cancer* (2008) 8(11):851–64. doi:10.1038/nrc2501
15. Lee CT, Boss MK, Dewhirst MW. Imaging tumor hypoxia to advance radiation oncology. *Antioxid Redox Signal* (2014) 21(2):313–37. doi:10.1089/ars.2013.5759
16. Ljungkvist ASE, Bussink J, Kaanders JH, Wiedenmann NE, Vlasman R, van der Kogel AJ. Dynamics of hypoxia, proliferation and apoptosis after irradiation in a murine tumor model. *Radiat Res* (2006) 165(3):326–36. doi:10.1667/RR3515.1
17. Matsumoto S, Yasui H, Mitchell JB, Krishna MC. Imaging cycling tumor hypoxia. *Cancer Res* (2010) 70(24):10019–23. doi:10.1158/0008-5472.CAN-10-2821
18. Vaupel P, Harrison L. Tumor hypoxia: causative factors, compensatory mechanisms, and cellular response. *Oncologist* (2004) 9(Suppl 5):4–9. doi:10.1634/theoncologist.9-90005-4
19. Chou CW, Wang CC, Wu CP, Lin YJ, Lee YC, Cheng YW, et al. Tumor cycling hypoxia induces chemoresistance in glioblastoma multiforme by upregulating the expression and function of ABCB1. *Neuro Oncol* (2012) 14(10):1227–38. doi:10.1093/neuonc/nos195
20. Span PN, Bussink J. Biology of hypoxia. *Semin Nucl Med* (2015) 45(2):101–9. doi:10.1053/j.semnuclmed.2014.10.002

21. Tellier C, Desmet D, Petit L, Finet L, Graux C, Raes M, et al. Cycling hypoxia induces a specific amplified inflammatory phenotype in endothelial cells and enhances tumor-promoting inflammation in vivo. *Neoplasia* (2015) 17(1): 66–78. doi:10.1016/j.neo.2014.11.003
22. Weinmann M, Belka C, Guner D, Goecke B, Muller I, Bamberg M, et al. Array-based comparative gene expression analysis of tumor cells with increased apoptosis resistance after hypoxic selection. *Oncogene* (2005) 24(38):5914–22. doi:10.1038/sj.onc.1208748
23. Weinmann M, Jendrossek V, Guner D, Goecke B, Belka C. Cyclic exposure to hypoxia and reoxygenation selects for tumor cells with defects in mitochondrial apoptotic pathways. *FASEB J* (2004) 18(15):1906–8. doi:10.1096/fj.04-1918fje
24. Matschke J, Riffkin H, Klein D, Handrick R, Ludemann L, Metzen E, et al. Targeted inhibition of glutamine-dependent glutathione metabolism overcomes death resistance induced by chronic cycling hypoxia. *Antioxid Redox Signal* (2016) 25(2):89–107. doi:10.1089/ars.2015.6589
25. Dewhirst MW. Intermittent hypoxia furthers the rationale for hypoxia-inducible factor-1 targeting. *Cancer Res* (2007) 67(3):854–5. doi:10.1158/0008-5472.CAN-06-4744
26. Song C, Hong BJ, Bok S, Lee CJ, Kim YE, Jeon SR, et al. Real-time tumor oxygenation changes after single high-dose radiation therapy in orthotopic and subcutaneous lung cancer in mice: clinical implication for stereotactic ablative radiation therapy schedule optimization. *Int J Radiat Oncol Biol Phys* (2016) 95(3):1022–31. doi:10.1016/j.ijrobp.2016.01.064
27. Levine AJ, Puzio-Kuter AM. The control of the metabolic switch in cancers by oncogenes and tumor suppressor genes. *Science* (2010) 330(6009):1340–4. doi:10.1126/science.1193494
28. Rouschop KM, Dubois LJ, Keulers TG, van den Beucken T, Lambin P, Bussink J, et al. PERK/eIF2alpha signaling protects therapy resistant hypoxic cells through induction of glutathione synthesis and protection against ROS. *Proc Natl Acad Sci U S A* (2013) 110(12):4622–7. doi:10.1073/pnas.1210633110
29. Hanahan D, Weinberg RA. Hallmarks of cancer: the next generation. *Cell* (2011) 144(5):646–74. doi:10.1016/j.cell.2011.02.013
30. Cairns RA, Harris IS, Mak TW. Regulation of cancer cell metabolism. *Nat Rev Cancer* (2011) 11(2):85–95. doi:10.1038/nrc2981
31. DeBerardinis RJ, Chandel NS. Fundamentals of cancer metabolism. *Sci Adv* (2016) 2(5):e1600200. doi:10.1126/sciadv.1600200
32. Nakashima R, Goto Y, Koyasu S, Kobayashi M, Morinibu A, Yoshimura M, et al. UCHL1-HIF-1 axis-mediated antioxidant property of cancer cells as a therapeutic target for radiosensitization. *Sci Rep* (2017) 7(1):6879. doi:10.1038/s41598-017-06605-1
33. Kuo ML, Sy AJ, Xue L, Chi M, Lee MT, Yen T, et al. RRM2B suppresses activation of the oxidative stress pathway and is up-regulated by p53 during senescence. *Sci Rep* (2012) 2:822. doi:10.1038/srep00822
34. Deponte M. The incomplete glutathione puzzle: just guessing at numbers and figures? *Antioxid Redox Signal* (2017) 27(15):1130–61. doi:10.1089/ars.2017.7123
35. Toledano MB, Huang ME. The unfinished puzzle of glutathione physiological functions, an old molecule that still retains many enigmas. *Antioxid Redox Signal* (2017) 27(15):1127–9. doi:10.1089/ars.2017.7230
36. Jiang L, Shestov AA, Swain P, Yang C, Parker SJ, Wang QA, et al. Reductive carboxylation supports redox homeostasis during anchorage-independent growth. *Nature* (2016) 532(7598):255–8. doi:10.1038/nature17393
37. Palmieri EM, Spera I, Menga A, Infantino V, Porcelli V, Iacobazzi V, et al. Acetylation of human mitochondrial citrate carrier modulates mitochondrial citrate/malate exchange activity to sustain NADPH production during macrophage activation. *Biochim Biophys Acta* (2015) 1847(8):729–38. doi:10.1016/j.bbabio.2015.04.009
38. Palmieri F. The mitochondrial transporter family (SLC25): physiological and pathological implications. *Pflugers Arch* (2004) 447(5):689–709. doi:10.1007/s00424-003-1099-7
39. Catalina-Rodriguez O, Kolukula VK, Tomita Y, Preet A, Palmieri F, Wellstein A, et al. The mitochondrial citrate transporter, CIC, is essential for mitochondrial homeostasis. *Oncotarget* (2012) 3(10):1220–35. doi:10.18632/oncotarget.714
40. Gyorffy B, Surowiak P, Budczies J, Lanczky A. Online survival analysis software to assess the prognostic value of biomarkers using transcriptomic data in non-small-cell lung cancer. *PLoS One* (2013) 8(12):e82241. doi:10.1371/journal.pone.0082241
41. Gyorffy B, Lanczky A, Eklund AC, Denkert C, Budczies J, Li Q, et al. An online survival analysis tool to rapidly assess the effect of 22,277 genes on breast cancer prognosis using microarray data of 1,809 patients. *Breast Cancer Res Treat* (2010) 123(3):725–31. doi:10.1007/s10549-009-0674-9
42. Kolukula VK, Sahu G, Wellstein A, Rodriguez OC, Preet A, Iacobazzi V, et al. SLC25A1, or CIC, is a novel transcriptional target of mutant p53 and a negative tumor prognostic marker. *Oncotarget* (2014) 5(5):1212–25. doi:10.18632/oncotarget.1831
43. Aluvila S, Sun J, Harrison DH, Walters DE, Kaplan RS. Inhibitors of the mitochondrial citrate transport protein: validation of the role of substrate binding residues and discovery of the first purely competitive inhibitor. *Mol Pharmacol* (2010) 77(1):26–34. doi:10.1124/mol.109.058750
44. Jiang L, Boufersaoui A, Yang C, Ko B, Rakheja D, Guevara G, et al. Quantitative metabolic flux analysis reveals an unconventional pathway of fatty acid synthesis in cancer cells deficient for the mitochondrial citrate transport protein. *Metab Eng* (2017) 43(Pt B):198–207. doi:10.1016/j.ymben.2016.11.004
45. Rogakou EP, Pilch DR, Orr AH, Ivanova VS, Bonner WM. DNA double-stranded breaks induce histone H2AX phosphorylation on serine 139. *J Biol Chem* (1998) 273(10):5858–68. doi:10.1074/jbc.273.10.5858
46. Sulkowski PL, Corso CD, Robinson ND, Scanlon SE, Purshouse KR, Bai H, et al. 2-Hydroxyglutarate produced by neomorphic IDH mutations suppresses homologous recombination and induces PARP inhibitor sensitivity. *Sci Transl Med* (2017) 9(375):eaal2463. doi:10.1126/scitranslmed.aal2463
47. Albanese C, Avantaggiati ML. The SLC25A1-p53 mutant crosstalk. *Aging (Albany NY)* (2015) 7(8):519–20. doi:10.18632/aging.100785
48. Wise DR, Ward PS, Shay JE, Cross JR, Gruber JJ, Sachdeva UM, et al. Hypoxia promotes isocitrate dehydrogenase-dependent carboxylation of alpha-ketoglutarate to citrate to support cell growth and viability. *Proc Natl Acad Sci U S A* (2011) 108(49):19611–6. doi:10.1073/pnas.1117773108
49. Infantino V, Iacobazzi V, Menga A, Avantaggiati ML, Palmieri F. A key role of the mitochondrial citrate carrier (SLC25A1) in TNFalpha- and IFNgamma-triggered inflammation. *Biochim Biophys Acta* (2014) 1839(11):1217–25. doi:10.1016/j.bbagrm.2014.07.013
50. Liemburg-Apers DC, Willems PH, Koopman WJ, Grefte S. Interactions between mitochondrial reactive oxygen species and cellular glucose metabolism. *Arch Toxicol* (2015) 89(8):1209–26. doi:10.1007/s00204-015-1520-y
51. Ye J, Fan J, Venneti S, Wan YW, Pawel BR, Zhang J, et al. Serine catabolism regulates mitochondrial redox control during hypoxia. *Cancer Discov* (2014) 4(12):1406–17. doi:10.1158/2159-8290.CD-14-0250
52. Latorre-Pellicer A, Moreno-Loshuertos R, Lechuga-Vieco AV, Sanchez-Cabo F, Torroja C, Acin-Perez R, et al. Mitochondrial and nuclear DNA matching shapes metabolism and healthy ageing. *Nature* (2016) 535(7613):561–5. doi:10.1038/nature18618
53. Schieber M, Chandel NS. ROS function in redox signaling and oxidative stress. *Curr Biol* (2014) 24(10):R453–62. doi:10.1016/j.cub.2014.03.034
54. Sullivan LB, Chandel NS. Mitochondrial reactive oxygen species and cancer. *Cancer Metab* (2014) 2:17. doi:10.1186/2049-3002-2-17
55. Sato A, Nakada K, Hayashi J. Mitochondrial dynamics and aging: mitochondrial interaction preventing individuals from expression of respiratory deficiency caused by mutant mtDNA. *Biochim Biophys Acta* (2006) 1763 (5–6):473–81. doi:10.1016/j.bbamcr.2006.03.001
56. Fulda S, Galluzzi L, Kroemer G. Targeting mitochondria for cancer therapy. *Nat Rev Drug Discov* (2010) 9(6):447–64. doi:10.1038/nrd3137
57. Wu CC, Bratton SB. Regulation of the intrinsic apoptosis pathway by reactive oxygen species. *Antioxid Redox Signal* (2013) 19(6):546–58. doi:10.1089/ars.2012.4905
58. Kamphorst JJ, Cross JR, Fan J, de Stanchina E, Mathew R, White EP, et al. Hypoxic and Ras-transformed cells support growth by scavenging unsaturated fatty acids from lysophospholipids. *Proc Natl Acad Sci U S A* (2013) 110(22):8882–7. doi:10.1073/pnas.1307237110
59. Matschke J, Wiebeck E, Hurst S, Rudner J, Jendrossek V. Role of SGK1 for fatty acid uptake, cell survival and radioresistance of NCI-H460 lung cancer cells exposed to acute or chronic cycling severe hypoxia. *Radiat Oncol* (2016) 11:75. doi:10.1186/s13014-016-0647-1
60. Eguchi M, Ozaki E, Yamauchi T, Ohta M, Higaki T, Masuda K, et al. Manifestation of recessive combined D-2-, L-2-hydroxyglutaric aciduria in combination with 22q11.2 deletion syndrome. *Am J Med Genet A* (2018) 176(2):351–8. doi:10.1002/ajmg.a.38578

61. Pop A, Williams M, Struys EA, Monne M, Jansen EEW, De Grassi A, et al. An overview of combined D-2- and L-2-hydroxyglutaric aciduria: functional analysis of CIC variants. *J Inherit Metab Dis* (2018) 41(2):169–80. doi:10.1007/s10545-017-0106-7
62. Dang L, White DW, Gross S, Bennett BD, Bittinger MA, Driggers EM, et al. Cancer-associated IDH1 mutations produce 2-hydroxyglutarate. *Nature* (2009) 462(7274):739–44. doi:10.1038/nature08617
63. Losman JA, Kaelin WG Jr. What a difference a hydroxyl makes: mutant IDH, (R)-2-hydroxyglutarate, and cancer. *Genes Dev* (2013) 27(8):836–52. doi:10.1101/gad.217406.113
64. Intlekofer AM, Dematteo RG, Venneti S, Finley LW, Lu C, Judkins AR, et al. Hypoxia induces production of L-2-hydroxyglutarate. *Cell Metab* (2015) 22(2):304–11. doi:10.1016/j.cmet.2015.06.023
65. Oldham WM, Clish CB, Yang Y, Loscalzo J. Hypoxia-mediated increases in L-2-hydroxyglutarate coordinate the metabolic response to reductive stress. *Cell Metab* (2015) 22(2):291–303. doi:10.1016/j.cmet.2015.06.021
66. Gagne M, Boulay K, Topisirovic I, Huot ME, Mallette FA. Oncogenic activities of IDH1/2 mutations: from epigenetics to cellular signaling. *Trends Cell Biol* (2017) 27(10):738–52. doi:10.1016/j.tcb.2017.06.002
67. Wang P, Wu J, Ma S, Zhang L, Yao J, Hoadley KA, et al. Oncometabolite D-2-hydroxyglutarate inhibits ALKBH DNA repair enzymes and sensitizes IDH mutant cells to alkylating agents. *Cell Rep* (2015) 13(11):2353–61. doi:10.1016/j.celrep.2015.11.029
68. Caradec J, Sirab N, Keumeugni C, Moutereau S, Chimingqi M, Matar C, et al. 'Desperate house genes': the dramatic example of hypoxia. *Br J Cancer* (2010) 102(6):1037–43. doi:10.1038/sj.bjc.6605573
69. Pfaffl MW. A new mathematical model for relative quantification in real-time RT-PCR. *Nucleic Acids Res* (2001) 29(9):e45. doi:10.1093/nar/29.9.e45
70. Rice GC, Bump EA, Shrieve DC, Lee W, Kovacs M. Quantitative analysis of cellular glutathione by flow cytometry utilizing monochlorobimane: some applications to radiation and drug resistance in vitro and in vivo. *Cancer Res* (1986) 46(12 Pt 1):6105–10.
71. Cox DP, Cardozo-Pelaez F. High throughput method for assessment of cellular reduced glutathione in mammalian cells. *J Environ Prot Sci* (2007) 1:23–8.
72. Oeck S, Malewicz NM, Hurst S, Al-Refae K, Krysztofiak A, Jendrossek V. The Focinator v2-0—graphical interface, four channels, colocalization analysis and cell phase identification. *Radiat Res* (2017) 188(1):114–20. doi:10.1667/RR14746.1
73. Oeck S, Malewicz NM, Hurst S, Rudner J, Jendrossek V. The Focinator—a new open-source tool for high-throughput foci evaluation of DNA damage. *Radiat Oncol* (2015) 10:163. doi:10.1186/s13014-015-0453-1
74. Franken NA, Rodermond HM, Stap J, Haveman J, van Bree C. Clonogenic assay of cells in vitro. *Nat Protoc* (2006) 1(5):2315–9. doi:10.1038/nprot.2006.339
75. Nicoletti I, Migliorati G, Pagliacci MC, Grignani F, Riccardi C. A rapid and simple method for measuring thymocyte apoptosis by propidium iodide staining and flow cytometry. *J Immunol Methods* (1991) 139(2):271–9. doi:10.1016/0022-1759(91)90198-O
76. Feoktistova M, Geserick P, Leverkus M. Crystal violet assay for determining viability of cultured cells. *Cold Spring Harb Protoc* (2016) 2016(4):343–6. doi:10.1101/pdb.prot087379

Conflict of Interest Statement: The authors declare that the research was conducted in the absence of any commercial or financial relationships that could be construed as a potential conflict of interest.

Originalarbeit 2: Hlouschek et al. (2018) Cancer Lett 439, 24-38.

Cancer Letters 439 (2018) 24–38

Contents lists available at ScienceDirect

Cancer Letters

journal homepage: www.elsevier.com/locate/canlet

Original Articles

Targeting SLC25A10 alleviates improved antioxidant capacity and associated radioresistance of cancer cells induced by chronic-cycling hypoxia

Julian Hlouschek, Violetta Ritter, Florian Wirsdörfer, Diana Klein, Verena Jendrossek, Johann Matschke*

Institute of Cell Biology (Cancer Research), University Hospital Essen, 45122, Essen, North Rhine-Westphalia, Germany

ARTICLE INFO

Keywords:
Chronic cycling hypoxia
Radiation resistance
Metabolic reprogramming
Antioxidant capacity
SLC25A11

ABSTRACT

High tumor heterogeneity and increased therapy resistance acquired in a hypoxic tumor microenvironment remain major obstacles to successful radiotherapy. Others and we have shown that adaptation of cancer cells to cycling severe hypoxia and intermittent reoxygenation stress (chronic-cycling hypoxia) increases cellular antioxidant capacity thereby supporting resistance to chemotherapy and radiotherapy. Here we explored the involvement of antioxidant-associated mitochondrial transport-systems for maintenance of redox-homeostasis in adaptation to chronic-cycling hypoxia and associated radioresistance.

Genetic or pharmacological inhibition of the mitochondrial dicarboxylate carrier (SLC25A10) or the oxoglutarate-carrier (SLC25A11) increased the cytotoxic effects of ionizing radiation (IR). But only targeting of SLC25A10 was effective in overcoming chronic-cycling hypoxia-induced enhanced death resistance *in vitro* and *in vivo* by disturbing increased antioxidant capacity. Furthermore, *in silico* analysis revealed that overexpression of SLC25A10 but not SLC25A11 is associated with reduced overall survival in lung- and breast-cancer patients.

Our study reveals a role of SLC25A10 in supporting both, redox- and energy-homeostasis, ensuring radioresistance of cancer cells with tolerance to chronic-cycling hypoxia thereby proposing a novel strategy to overcome a mechanism of hypoxia-induced therapy resistance with potential clinical relevance regarding decreased patient survival.

1. Introduction

Metabolic reprogramming is an emerging hallmark of cancer that is associated with poor prognosis [1,2]. Herein the adverse microenvironment of malignant solid tumors characterized by a reduced availability of oxygen (tumor hypoxia) and nutrients as well as low pH is considered as an important driver of metabolic reprogramming [3,4]. Various reports associate tumor hypoxia with malignant progression, resistance of cancer cells to chemotherapy and radiotherapy (RT), and poor clinical outcome [5–7].

Increasing flexibility of cancer cells to maintain cellular redox homeostasis and high antioxidant capacity are part of the metabolic reprogramming observed in cancer cells during malignant progression [8]. In line with that observation we have recently demonstrated that increased antioxidant capacity is a particular feature of cancer cells with tolerance to cycling severe hypoxia and intermittent reoxygenation, subsequently designated as chronic-cycling hypoxia [9]. Mechanistically we could link improved antioxidant defence to up-regulation of glutamic oxaloacetic transaminase 1 (GOT1) resulting in a glutamine-dependent increase in the levels of the major cellular

Abbreviations: B2M, β2-microglobulin; BMA, butylmalonate; ctrl, control; DAB, diaminobenzidine; DHE, dihydroethidium; eIF2α, eukaryotic initiation factor 2α; ETC, electronical transport chain; FC, fold change; GEE, glutathione ethyl ester; GOT1, glutamic oxaloacetic transaminase 1; GSH, glutathione; Gy, Gray; H&E, haematoxylin and eosin; HCC, hepatocellular carcinoma; HIF1, Hypoxia-inducible factor 1; IHC, immunohistochemistry; IR, ionizing radiation; MPC1, mitochondrial pyruvate carrier 1; mROS, mitochondrial reactive oxygen species; MT, Mito Tempo; ns, not significant; NSCLC, non-small cell lung cancer; OCR, oxygen consumption rate; PEP-CK, phosphoenolpyruvate carboxykinase; PER, proton efflux rate; PERK, double-stranded RNA-activated protein kinase-like endoplasmic reticulumkinase; PFA, paraformaldehyde; PI, propidium iodide; PSA, phenylsuccinate; qRT-PCR, quantitative real-time PCR; ROS, reactive oxygen species; ROX, 6-Carboxyl-X-Rhodamine; RT, Radiotherapy; SLC25A1, mitochondrial citrate carrier; SLC25A10, mitochondrial dicarboxylate carrier; SLC25A11, mitochondrial oxoglutarate carrier; TCA, tricarboxylic acid cycle; UCHL1, Ubiquitin C-terminal hydrolase-L1

* Corresponding author. Institute of Cell Biology (Cancer Research), University Hospital Essen, Virchowstrasse 173, 45122, Essen, Germany.
E-mail address: johann.matschke@uk-essen.de (J. Matschke).

https://doi.org/10.1016/j.canlet.2018.09.002
Received 18 June 2018; Received in revised form 22 August 2018; Accepted 3 September 2018

antioxidant molecule glutathione (GSH) and associated radioresistance [9]. Further mechanisms of increased antioxidant capacity of hypoxic or severe hypoxia/reoxygenation-tolerant cancer cells leading to radioresistance include cysteine-dependent novel synthesis of GSH as a result of ER stress downstream signalling of double-stranded RNA-activated protein kinase-like endoplasmic reticulum kinase (PERK)/eukaryotic initiation factor 2α (eIF2α)-dependent arm of the unfolded protein response [10]. But also increased NADPH production for GSH regeneration in the pentose phosphate pathway via the Ubiquitin C-terminal hydrolase-L1 (UCHL1)/Hypoxia-inducible factor 1 (HIF1) axis [11] has been described. In our hands, up-regulated expression of the mitochondrial citrate carrier SLC25A1 in response to chronic-cycling hypoxia sustained NADPH pools and mitochondrial redox homeostasis [12].

Generally, up-regulation of GSH strongly correlates with cancer initiation and progression in various tumor entities [13]. GSH is critical for various cellular processes like protein folding, redox signalling and defence against reactive oxygen species (ROS), but also for detoxification of xenobiotics [14]. Of note, elevated levels of GSH acquired during malignant progression have been linked to cancer cell resistance against pro-oxidant anticancer treatments making pathways involved in sustaining high GSH levels promising therapeutic targets to overcome cancer cell resistance to radiotherapy and certain anticancer drugs, particularly in hypoxic tumors [13].

In own previous work we demonstrated that pharmacologic inhibition of GOT1 or SLC25A1 in combination with ionizing radiation was able to overcome increased radioresistance induced by adaptation to chronic-cycling hypoxia amongst others by disturbing cellular and mitochondrial redox homeostasis [9,12].

Together with glycolytic metabolism and some other metabolic fluxes, mitochondria play a pivotal role in therapy resistance of cancer cells in terms of energy provision, redox balance, oncogenic signalling and intrinsic apoptosis [15–18]. Herein, mitochondrial GSH (mGSH) seems to be critical to regulate mitochondrial redox homeostasis and to protect cells from cardiolipin oxidation, subsequent cytochrome *c* release and intrinsic apoptosis [13,19,20]. We therefore speculate that interference with mGSH levels may be particularly suited to overcome apoptosis resistance of cancer cells and may therefore be suited to sensitize cancer cells to pro-oxidant treatments such as radiotherapy.

However, GSH is exclusively synthesized in the cytosol and the inner mitochondrial membrane is impermeable for GSH so that specific transport systems for the maintenance of GSH are required which are not fully understood, particularly in cancer cells [19,21].

Aim of the present study was to further elucidate and improve the concept of targeting antioxidant-associated mitochondrial transport systems to overcome chronic-cycling hypoxia-induced resistance to RT focussing on the role of mitochondrial dicarboxylate carrier (SLC25A10) and mitochondrial 2-oxoglutarate carrier (SLC25A11), two potential mGSH transporters validated in various preclinical models [22–26]. We speculated that pharmacologic inhibition of these assumed mGSH and carboxylate transporters might be an attractive strategy as it should interfere with two assumed resistance mechanisms at the same time, namely antioxidant defence and cellular energy metabolism.

2. Materials and methods

2.1. Reagents and cell lines

If not stated otherwise, all chemicals were purchased from Sigma Aldrich (St. Louis, MO, USA). NCI-H460 lung adenocarcinoma cells, DU145 prostate cancer cells and T98G glioblastoma cells were obtained from ATCC (Bethesda, Maryland, USA) and were routinely tested for mycoplasma. NCI-H460, DU145 or T98G cells with tolerance to cycling severe hypoxia/re-oxygenation stress were generated by exposure to 16 cycles (T98G) or 25 cycles (NCI-H460, DU145) of severe hypoxia (48 h, < 0.1% O_2) and re-oxygenation (120 h air plus 5% CO_2 referred as 20% O_2) as described earlier [9]. These hypoxia/reoxygenation-tolerant cells are termed "anoxia-tolerant cells" throughout the manuscript. Control cells were cultured in parallel under standard ambient O_2 conditions (20% O_2 plus 5% CO_2; the control cells are termed "oxic cells" throughout the manuscript) [9,12,27]. Upon selection, cancer cells were routinely grown in RPMI 1640 medium. supplemented with 10% (v/v) fetal calf serum (Gibco/Life Technologies, Carlsbad, CA, USA) and maintained in a humidified incubator at 37 °C and 5% CO_2 (referred to as "normoxia" or "normoxic conditions", Nx). For severely hypoxic conditions cells were grown in a humidified hypoxia work station (In vivo 400, Ruskinn Technology Ltd., Bridgend, Great Britain) at 37 °C, 0.2% O_2, and 5% CO_2 (referred to as "hypoxia" or "hypoxic conditions", Hx).

2.2. Patient survival data

Patient array data were obtained from and analyzed by Kaplan Meier-plotter tool (kmplot.com) as described elsewhere [28,29]. The cohort was split by median of *SLC25A10* or *SLC25A11*-expression ("High" and "Low", respectively). Analysis was performed in the cohort without additional restrictions including lung cancer or breast cancer patients as described in detail elsewhere [28,29]. For further details of used settings please refer to Supplementary Tables 1–4.

2.3. qRT-PCR analysis

cDNA was synthesized from 1 µg of total RNA using QuantiTect Reverse Transcription Kit (Qiagen, Hilden, Germany) according to the manufacturer's protocol. Specific primers were synthesized based on available sequences for each mentioned gene. Primer sets were designed with the Blast web tool (U.S. National Centre for Biotechnology Information, Bethesda, MD, USA). PCR products were 150–200 bp in size. We used published β2-microglobulin (B2M) primer sequences as housekeeping gene [30]. qRT–PCR and cycling conditions were performed using specific oligonucleotide primers (*B2M* forward: TGCTGT CTCCATGTTTGATGTATCT; reverse: TCTCTGCTCCCCACCTCTAAGT; *SLC25A10* forward: CAGGAGACTGTTCTCGGGTG; reverse: GTCACCA GCGGCTGCAATA; *SLC25A11* forward: CCCTAAGTCCGTCAAGTTC CTG; reverse: GCCCAGTGTAAATGCCCCTC) and using qPCR kit for SYBR® Green I, 6-Carboxyl-X-Rhodamine (ROX) (Eurogentec, Cologne, Germany) according to the manufacturer's protocol. Reactions were carried out on an ABI Prism 7900HT using MicroAmp Optical 384 well Reaction plates (Applied Biosystems by Life Technologies, Bleijswijk, Netherlands) and BIO-RAD PCR Sealers Microseal "B" Film Adhesive seal (optically clear; BIO-RAD, Munich, Germany). Melting curves were obtained after each PCR run and showed single PCR products. cDNAs were run in triplicate, without reverse transcriptase and no-template controls were run in duplicates. Expression ratios were calculated using the geometric mean expression of the housekeeping gene B2M to normalize the expression data for the genes of interest according to the $2^{-\Delta\Delta Ct}$ -method as described by others [31].

2.4. Western blot analysis

Anti-mouse SLC25A10 monoclonal antibody (EMD Millipore Corporation, Temecula, CA, USA), anti-mouse SLC25A11 monoclonal antibody (Santa Cruz Biotechnology, Dallas, TX, USA) and anti-mouse ß-actin from Sigma Aldrich (St. Louis, MO, USA) were used for Western blot analysis. After harvesting, cells were lysed in 75 µl of RIPA buffer as described previously [12]. Protein was separated by 12% sodium dodecyl sulfate polyacrylamide gel electrophoresis (SDS-PAGE) under reducing conditions and transferred onto polyvinylidene fluoride (PVDF) membranes (Roth, Karlsruhe, Germany). Blots were blocked in RotiBlock (Roth, Karlsruhe, Germany) for 1 h at room temperature. The membranes were incubated overnight at 4 °C with the respective primary antibodies. The secondary antibody was incubated for 1 h at room

temperature. Detection of antibody binding was performed by enhanced chemiluminescence (ECL Western Blotting Analysis System; GE Healthcare/Amersham Biosciences, Freiburg, Germany). Densitometry analysis was performed using ImageJ 2.00 (National Institutes of Health, Bethesda, MD, USA).

2.5. Animal experiments

Animal experiments were conducted according to the German animal welfare regulations and approved by the local authorities (registration number Az. 84–02.04.2013.A092; Az. 84–02.04.2014.A481). Immunodeficient NMRI (nu/nu) nude mice were purchased from the University Hospital Essen (age 6–12 weeks). Animals were housed in an individually ventilated cage rack system (Techniplast, West Chester, PA, USA) and fed with sterile high calorie laboratory food (Sniff, Soest, Germany). Xenograft tumors of anoxia-tolerant NCI-H460 cells were generated by a subcutaneous injection of 5×10^5 cells in 50 µl RPMI mixed with 50% matrigel (growth factor reduced Matrigel Matrix, Corning, Tewksbury, MA, USA) into the right hind leg. Mice were randomly allocated to the following different treatment groups (7 mice/group) when the tumor volume reached 80–100 mm^3 (about 4 days after inoculation): i) control (sham irradiation); ii) irradiation with a single dose 5 Gy (day 4); iii) BMA treatment (25 mg/kg dissolved in PBS) 5 times every second day (day 4 - day 12); iv) combined treatment with 5 Gy day 4 plus 5 × 25 mg/kg BMA every second day (day 4 - day 12). On the first of day of treatment (day 4) BMA was given 2 h before irradiation via intraperitoneal injection in a total volume of 50 µl (Fig. 6A). PBS was used as a solvent control. For radiation therapy mice were anesthetized (2% isoflurane) and tumors were exposed to a single dose of 5 Gy ± 5% in 5 mm tissue depth (~1.53 Gy/min, 300 kV, filter: 0.5 mm Cu, 10 mA, focus distance: 60 cm) using a collimated beam (field size: 25 × 13 mm) with a XStrahl RS 320 cabinet irradiator (XStrahl Limited, Camberly, Surrey, Great Britain). 1 h before euthanization, 60 mg/kg pimonidazole hydrochloride (Hydroxyprobe, Burlington, MA, USA) was injected intraperitoneal to 5 control and BMA-treated mice for immunohistochemistry.

2.6. Immunohistochemistry

For immunostaining of SLC25A10 and pimonidazole using the Mouse on Mouse (M.O.M.™) ImmPRESS™ HRP (Peroxidase) Polymer Kit (Vector Laboratories, Burlingame, USA), tissue slides of NCI-H460 anoxia-tolerant xenograft tumors (n = 5 each) were deparaffinised, rehydrated and steam boiled in citrate buffer with pH 6. Endogenous peroxidase was blocked with BLOXALL (Vector Laboratories, Burlingame, USA) for 10min. Slides were blocked for 1 h using M.O.M. Ig blocking reagent (Vector Laboratories, Burlingame, USA) and subsequently incubated overnight at 4 °C with anti-mouse SLC25A10 monoclonal antibody (EMD Millipore Corporation, Temecula, CA, USA) or anti-mouse Hypoxyprobe™ Mab-1 antibody for detection of pimonidazole (Hydroxyprobe, Burlington, MA, USA). Primary antibodies were detected by secondary antibodies linked to horseradish peroxidase and subsequent diaminobenzidine (DAB) staining, including negative controls without primary antibody for each animal. Nuclei were counterstained using haematoxylin.

Additionally, tumor tissue slides were stained with haematoxylin and eosin (H&E) (Roth, Karlsruhe, Germany).

Slides were then analyzed microscopically and pictures of corresponding regions (oxygenated and hypoxic) were taken with a 10× objective. Semi-quantification of DAB-stained slides was performed by using Fiji [32]. ΔIntensity (DAB) as indicated in Fig. 6D of each staining was calculated by subtraction of intensity (DAB) of respective negative control region.

2.7. Transfections, irradiation and treatment

To achieve downregulation of SLC25A10 or SLC25A11 on protein level, cells were transfected with 45 nm siRNA pools targeting SLC25A10, SLC25A11, or non-targeting controls (SMARTpool: ON-TARGETplus, Dharmacon/Horizon Discovery, Cambridge, UK) with 3 µl TransIT-siQUEST (Mirus Bio, Madison, WI, USA) and 100 µl optiMEM (Gibco/Life Technologies, Carlsbad, CA, USA) for 24 h in 1 ml total reaction volume, followed by medium exchange according to manufacturer's protocols. 48 h after start of transfection, sufficient protein downregulation was achieved and additional treatments (e.g. irradiation) were performed.

Irradiation was performed at room temperature with an X-ray machine (Precision X-Ray Inc., North Branford, CT) operated at 320 kV, 12.5 mA with a 1.65 mm Al filter, at a distance of 50 cm and a dose rate of 3.71 Gy/min. Cells were returned to the incubator immediately after exposure to IR. For irradiation under hypoxic conditions, hypoxic cell dishes were kept in BD GasPak EZ Pouch System (Becton Dickinson, Heidelberg, Germany).

BMA and PSA were purchased from Sigma-Aldrich (St. Louis, MO, USA). GSH-Ethylester (GEE) and MitoTempo (MT) were purchased from Cayman Chemical (Ann Arbor, MI, USA). For rescue experiments of mROS induction or clonogenic survival, cells were pretreated with GEE or MT for 2 h before addition of BMA or PSA. In terms of combined treatments of inhibition and irradiation, BMA or PSA were added 2 h prior to irradiation.

2.8. Determination of redox homeostasis

NADH levels were measured using NADH Glo Assay (Promega, Madison, WI, USA) according to manufacturer's protocol. Briefly, adherent cells in 96 well plates were lysed and heated under acidic and basic conditions to measure NAD^+ and NADH individually using a luciferase-coupled enzymatic reaction. In parallel, technical replicates were fixed with 4% paraformaldehyde and stained with 10 µg/ml solution of fluorescent dye Hoechst 33342 (Thermo Scientific, Waltham, MA, USA) for normalization to DNA content. Luminescence and fluorescence were measured in triplicates using a BioTek Synergy Microplate reader (BioTek, Winooski, NH, USA).

Levels of reduced Glutathione (GSH) were determined by using monochlorobimane (MCB) which was described to be specific for GSH metabolized by Glutathione-S-transferase, leading to a fluorescent adduct [33]. Intensity of GSH-fluorescence was measured with a BioTek Synergy Microplate reader (BioTek, Winooski, NH, USA) using 10 µM MCB with 15 min of pre-incubation as described previously [12].

To quantify mitochondrial ROS production, cells were stained for 30 min at 37 °C with 5 µM of MitoSox (Molecular Probes/Invitrogen, Carlsbad, CA USA). To quantify cellular ROS production, cells were stained for 30 min at 37 °C with 5 µM of Dihydroethidium (DHE) (Molecular Probes/Invitrogen, Carlsbad, CA USA). MitoSox- or DHE-positive cells were detected by flow cytometry (BD FACS Calibur, Becton Dickinson, Heidelberg, Germany; FL-2). Fractions of gated positive cells (at least 10.000) with higher fluorescence were evaluated.

2.9. Determination of mitochondrial glutathione

For measurement of mGSH, cells in tissue flasks were pretreated with potential mGSH inhibitors BMA (8 mM) or PSA (8 mM) for 2 h. After harvesting, mitochondria of 3×10^7 cells were isolated using Mitochondria Isolation Kit for Mammalian Cells (Thermo Scientific, Waltham, MA, USA) according to manufacturer's protocol (reagent-based method). Mitochondria were resuspended in a protective buffer containing 220 mM mannitol, 70 mM sucrose, 10 mM KH_2PO_4, 10 mM pyruvate, 10 mM malate, 5 mM $MgCl_2$, 4 mM ADP, 2 mM HEPES, 1 mM EGTA and 0,6% fatty acid free BSA. Since the use of fluorescent dye monochlorobimane (MCB) has been demonstrated to be suitable to

measure mGSH [34,35], isolated mitochondria were transferred to 96-well plates and incubated with 10 µM MCB and 1U/ml Glutathione-S-transferase for 30 min at 37 °C. Intensity of mGSH-fluorescence was measured with a BioTek Synergy Microplate reader (BioTek, Winooski, NH, USA).

2.10. Extracellular flux analysis

NCI-H460 cells were plated at 7.500 cells/well in XF96 microplates (Seahorse Bioscience, Billerica, MA, USA) in RPMI Medium with 10% FCS according to manufacturer's recommendations 48 h prior to the assay. Treatment with 8 mM BMA was performed for 24 h.

For Mito Stress Test, medium was exchanged to XF base medium (Seahorse Bioscience, Billerica, MA, USA) with 1 mM Pyruvate, 2 mM Glutamine and 10 mM Glucose and incubated at 37 °C without CO_2 1 h prior to the assay. During assay, OCR was measured using a Seahorse XFe 96 analyzer. Mito Stress Test Kit containing 1 µM Oligomycin, 2 µM Carbonyl cyanide-4-(trifluoromethoxy)phenylhydrazone (FCCP), 0,5 µM Rotenone and 0,5 µM Antimycin A was performed according to manufacturer's protocol.

For Glycolytic Rate Assay, medium was exchanged to XF base medium without phenol red (Seahorse Bioscience, Billerica, MA, USA) with 2 mM glutamine, 10 mM glucose, 1 mM pyruvate, and 5 mM HEPES and incubated at 37 °C without CO_2 1 h prior to the assay. During assay, ECAR was measured using a Seahorse XFe 96 analyzer. Glycolytic Rate Assay Kit containing 0,5 µM Rotenone, 0,5 µM Antimycin A and 50 mM 2-Desoxyglucose was performed according to manufacturer's protocol. PER was calculated by Wave 2.6 (Seahorse Bioscience, Billerica, MA, USA) software after the assay.

For individual normalization to DNA content, fluorescence was measured after cells were fixed with 4% PFA and stained with 10 µg/ml Hoechst 33342 solution after each assay. Data were analyzed using Wave 2.6 software.

2.11. Colony formation assays

Clonogenic cell survival in response to the respective treatments was determined comparing the clonogenic survival of cells cultured under normoxic and severely hypoxic conditions. For treatment in normoxia, exponentially growing cells were seeded in tissue culture flasks, incubated under standard culturing conditions (20% O_2, 5% CO_2, 37 °C) and irradiated 24 h later (0–5 Gy) without or with prior BMA (8 mM) or PSA (8 mM) treatment. BMA or PSA treatment was performed 2 h prior to irradiation. For treatment in hypoxia, tissue culture flasks of exponentially growing cells were exposed to severe hypoxia (0.2% O_2) 2 h prior to BMA or PSA treatment and 4 h prior to irradiation, respectively. After completion of the treatments, cells were incubated for 24 h under normoxic or hypoxic conditions, then washed, collected (0.05% Trypsin, 0.01 EDTA), and plated to 6 well plates at densities of 200–3200 cells per well in inhibitor-free media (delayed plating). The cell viability was checked before plating the cells by using CASY COUNT (Omni Life Science, Bremen, Germany) and only the number of viable cells were used for the calculation of necessary cell numbers for plating. Plates were subsequently incubated for 9 days under standard normoxic conditions before quantification of colony formation. For this, cells were fixed in 3.7% formaldehyde and 70% ethanol, stained with 0.05% Coomassie blue, and colonies of at least 50 cells were counted by GelCount (Oxford Optronix, Oxfordshire, Great Britain). The plating efficiency and surviving fraction (SF) to corresponding normoxic and hypoxic controls were calculated as described elsewhere [36].

2.12. Short term cell death and proliferation assays

The fraction of dead cells was quantified by flow cytometry (FACS Calibur, Becton Dickinson Heidelberg, Germany; FL-2) of PI–stained cells. Cells were incubated for 30 min in the dark with PI (10 µg/ml) in PBS and measured within 1 h. Fractions of gated positive cells (at least 10.000) with higher fluorescence were evaluated.

For quantification of apoptotic DNA-fragmentation (sub-G1 population) of gated positive cells (at least 10.000), cells were incubated for 30 min in the dark with a staining solution containing 50 µg/ml PI in a hypotonic citrate buffer 0.1% sodium citrate and 0.05% Triton X-100 and subsequently analyzed by flow cytometry (FACS Calibur, Becton Dickinson, Heidelberg, Germany; FL-2) [37].

For determination of cell proliferation and viability, cells were washed with PBS (1×), fixed with Glutaraldehyde (0.1% in PBS), and stained with crystal violet (0.1% in PBS). The dye was released by TritonX-100 (0.2% in PBS) and measured spectrophotometrically at 540 nm as described elsewhere [27].

2.13. Statistics

Data represent mean values of at least 3 independent experiments ± standard error of mean (SEM) except for Fig. 5A and B which shows data from n = 12–18 wells from 2 independent experiments.

Data analysis was performed by two-way ANOVA test using parametric methods and employing Tukey multiple comparison post-test where appropriate or by unpaired Student's t-test using Prism6 software (Graph Pad Inc., La Jolla, USA). If not indicated differently, asterisks above bars refer to comparison with corresponding controls. P-values ≤ 0.05 were considered significant, P-values > 0.05 as not significant (ns).

3. Results

3.1. Exposure to chronic-cycling hypoxia induces expression of SLC25A10 but not SLC25A11 and correlates with reduced overall survival in cancer patients

To investigate a potential role of SLC25A10 or SLC25A11 in adaptation to chronic-cycling hypoxia we first analyzed expression of SLC25A10 and SLC25A11 on the mRNA level using our established models of so-called "anoxia-tolerant" cancer cell lines that had been generated by exposure to up to 25 cycles of severe hypoxia (48 h) followed by intermittent reoxygenation (120 h) [9]. These anoxia-tolerant cancer cells are characterized by increased resistance to stimuli of the intrinsic apoptosis pathway including genotoxic chemotherapy or radiotherapy, when compared to the non-selected control cells, termed "oxic" control cells, as described earlier [9,27,38].

Our data indicate an up-regulation of *SLC25A10* mRNA-expression in all three investigated anoxia-tolerant cancer cell lines compared to oxic control cells (Fig. 1A: NCI-H460, NSCLC; Fig. 1B: DU145, prostate cancer; Fig. 1C T98G, glioblastoma). Instead, *SLC25A11* mRNA-expression did not differ between the three examined anoxia-tolerant cells and the respective oxic control cells. Furthermore, we confirmed increased expression of SLC25A10 and no changes in SLC25A11 expression in anoxia-tolerant NCI-H460 cells on the protein level (Fig. 1D).

To gain insight into a potential clinical relevance of our findings for cellular adaptation mechanisms contributing to cancer therapy resistance, we additionally performed an *in silico* analysis of publically available datasets using the Kaplan Meier Plotter tool (kmplot.com [28,29]). The parameters of our *in silico* analysis are given in Supplementary Tables 1–4. In line with our *in vitro* findings, these *in silico* analyses revealed an association of *SLC25A10*-overexpression on the mRNA level with reduced overall survival in patients suffering from lung cancer (Fig. 1E) or breast cancer (Fig. 1G), respectively. In contrast, no such association could be detected when analysing *SLC25A11* overexpression (Fig. 1F and H). Furthermore, when comparing the expression levels of *SLC25A10* and *SLC25A11* between cancer and normal tissues, we found that *SLC25A10* was overexpressed in all tumor types examined by the tool, whereas *SLC25A11* revealed a divergent

expression pattern and even lower expression in lung cancer tissue compared to normal lung tissue (Fig. 1I).

Altogether these findings pointed to a higher relevance of SLC25A10 for both, anoxia tolerance *in vitro* and overall survival of lung cancer patients in the clinical situation. On the basis of the results from our *in vitro* and *in silico* investigations, we decided to focus on SLC25A10 in our further experiments and to perform our mechanistic studies mainly in our NCI-H460 NSCLC cell model.

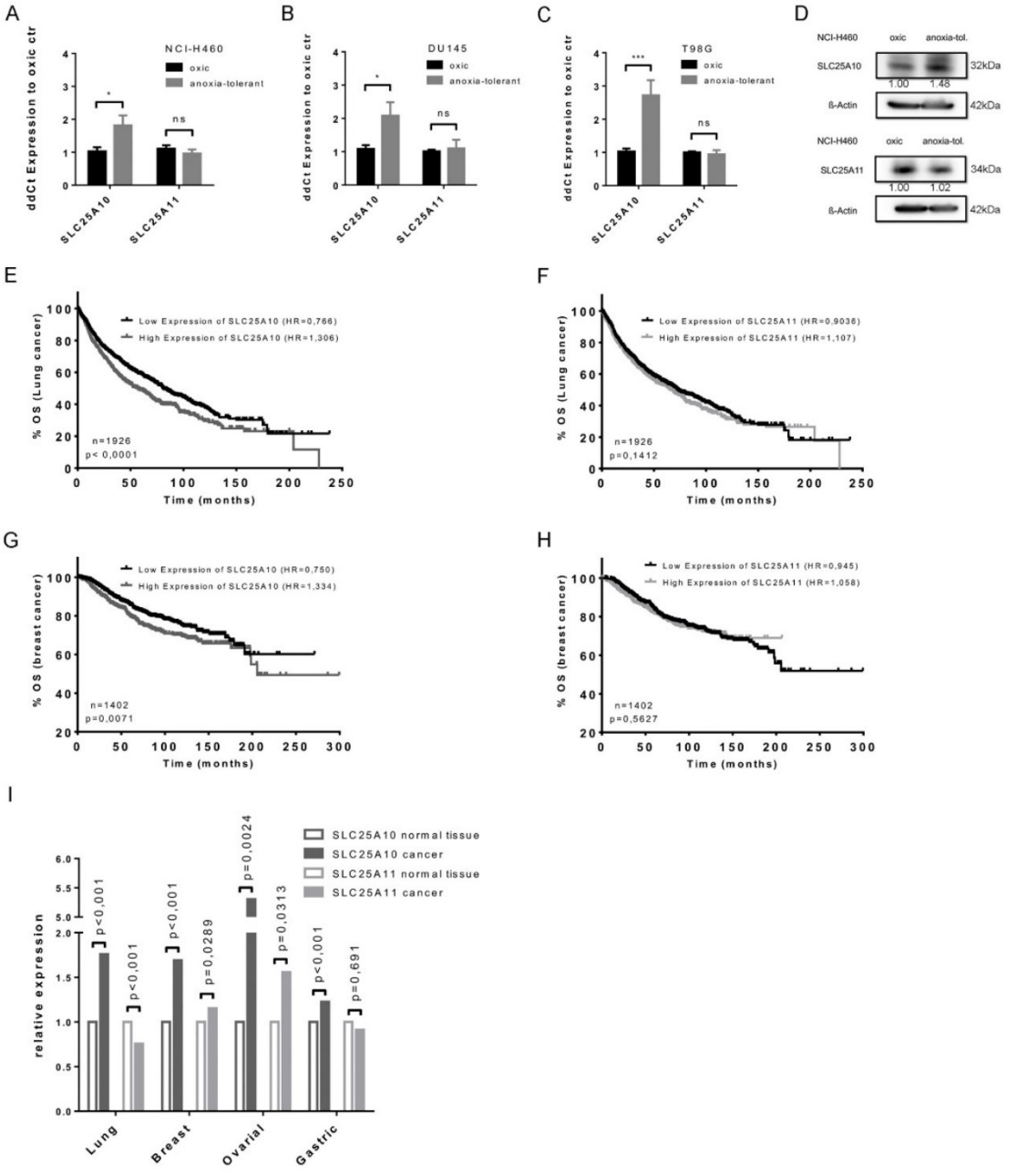

(caption on next page)

Fig. 1. Elevated expression of SLC25A10 but not SCL25A11 is indicated after chronic-cycling hypoxia selection *in vitro* and leads to lowered cancer patient overall survival.
Basal expression of SLC25A10 and SLC25A11 was determined in cancer cells with tolerance to chronic-cycling hypoxia (anoxia-tolerant) and respective oxic control cells. **A)** qRT-PCR analysis of *SLC25A10* and *SLC25A11* expression normalized to oxic control (ctrl) in NCI-H460 cells. **B)** qRT-PCR analysis of *SLC25A10* and *SLC25A11* expression normalized to oxic control (ctrl) in DU145 cells. **C)** qRT-PCR analysis of *SLC25A10* and *SLC25A11* expression normalized to oxic control (ctrl) in T98G cells. **D)** Western blot analysis of SLC25A10 and SLC25A11 protein expression in NCI-H460 cells. Relative quantification is depicted with numbers under the appropriate protein band. Mean values ± SEM are shown, n = 3–4 (*p ≤ 0.05, ***p ≤ 0.001; *t*-test).
Association between gene expression and overall survival (OS) of cancer patients and comparison between cancer and normal tissue expression was analyzed with the Kaplan Meier Plotter (kmplot.com). **E)** OS in lung cancer patients with different SLC25A10 expression levels. **F)** OS in lung cancer patients with different SLC25A11 expression levels. **G)** OS in breast cancer patients with different SLC25A10 expression levels. **H)** OS in breast cancer patients with different SLC25A11 expression levels. **I)** Comparison of SLC25A10 or SLC25A11 expression between cancer and normal tissue in lung, breast, ovarial or gastric cancer. For the analysis the cohort was split by median of gene expression ("High" and "Low"). Hazard ratio (HR) and number of patients (n) is indicated for each survival curve.

3.2. Genetic and pharmacologic inhibition of SLC25A10 counteract increased radioresistance induced by adaptation of cancer cells to chronic-cycling hypoxia

Next, we aimed to explore if genetic or pharmacologic SLC25A10-inhibition would affect survival of cancer cells when given alone or in combination with ionizing radiation (IR) (single dose irradiation with 10 Gy) in short-term assays. Knockdown of SLC25A10 by using an RNAi-approach (Fig. 2A) as well as pharmacological SLC25A10-inhibition using 8 mM butylmalonate (BMA [26,39]; Fig. 2C) induced cell death within 72 h after treatment with higher potency to the anoxia-tolerant than the oxic control cells. Effective reduction of SLC25A10 expression in NCI-H460 cells is shown in Fig. 2B. The above BMA working-concentration had been established by determination of the IC_{50} values on the basis of the drug effects on cell proliferation/viability monitored by crystal violet assay which amounted to 8–11 mM in all oxic and anoxia-tolerant cell lines (Suppl. Fig. 1A).

As expected, the cytotoxic effect of IR alone was always lower in the anoxia-tolerant cells compared to the oxic controls confirming reduced sensitivity of the anoxia-tolerant cancer cells to the cytotoxic effects of IR observed earlier. However, combined treatment of NCI-H460 lung cancer cells with BMA and IR significantly increased the sensitivity to the cytotoxic effects of IR (Fig. 2C). Of note, the combination effect was more pronounced in anoxia-tolerant NCI-H460 cells than in oxic control cells pointing to a relevance of SLC25A10 for the enhanced protection against radiation-induced cell death in these cells (Fig. 2A and C). Similar observations were made when treating oxic and anoxia-tolerant DU145 prostate cancer or T98G glioblastoma cells with BMA, IR or in combination (Fig. 2D). Moreover, combination of IR with a dose of 5Gy and BMA-treatment significantly reduced the cell proliferation/viability of both NCI-H460 cell lines compared to the single IR-treatment (Suppl. Fig. 1D and E). The obtained results confirm the data obtained using determination of cell death by flow cytometry (% of PI-positive cells, Fig. 2C) that pre-treatment of BMA is particularly suited to increase the antineoplastic action of ionizing radiation in anoxia-tolerant cells.

To evaluate if drug-treatment was also effective in reducing the survival of clonogenic tumor cells we next performed standard long-term colony formation assays (see treatment schedule, Fig. 2E). Our results indicated that inhibition of SLC25A10 by BMA alone reduced clonogenic survival particularly in anoxia-tolerant cells whereas exposure to IR alone was more effective in reducing the survival of clonogenic oxic control cells (Fig. 2F). Importantly, the combination of BMA and IR sensitized both, oxic and anoxia-tolerant cells, to the cytotoxic action of IR and even to counteract increased radioresistance of the anoxia-tolerant NCI-H460 cells (Fig. 2F). Thereby the long-term colony formation assays corroborated the initial observation from the short-term survival assays.

Next, we explored if BMA was also effective when treatment was performed in acute severe hypoxia (Hx, 0.2% O_2). Of note, BMA reduced clonogenic survival of NCI-H460 cells when treatment was performed in acute Hx, particularly in the anoxia-tolerant NCI-H460 cells (Suppl. Fig. 2A and B). Moreover, BMA effectively increased the radiation-induced eradication of clonogenic NCI-H460 cells; BMA-mediated radiosensitization was even enhanced when compared to treatment in normoxia, especially in the anoxia-tolerant NCI-H460 cells (Suppl. Fig. 2C and D).

Though SLC25A11 had not been associated with anoxia-tolerance or poor patient survival, we also studied potential consequences of genetic or pharmacologic SLC25A11 inhibition for cell survival and radiosensitivity, as SLC25A11 had been linked to mGSH uptake. Pharmacologic inhibition of the alternatively assumed mGSH carrier SLC25A11 using phenylsuccinate (PSA) effectively decreased mGSH levels (Suppl. Fig. 1C). Moreover, pre-treatment of the cancer cells with the mROS-scavenger MitoTempo (MT) or with glutathione-ethylester (GEE) also rescued these cells from PSA-induced mROS and clonogenic death (Suppl. Fig. 3E and F). Importantly, RNAi-mediated SLC25A11-downregulation (Suppl. Fig. 3A) or pharmacological inhibition using 8 mM phenylsuccinate (PSA [25,26]) increased radiation-induced death of oxic and anoxia-tolerant NCI-H460 cells, but was not able to overcome increased resistance of the anoxia-tolerant NCI-H460 cells to IR-induced cell death (Suppl. Fig. 3B and C). In addition, PSA-mediated inhibition of SLC25A11 did not counteract the increased radioresistance of the anoxia-tolerant NCI-H460 cells in long-term colony formation assays (Suppl. Fig. 3D). These findings suggest that SLC25A11 might not be critical to radiation resistance of NCI-H460 cells acquired during adaptation to chronic-cycling hypoxia and thus not be a favourable target for their treatment.

Accordingly, comparing inhibitory drug concentrations by using crystal violet assay revealed overall comparable antineoplastic effects of BMA and PSA (Suppl. Fig. 1A and B). The IC_{50} values for BMA and PSA amounted to approximately 8–11 mM for all cell lines used without significant differences between the oxic and anoxia-tolerant cells (Suppl. Fig. 1A and B).

3.3. SLC25A10 sustains improved antioxidant capacity of anoxia-tolerant cancer cells

The observation that SLC25A10 might participate in the import of GSH into the mitochondrial matrix, prompted us to investigate the influence of pharmacological inhibition of SLC25A10 on various parameters of cellular and mitochondrial redox homeostasis. BMA-treatment decreased cellular levels of reduced GSH in oxic and anoxia-tolerant NCI-H460 cells, though the effect was more pronounced in the anoxia-tolerant cells (Fig. 3A–C). Similarly, BMA treatment increased cellular ROS levels to a higher extent in the anoxia-tolerant NCI-H460 cells than in oxic control cells (Fig. 3D and E). Finally, we observed that pharmacologic inhibition of SLC25A10 also increased mitochondrial ROS (mROS) formation, and this effect was again more pronounced in the anoxia-tolerant NCI-H460 cells (Fig. 3F and G). BMA-treatment had always a more pronounced effect on cellular and mitochondrial ROS-levels in the anoxia-tolerant cell variants of all examined cell lines when evaluated as fold-changes (Fig. 3E and G and Suppl. Fig. 5 for original data).

To corroborate our findings about the BMA-effects at the level of SLC25A10 we additionally repeated the above experiments with a genetic approach using RNAi-mediated SLC25A10 down-regulation. As

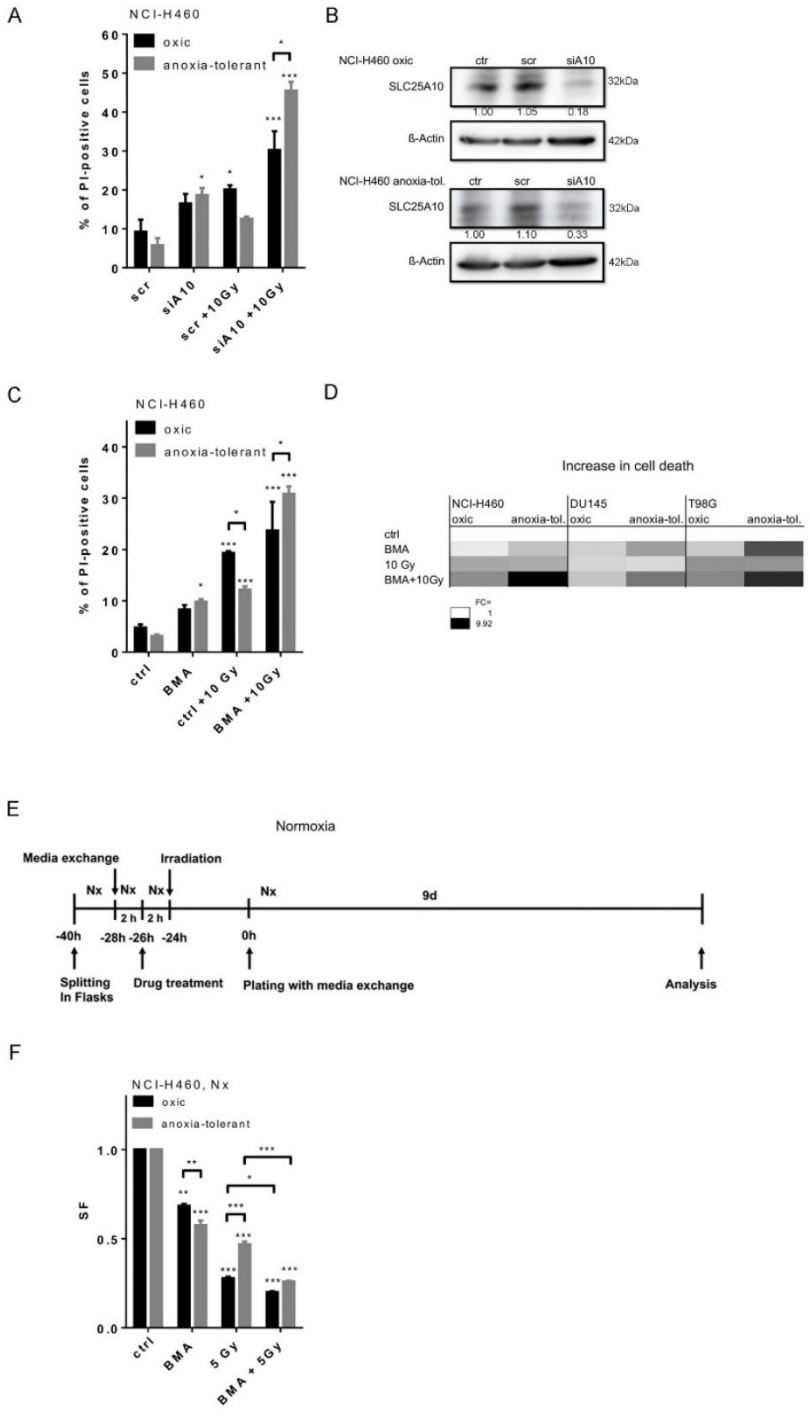

Fig. 2. Targeting of SLC25A10 overcomes chronic-cycling hypoxia induced radioresistance.
Impact of SLC25A10 genetic knockdown by RNAi (siA10) or inhibition by BMA (8 mM) alone or in combination with exposure to ionizing radiation (IR; 5–10Gy) on cell death and clonogenic survival was examined. **A)** Fraction of dead cells 72 h after knockdown of SLC25A10 by RNAi with or without IR determined by flow cytometry. **B)** Western blots indicate SLC25A10 protein downregulation 48 h after start of transfection at the timepoint of IR. Relative quantification is depicted with numbers under the appropriate protein band. **C)** Bar graph indicates fraction of dead cells 72 h after BMA-mediated inhibition of SLC25A10 with or without IR determined by flow cytometry in NCI-H460 oxic and anoxia-tolerant cells. **D)** Heat maps indicate fold change (FC) of cell death induction in NCI-H460, DU145 or T98G oxic and anoxia-tolerant cells calculated to respective controls (ctrl). Bar graphs with measured % of PI-positive oxic and anoxia-tolerant DU145 and T98G cells can be found in Suppl. Fig. 5. **E)** Schematic representation of the experimental timeline in normoxia (Nx). **F)** Survival fraction (SF) of clonogenic survival of NCI-H460 oxic and anoxia-tolerant cells upon BMA-treatment and IR with 5Gy under normoxic (Nx, 21% O_2) conditions is presented in a bar graph. 24 h after treatment cells were collected and plated at different cell numbers in full medium without the inhibitor and grown under Nx for 9 days.
Mean values ± SEM are shown, n = 3–5 (*p ≤ 0.05, **p ≤ 0.01, ***p ≤ 0.001; 2-way ANOVA with Tukey post-test).

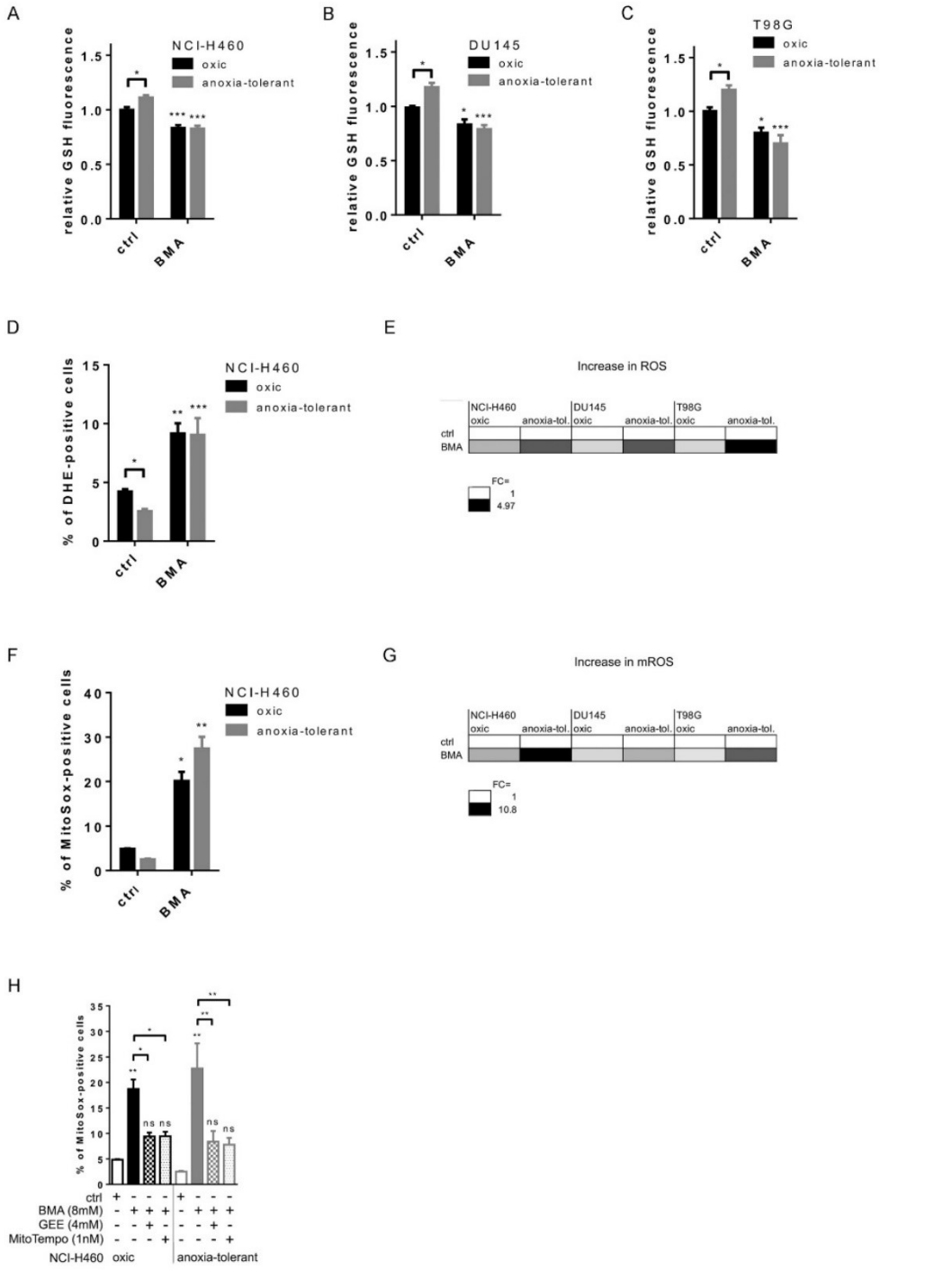

(caption on next page)

Fig. 3. SLC25A10 sustains improved antioxidant capacity of anoxia-tolerant cancer cells.
Impact of SLC25A10-inhibition with 8 mM BMA on antioxidant capacity and ROS formation of oxic and anoxia-tolerant cells. **A)-C)** Relative levels of reduced glutathione (GSH) after 2 h of BMA-treatment. Bar graph indicates GSH levels relative to untreated oxic control in NCI-H460 **(A)**, DU145 **(B)** or T98G **(C)** oxic and anoxia-tolerant cells. **D)** Fraction of DHE-positive cells stained for cellular ROS determined by flow cytometry in NCI-H460 oxic and anoxia-tolerant cells after 24 h of BMA-treatment. **E)** Fold change of ROS induction (DHE-positive cells determined by flow cytometry) in NCI-H460, DU145 or T98G oxic and anoxia-tolerant cells after 24 h of BMA-treatment calculated to the corresponding untreated control. Bar graphs with measured % of DHE-positive oxic and anoxia-tolerant DU145 and T98G cells can be found in Suppl. Fig. 5C and D. **F)** Fraction of MitoSox-positive cells stained for mitochondrial (m) ROS determined by flow cytometry in NCI-H460 oxic and anoxia-tolerant cells after 24 h of BMA-treatment. **G)** Fold change of mROS induction (MitoSox-positive cells determined by flow cytometry) in NCI-H460, DU145 or T98G oxic and anoxia-tolerant cells after 24 h of BMA-treatment represented in a color coded heat map. Bar graphs with measured % of MitoSox-positive oxic and anoxia-tolerant DU145 and T98G cells can be found in Suppl. Fig. 5A and B. **H)** Rescue of BMA-mediated mROS-induction (fraction of MitoSox-positive cells determined by flow cytometry) after 24 h by 2 h additional pre-treatment with 4 mM cell- and mitochondria-permeable glutathione-ethylester (GEE) or 1 nM mitochondrial ROS scavenger Mito Tempo (MT) in NCI-H460 oxic and anoxia-tolerant cells.
Mean values ± SEM are shown, n = 3–4 (*p ≤ 0.05, **p ≤ 0.01, ***p ≤ 0.001; 2-way ANOVA with Tukey post-test).

shown in Suppl. Fig. 3 we could confirm the enhanced effect of SLC25A10-inhibition on cellular ROS and mROS formation in anoxia-tolerant NCI-H460 cells by using siRNA (Suppl. Fig. 4).

To prove that the BMA-mediated increase of mROS but also associated decrease of mGSH (Suppl. Fig. 1C) is directly caused and not a secondary consequence of toxic side effects of the drug, we verified if we could rescue the cells from mROS increase by abrogation of BMA-induced mROS formation using either mROS-scavenger MitoTempo (MT) or by artificially increasing cellular and mitochondrial GSH levels using cell- and mitochondria-permeable glutathione-ethylester (GEE). As indicated in Fig. 3H and 2 h pre-treatment and presence of MT or GEE significantly decreased BMA-mediated mROS-induction within 24 h in both oxic and anoxia-tolerant NCI-H460 cells. Of note, treatment with GEE or MT alone did not alter mROS levels (data not shown).

3.4. SLC25A10 sustains improved death resistance of anoxia-tolerant cancer cells

Considering the initial observation that genetic or pharmacologic inhibition of SLC25A10 increases cell death (Fig. 2A and C; Suppl. Fig. 4D and E), we investigated the influence of SLC25A10-targeting on the induction of apoptosis after 72 h. Both, BMA-treatment (Fig. 4A) and RNAi-mediated SLC25A10-knockdown (Suppl. Fig. 4C) significantly increased apoptotic cell death in anoxia-tolerant NCI-H460 cells as revealed by increased subG1 fraction (Fig. 4A and B). Again, the more pronounced effects on apoptosis induction was also present in DU145 and T98G anoxia-tolerant cancer cells, hinting to a broader relevance of our findings (Fig. 4B).

Remarkably, cell death induction upon BMA-treatment (Suppl. Fig. 2A and B) or SLC25A10-targeting by RNAi (Suppl. Fig. 4 E) was enhanced in acute Hx compared to the appropriate normoxic condition. Of note, a more pronounced effect to anoxia-tolerant cells was observed (Suppl. Fig. 2B).

Importantly, BMA-mediated reduction in long-term clonogenic survival of oxic and anoxia-tolerant NCI-H460 cells was rescued by pre-treating cells either with the mROS-scavenger MitoTempo (MT) or with cell- and mitochondria-permeable glutathione-ethylester (GEE) (Fig. 4C). These results confirm that the radiosensitizing effect of BMA-treatment is indeed due to BMA-mediated disturbance of cellular GSH or mGSH causing an increase in mROS. Of note, the GEE/MT-mediated rescue of clonogenic survival was even more effective in anoxia-tolerant cells with higher SLC25A10 expression than in oxic control cells (Fig. 4C).

3.5. Inhibition of SLC25A10 lowers energy metabolism particularly in anoxia-tolerant cancer cells

SLC25A10 is a carrier for dicarboxylates such as malate or succinate [39], and thus plays a role in energy metabolism besides its assumed function in the maintenance of redox homeostasis. To explore a potential impact of SLC25A10-inhibition on cell metabolism we compared the effect of hypoxic selection and BMA-treatment on parameters of mitochondrial respiration using Seahorse technology. As shown in Fig. 5A basal respiration, ATP-production and spare respiratory capacity were slightly enhanced in NCI-H460 anoxia-tolerant cells (Fig. 5A, right panel) in comparison to the respective oxic control cells (Fig. 5A, middle panel), in line with our previous findings [12]. BMA-treatment for 24 h led to decreased parameters of mitochondrial respiration, in particular spare respiratory capacity, especially in anoxia-tolerant cells (Fig. 5A, left panel). Herein, spare respiratory capacity considers the maximal possible increase in respiration after uncoupling of the electron transport chain (ETC).

To examine whether this reduction of mitochondrial respiration and ATP-production is compensated by increased anaerobic glycolysis, we next examined glycolytic activity after BMA-treatment (Fig. 5B). Again, anoxia-tolerant NCI-H460 cells (Fig. 5B, right panel) displayed slightly enhanced basal and compensatory glycolytic rate when compared to oxic control cells (Fig. 5B, middle panel). BMA-treatment for 24 h reduced basal and compensatory glycolytic rates in both cell lines (Fig. 5B). However, in terms of compensatory glycolysis, which is determined after inhibition of ETC, the effect of BMA treatment was again more pronounced in anoxia-tolerant cells (Fig. 5B).

Another crucial factor for maintenance of cellular energy homeostasis is NADH. Reduced NADH is regenerated in the TCA-cycle as well as during glycolysis. We therefore also explored a potential impact of BMA treatment on cellular NADH levels. In line with the effects of BMA on mitochondrial respiration and glycolysis, our data show a decrease of NADH levels (Fig. 5C) and an increase in the NAD^+/NADH ratio at 24 h after BMA-treatment, though these effects were only significant in anoxia-tolerant NCI-H460 cells (Fig. 5C and D). The more pronounced effects of BMA on NADH and the NAD^+/NADH ratio in anoxia-tolerant cells, hint to a higher sensitivity of these cells to BMA-mediated disturbance of energy homeostasis.

3.6. Pharmacologic inhibition of SLC25A10 increases the efficacy of radiotherapy in xenograft tumors generated from anoxia-tolerant NCI-H460 lung cancer cells in vivo

We have previously shown that xenograft tumors derived from NCI-H460 anoxia-tolerant cells display higher resistance to RT *in vivo* than tumors derived from NCI-H460 oxic control cells [9]. To explore the therapeutic potential of our innovative treatment strategy for sensitization of anoxia-tolerant cancer cells to the cytotoxic action of RT derived from our *in vitro* and *in silico* analyses, we investigated the effect of treatment with the SLC25A10 inhibitor BMA alone or in combination with a single-dose RT (5Gy) on the growth of anoxia-tolerant NCI-H460 xenograft tumors in NMRI nu/nu mice. The treatment schedule is shown in Fig. 6A.

Treatment of anoxia-tolerant NCI-H460 xenograft tumors with either BMA alone (5 × 25 mg/kg every second day i.p.) or RT (5 Gy) alone led to a delay of tumor growth by 2 days until the tumors reached the 6-fold volume of the volume at the start of treatment when compared to untreated controls. Importantly, treatment of tumor-bearing mice with BMA in combination with RT (5 Gy) led to a significant

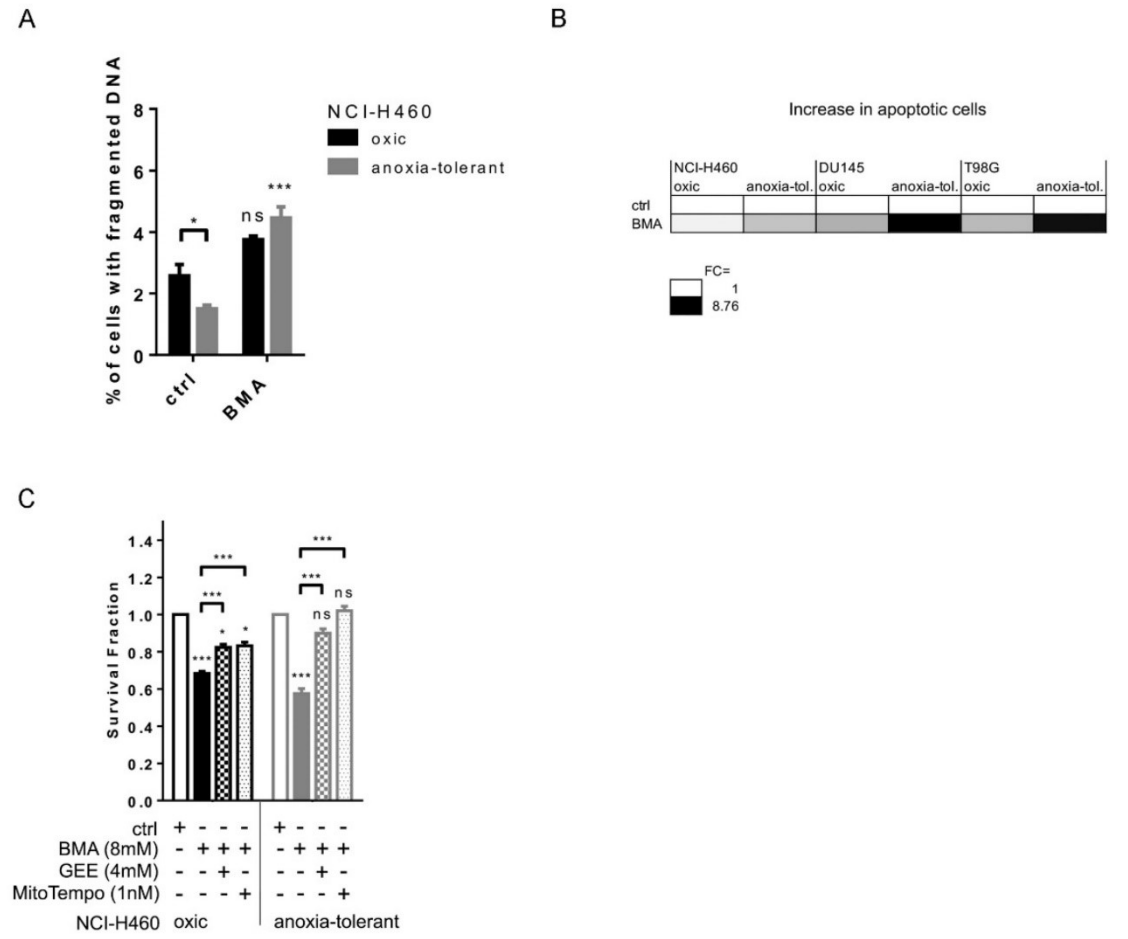

Fig. 4. SLC25A10 sustains improved death resistance of anoxia-tolerant cancer cells.
Impact of pharmacological SLC25A10 inhibition by using 8 mM BMA on induction of apoptosis in oxic and anoxia-tolerant cells. **A)** Fraction of apoptotic cells with fragmented DNA determined by flow cytometry (PI staining in a hypotonic citrate buffer) in NCI-H460 oxic and anoxia-tolerant cells after 72 h of BMA-treatment. **B)** Fold change of induction of apoptosis and DNA fragmentation (PI staining in a hypotonic citrate buffer) in NCI-H460, DU145 or T98G oxic and anoxia-tolerant cells after 72 h of BMA-treatment. Bar graphs with measured raw values (% of cells with fragmented DNA) of oxic and anoxia-tolerant DU145 and T98G cells can be found in Suppl. Fig. 5G and H. **C)** Rescue of BMA-mediated reduction of clonogenic survival fraction (SF) by 2 h additional pretreatment with 4 mM cell- and mitochondria-permeable glutathione-ethylester (GEE) or 1 nM mitochondrial ROS scavenger MitoTempo (MT) in NCI-H460 oxic and anoxia-tolerant cells. 24 h after treatment cells were collected and plated at different cell numbers in full medium without drugs and grown for 9 days.
Mean values ± SEM are shown, n = 3–4 (*p ≤ 0.05, **p ≤ 0.01, ***p ≤ 0.001; 2-way ANOVA with Tukey post-test).

increase in the efficacy of RT as demonstrated by a remarkable growth delay of 8 days until tumors reached the 6-fold volume when compared to RT alone (Fig. 6B).

3.7. Expression of SLC25A10 is a marker for tumor heterogeneity associated with tumor hypoxia in vivo

To gain further insight into a potential clinical relevance of SLC25A10 expression for tumor progression and therapy resistance we examined the *in vivo* expression of SLC25A10 in xenograft tumors generated from anoxia-tolerant NCI-H460 cells by using immunohistochemistry (IHC). We used staining with the hypoxia marker pimonidazole to reveal potential hypoxia-induced differences in transporter expression. Of note, we found that SLC25A10 expression was mostly associated with pimonidazole-positive hypoxic tumor fractions (Fig. 6C). Semi-quantitative analysis of the IHC sections revealed enhanced SLC25A10 expression in pimonidazole-positive hypoxic tumor regions compared to oxygenated, pimonidazole-negative tumor regions (Fig. 6D). Importantly, BMA-treatment *in vivo* did not suppress the generation of hypoxic tumor regions and did not abrogate the association between SLC25A10 expression and tumor hypoxia (Suppl. Fig. 7).

Taken together, our data strongly suggest that SLC25A10-inhibition could be a novel and effective strategy to target increased radioresistance associated with improved antioxidant defence, especially in hypoxic tumor fractions with up-regulated SLC25A10 expression (Fig. 6E).

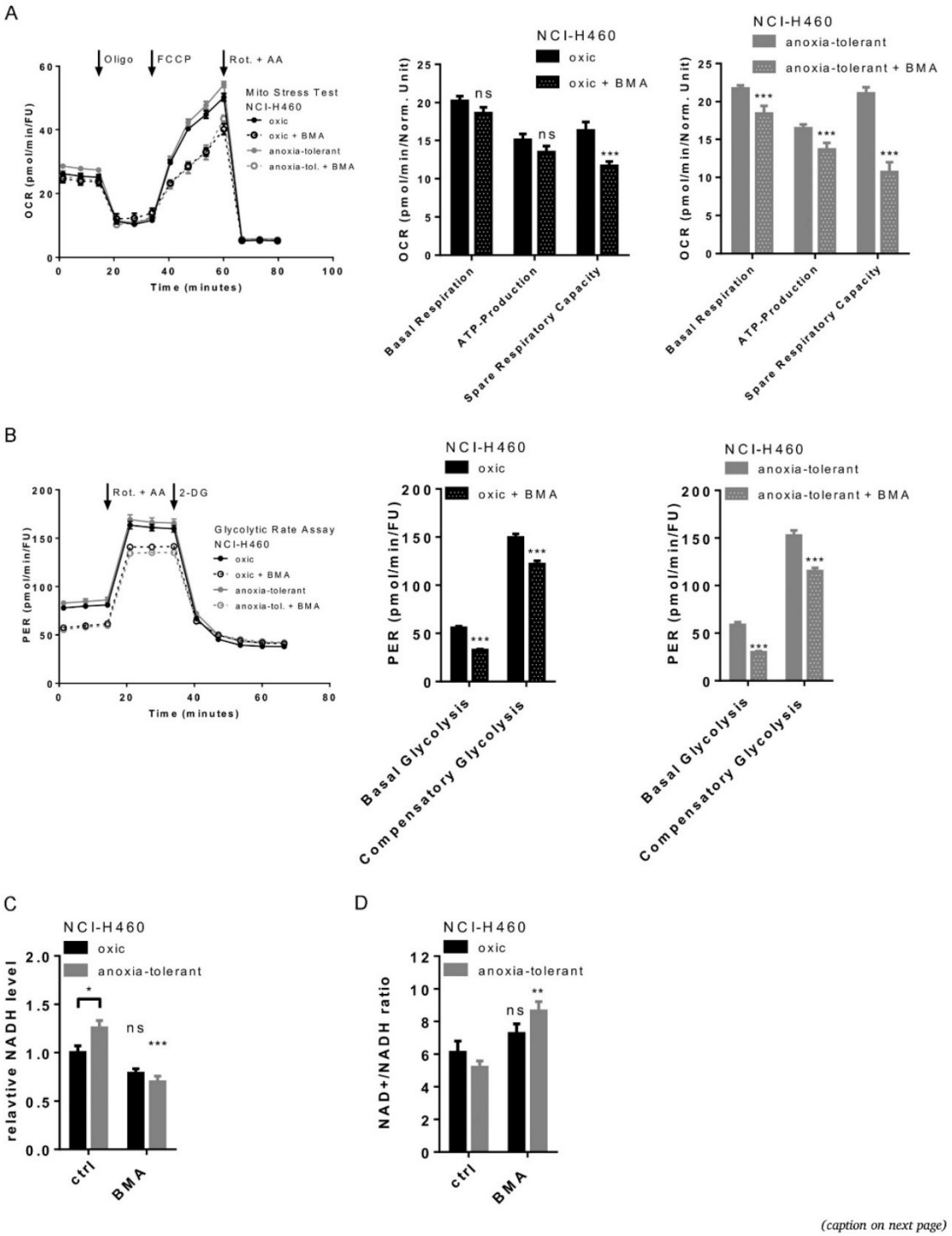

(caption on next page)

Fig. 5. Inhibition of SLC25A10 lowers cellular metabolism particularly in anoxia-tolerant cancer cells.
NCI-H460 oxic and anoxia-tolerant cells were treated for 24 h with 8 mM BMA and various parameters of cell metabolism were determined by using a Seahorse XFe 96 analyzer. NADH was measured by using a luciferase-coupled enzymatic reaction. **A)** Oxygen consumption rate (OCR) was measured using Mito Stress Test Kit and normalized to Hoechst 33342 fluorescence units (FU). Real-time Injection of Oligomycin (Oligo, 1 μM), FCCP (2 μM), Rotenone (Rot, 0.5 μM) and Antimycin A (AA, 0.5 μM) was performed and OCR was measured. Calculated parameters of the assay are indicated in bar graphs. **B)** Proton efflux rate (PER) was calculated from extracellular acidification rate measured using Glycolytic Rate Assay and normalized to Hoechst 33342 fluorescence units (FU). Real-time Injection of Rotenone (Rot, 0.5 μM), Antimycin A (AA, 0.5 μM) and 2-Desoxyglucose (2-DG, 50 mM). Calculated parameters of the assay are indicated in bar graphs. **C)** NADH levels (normalized to Hoechst 33342 fluorescence; DNA content) relative to oxic control after 24 h of BMA-treatment **D)** NAD^+/NADH ratio after 24 h of BMA-treatment.
Mean values ± SEM are shown, A) and B) from n = 12–18 wells (2 independent experiments); C) n = 3 (*p ≤ 0.05, **p < 0,01, ***p ≤ 0.001; A + B: *t*-test; C + D: two-way ANOVA with Tukey post-test).

4. Discussion

There is a high need in the development of novel therapeutic approaches overcoming hypoxia-mediated resistance [6,40–42]. Moreover, high tumor heterogeneity induced for example by acute or chronic (cycling) hypoxia is a major obstacle to successful RT. With the present work we reveal high expression of the mitochondrial dicarboxylate carrier SLC25A10 as a potential marker for hypoxic tumor fractions and hypoxia-induced radiation resistance in preclinical investigations. Mechanistically, we provide evidence for a link between high SLC25A10-expression in anoxia-tolerant cancer cells, improved antioxidant capacity, and associated radiation resistance. Even more important, pharmacologic inhibition of SLC25A10 proved to be an effective novel therapeutic strategy to counteract increased radioresistance induced by chronic-cycling hypoxia *in vitro* and *in vivo*. Finally, our *in silico* analyses point to an association of high SLC25A10 expression with poor overall survival, at least in lung and breast cancer patients. We speculate that up-regulation of SLC25A10 induced for example in hypoxic tumor fractions might impact patient survival in the clinical situation amongst others by increasing resistance to pro-oxidant therapies.

In more detail, we found that exposure to chronic-cycling hypoxia induced up-regulated expression of the mitochondrial dicarboxylate carrier SLC25A10 but not of the oxoglutarate carrier SLC25A11 in anoxia-tolerant cancer cells on the mRNA and protein level *in vitro*. Both transporters had been implicated in mitochondrial GSH (mGSH) transport to sustain metabolic reprogramming and antioxidant defense in cancer cells [19,21,43]. Herein, earlier studies already revealed an association of SLC25A10 expression to increased growth of A549 lung cancer cells with resistance to treatment with cisplatin [43] and high growth capacity of ovarian cancer cells [44]. Interestingly, *SLC25A10* is regulated by the transcription factor BTB and CNC homology 1 (BACH1) [45] that is induced in hypoxia [46].

Here we substantially extended these findings by linking adaptation of cancer cells to acute and chronic-cycling hypoxia to up-regulated expression of SLC25A10 and increased radioresistance. Moreover, we provide evidence that genetic or pharmacologic SLC25A10-inhibition increases the sensitivity of cancer cells to IR and even counteract the increased radioresistance induced by chronic-cycling hypoxia *in vitro* and *in vivo* by disturbing the up-regulated antioxidant capacity of the anoxia-tolerant cancer cells. This suggests that inhibition of SLC25A10 might be a promising strategy for increasing the efficacy of IR, particularly in SLC25A10-positive tumors with significant hypoxic fractions. However, our *in vivo* model using athymic mice has also some limitations since it misses out possible immune reactions induced by the treatment such as immunogenic cell death or activation of the adaptive immune system [47,48].

An earlier report linked reduced cell growth and enhanced cisplatin sensitivity upon genetic inhibition of SLC25A10 to altered NADPH redox states and decreased levels of mitochondrial thioredoxin (TXN) 2, [43]. Instead, an interplay and compensatory activity between TXN and GSH pathways had been proposed to support drug resistance in different cancer models [13]. In line with the former findings [43], in our hands inhibition of SLC25A10 decreased mitochondrial and cellular GSH-pools, caused mROS formation, and induced apoptotic cell death, arguing against the suggested concept of acquired resistance through a compensatory interplay between GSH and TXN pathways. Thereby our data are consistent with findings of others reporting that SLC25A10-inhibition increases formation of mROS, induces loss of mitochondrial membrane potential, release of cytochrome *c*, and induction of intrinsic apoptosis as a result of mGSH-depletion [19,49,50].

However, so far the transport of GSH into the mitochondrial matrix is not fully understood [19,21,49]. Particularly, the participation of SLC25A10 in mGSH transport was still controversial [25,26,51–53]. We show here that treatment of cancer cells with the SLC25A10-inhibitor BMA depleted mGSH levels, as determined in mitochondria isolated 2 h after treatment by using monochlorobimane (MCB). This suggests that pharmacologic inhibition of SLC25A10 indeed affects the proper import of GSH into the mitochondrial matrix and thus induction of mROS. Together with the observation that BMA-induced eradication of clonogenic tumor cells was effectively rescued by pre-treatment of the cells with a mitochondrial ROS scavenger MitoTempo (MT) or by artificially increasing mGSH-levels using GEE, respectively, our findings implicate that SLC25A10 indeed participates in mGSH uptake and that depletion of mGSH and generation of mROS contribute to the cytotoxic and radiosensitizing effects of SLC25A10-inhibition. Similar observations were made when using the SLC25A11 inhibitor PSA. It thus appears that both, SLC25A10 and SLC25A11, participate in redox homeostasis of cancer cells at the level of the mitochondria and that pharmacologic inhibition of these antioxidant-associated mitochondrial transport systems enhances cancer cell radiosensitivity.

However, we observed only increased expression of SLC25A10 but not SLC25A11 in our anoxia-tolerant cancer cells. Moreover, genetic or pharmacological inhibition of SLC25A11 with PSA was not capable to overcome increased radioresistance of anoxia-tolerant cancer cells demonstrating that SLC25A11 has minor relevance to therapy resistance caused by cellular adaptation to chronic-cycling hypoxia in the investigated cell lines. Interestingly, SLC25A11-overexpression did also not correlate to poor overall survival in our *in silico* analyses of publically available datasets from cancer patients.

In contrast, a recent study revealed a higher expression of SLC25A11 but not SLC25A10 in patient-derived HCC samples (n = 8) when compared to normal tissue [22]. Moreover, knockdown of SLC25A11 impaired cell growth, induced cell death, and sensitized HCC cells to hypoxia-induced ROS generation in a liver cancer model and this was associated with depletion of mGSH [22]. Despite similar observations regarding tumor-promoting effects of the two assumed mitochondrial GSH carriers with respect to maintenance of cellular and mitochondrial redox balance, our *in silico* analysis revealed a more prominent overexpression of SLC25A10 in patient samples from lung, breast, gastric and ovarian cancer compared to the respective normal tissues when compared to SLC25A11, and only high expression of SLC25A10 was associated with poor overall survival in breast and lung cancer patients.

The obvious differences regarding the relative importance of SLC25A10 and SLC25A11 point to tissue-specific requirements in these two transporters to maintain mGSH. However, it cannot be excluded that the small number of patient samples in the HCC study [22], distinct methods for the evaluation of SLC25A10 and SLC25A11 expression, or both might contribute to the conflicting findings. Nevertheless, a

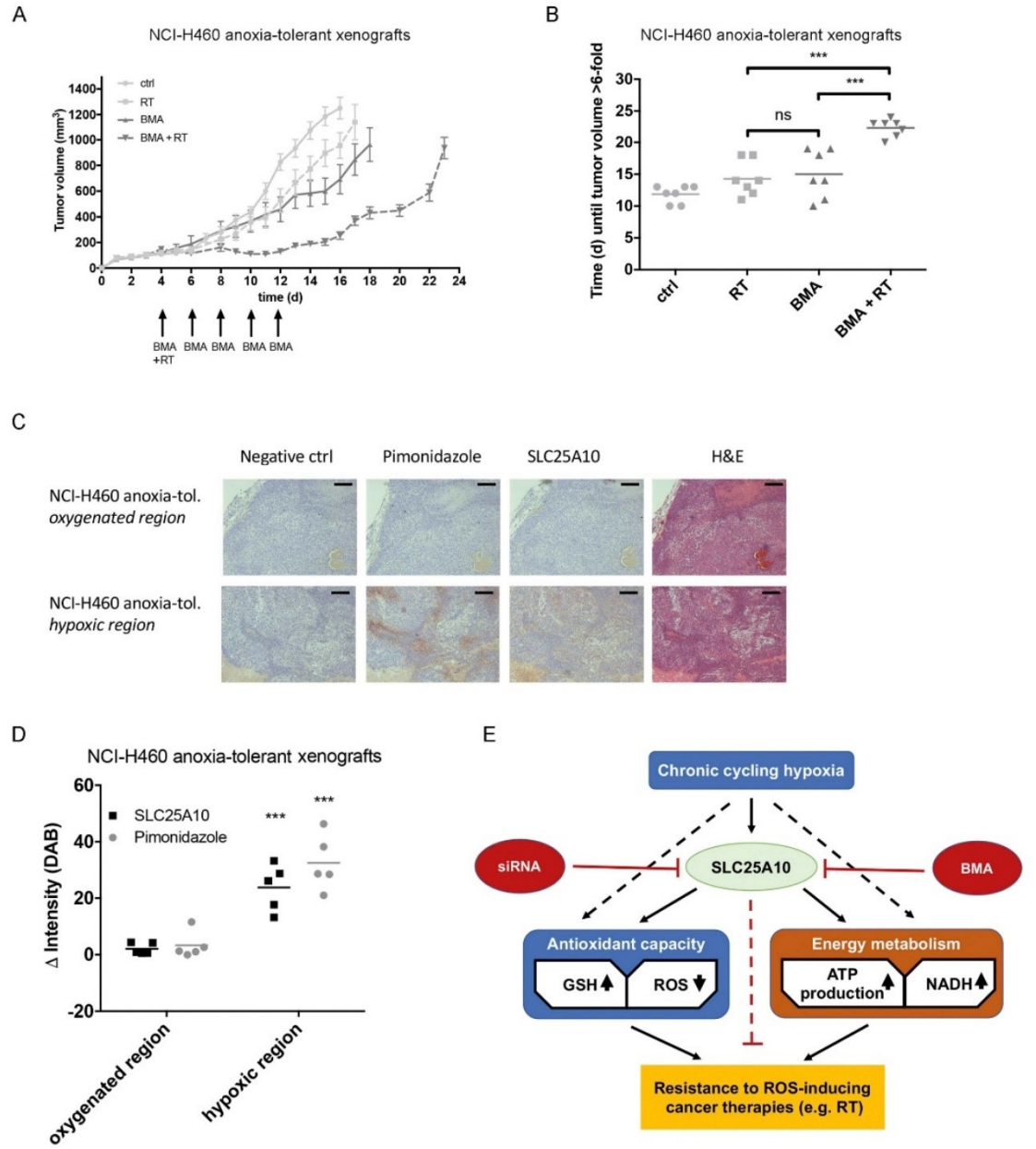

Fig. 6. BMA-mediated SLC25A10 inhibition improves efficacy of radiotherapy (RT) in anoxia-tolerant xenograft tumors.
Reduction of xenograft tumor growth of NCI-H460 anoxia-tolerant cancer cells when treated with BMA, RT or both. Especially hypoxic xenograft tumor regions displayed increased levels of SLC25A10 *in vivo*. **A)** Growth curve of NCI-H460 anoxia-tolerant xenograft tumors treated with BMA (5 × 25 mg/kg BMA every second day i.p.), single dose RT (5Gy) or both. Arrows below graph indicate treatment schedule. **B)** Time until tumor volume of NCI-H460 anoxia-tolerant xenograft tumors treated with BMA (5 × 25 mg/kg every second day i.p.), RT (5Gy single dose) or both reached 6-fold volume compared to volume at time of first treatment. **C)** Tumors of untreated NCI-H460 anoxia-tolerant cells were analyzed by immunohistochemistry (DAB-staining) for tumor hypoxia (pimonidazole-staining) and SLC25A10 levels. Representative pictures of corresponding regions (oxygenated and hypoxic) were taken with a 10× objective. **D)** Semi-quantification of DAB-stained slides in tumors derived from NCI-H460 anoxia-tolerant cells. Δ Intensity (DAB) of each staining was calculated by subtraction of intensity (DAB) of respective negative control region. **E)** Potential role of SLC25A10 in chronic-cycling hypoxia-mediated resistance to ROS-inducing treatments. Straight lines represent direct effects, Interleaved lines represent indirect effects. BMA: butylmalonate.
Mean values ± SEM are shown, data from A&B: n = 7, data from C&D n = 5 animals per group (***p ≤ 0.001; 2-way ANOVA with Tukey post-test).

potential role of SLC25A10 or SLC25A11 as biomarkers and therapeutic targets for aggressive cancers with pronounced tumor hypoxia and associated therapy resistance will require a proper and broad validation in large patient cohorts [54,55]. Generally, various members of the SLC25 carrier family seem to play a role in cancer [56]. Beside mitochondrial carboxylate carriers, also amino acid carriers and the mitochondrial pyruvate carrier 1 (MPC1) participate in metabolic reprogramming in cancer, whereas several uncoupling proteins are discussed to participate in antioxidant defence [56].

However, when analysing the mechanisms underlying SLC25A10-dependent mitochondrial redox homeostasis and radioresistance, it is important to consider that SLC25A10 not only shuttles GSH but mainly functions as a mitochondrial carboxylate carrier and participates, amongst others, in the bidirectional transport of malate between the cytosol and the mitochondrial matrix. By participation in balancing mitochondrial and cytosolic malate pools, SLC25A10 contributes to antiport with citrate mediated by the mitochondrial citrate carrier SLC25A1 [39]. In turn, isocitrate - isomerized from citrate – is used by isocitrate dehydrogenase 1 (IDH1, cytosolic) and isocitrate dehydrogenase 2 (IDH2, mitochondrial) to regenerate NADPH and in turn mGSH, making additional indirect effects of SLC25A10-dependent transport of malate on mitochondrial redox homeostasis highly likely [57]. Herein, our previous work revealed up-regulated expression of the mitochondrial citrate carrier SLC25A1 together with IDH2 in anoxia-tolerant cancer cells to support mitochondrial and cellular NADPH pools and redox homeostasis [12].

Here we extend these findings highlighting SLC25A10 as another antioxidant-associated mitochondrial transport system involved in increased antioxidant defence of cancer cells amenable to therapeutic inhibition. Our data also demonstrate that up-regulation of SLC25A10 not only improves cellular redox homeostasis but also supports cellular energy metabolism highlighting a dual but interconnected resistance mechanism on a functional level. Thereby our work supports various reports highlighting the importance of cellular redox balance for regulation of the mitochondrial metabolism at various levels. For example, we observed that mitochondrial respiration was decreased upon BMA-mediated SLC25A10 inhibition. Herein, depletion of (m)GSH has been reported to impair s-glutathionylation of proteins [20,21]. Enzymes of the TCA cycle and also complexes I, III and V of the ETC are functionally altered by s-glutathionylation [21]. Thus, up-regulation of mGSH by increased SLC25A10-expression might support mitochondrial respiration, while SLC25A10-inhibition would abrogate growth and resistance-promoting mitochondrial respiration. Consequently, disturbance of mGSH upon SLC25A10-inhibition might facilitate cell death by disturbing ETC-dependent energy homeostasis.

Further potential consequences of BMA-treatment on mitochondrial function might be observed because mitochondrial GTPase optic atrophy 1 (OPA1) was shown to sense energy homeostasis by interaction with SLC25 proteins, among others SLC25A10 [58]. Thus, BMA-treatment might also disturb the interaction between SLC25A10 and OPA1 in our cell systems and impair proper sensing of energy homeostasis thereby contributing to the observed decrease in mitochondrial respiration, especially in anoxia-tolerant cells.

Finally, we observed that SLC25A10-inhibition decreased glycolytic activity and NADH levels, which are also crucial for cellular energy homeostasis [20,59]. For example, under physiological conditions SLC25A10 participates in gluconeogenesis by providing malate for oxidation to oxaloacetate as substrate for phosphoenolpyruvate carboxykinase (PEP-CK) [39]. Though the role of gluconeogenesis in cancer is not fully understood, increasing evidence indicates that lung cancer cells use gluconeogenic enzymes like PEP-CK to sustain growth, particularly under reduced nutrient supply [60,61]. A disturbance of this process might thus contribute to BMA-mediated radiosensitization in our anoxia-tolerant cancer cells.

Taken together, our study reveals a novel role of SLC25A10 in redox- and energy-homeostasis of cancer cells with tolerance to chronic-cycling hypoxia and provides first evidence that SLC25A10-inhibition might be suited to improve treatment outcome in combination with radiation by targeting both, improved antioxidant defence and energy metabolism of cancer cells with tolerance to chronic cycling hypoxia, especially in solid tumors with hypoxic cell fractions. The observed association of high SLC25A10 expression with poor overall survival of lung and breast cancer patients points to a potential clinical relevance of our findings. It will be crucial to extend these findings on patient samples and further validate the use of targeting mitochondrial transport systems supporting redox and energy homeostasis to overcome hypoxia-induced radioresistance and to possibly improve treatment outcome in patients, especially with highly heterogeneous and hypoxic tumors in the future.

Author contributions

J.M., J.H. and V.J. designed and conceptualized the research; J.H., J.M. and V.R. performed experiments; J.M. and J.H. analyzed, validated and visualized the results; F.W. provided expertise in immunohistochemistry; D.K. provided expertise with animal experiments; J.M., J.H., and V.J. wrote the original manuscript draft; J.M. and V.J. supervised the work; V.J. acquired the funding. All authors critically revised, edited and approved the final version of the manuscript.

Funding

This work was supported by Grants of the German Research Association (grant number DFG GRK1739/2) and the Deutsche Krebshilfe/Mildred-Scheel-Stiftung (grant numbers 110355 and 70112711) to V.J.

Author disclosure statement

The authors state that there are no personal or institutional conflicts of interest.

Acknowledgements

We thank E. Gau for excellent technical support, C. Hansel for experimental assistance, M. Schuler for very helpful discussions and *Brigitte und Dr. Konstanze Wegener-Stiftung* for funding of the Seahorse XFe 96 analyzer.

Appendix A. Supplementary data

Supplementary data related to this article can be found at https://doi.org/10.1016/j.canlet.2018.09.002.

References

[1] D. Hanahan, R.A. Weinberg, Hallmarks of cancer: the next generation, Cell 144 (2011) 646–674.
[2] J.C. van der Mijn, D.J. Panka, A.K. Geissler, H.M. Verheul, J.W. Mier, Novel drugs that target the metabolic reprogramming in renal cell cancer, Canc. Metabol. 4 (2016) 14.
[3] J. Abrego, V. Gunda, E. Vernucci, S.K. Shukla, R.J. King, A. Dasgupta, G. Goode, D. Murthy, F. Yu, P.K. Singh, GOT1-mediated anaplerotic glutamine metabolism regulates chronic acidosis stress in pancreatic cancer cells, Canc. Lett. 400 (2017) 37–46.
[4] W. Zeng, P. Liu, W. Pan, S.R. Singh, Y. Wei, Hypoxia and hypoxia inducible factors in tumor metabolism, Canc. Lett. 356 (2015) 263–267.
[5] P. Vaupel, Tumor microenvironmental physiology and its implications for radiation oncology, Semin. Radiat. Oncol. 14 (2004) 198–206.
[6] A. Salem, M.C. Asselin, B. Reymen, A. Jackson, P. Lambin, C.M.L. West, J.P.B. O'Connor, C. Faivre-Finn, Targeting hypoxia to improve non-small cell lung cancer outcome, J. Natl. Cancer Inst. 110 (2018).
[7] H. Kim, Q. Lin, Z. Yun, The hypoxic tumor microenvironment in vivo selects tumor cells with increased survival against genotoxic stresses, Canc. Lett. 431 (2018) 142–149.
[8] R.J. DeBerardinis, N.S. Chandel, Fundamentals of cancer metabolism, Sci. Adv. 2

(2016) e1600200.
[9] J. Matschke, H. Riffkin, D. Klein, R. Handrick, L. Ludemann, E. Metzen, T. Shlomi, M. Stuschke, V. Jendrossek, Targeted inhibition of glutamine-dependent glutathione metabolism overcomes death resistance induced by chronic cycling hypoxia, Antioxidants Redox Signal. 25 (2016) 89–107.
[10] K.M. Rouschop, L.J. Dubois, T.G. Keulers, T. van den Beucken, P. Lambin, J. Bussink, A.J. van der Kogel, M. Koritzinsky, B.G. Wouters, PERK/eIF2alpha signaling protects therapy resistant hypoxic cells through induction of glutathione synthesis and protection against ROS, Proc. Natl. Acad. Sci. U. S. A. 110 (2013) 4622–4627.
[11] R. Nakashima, Y. Goto, S. Koyasu, M. Kobayashi, A. Morinibu, M. Yoshimura, M. Hiraoka, E.M. Hammond, H. Harada, UCHL1-HIF-1 axis-mediated antioxidant property of cancer cells as a therapeutic target for radiosensitization, Sci. Rep. 7 (2017) 6879.
[12] J. Hlouschek, C. Hansel, V. Jendrossek, J. Matschke, The mitochondrial citrate Carrier (SLC25A1) sustains redox homeostasis and mitochondrial metabolism supporting radioresistance of cancer cells with tolerance to cycling severe hypoxia, Front. Oncol. 8 (2018) 170.
[13] E. Hatem, N. El Banna, M.E. Huang, Multifaceted roles of glutathione and glutathione-based systems in carcinogenesis and anticancer drug resistance, Antioxidants Redox Signal. 27 (2017) 1217–1234.
[14] M. Deponte, The incomplete glutathione puzzle: just guessing at numbers and figures? Antioxidants Redox Signal. 27 (2017) 1130–1161.
[15] W.X. Zong, J.D. Rabinowitz, E. White, Mitochondria and cancer, Mol. Cell. 61 (2016) 667–676.
[16] P.B. Esparza-Molto, J.M. Cuezva, The role of mitochondrial H(+)-ATP synthase in cancer, Front. Oncol. 8 (2018) 53.
[17] M.C. De Santis, P.E. Porporato, M. Martini, A. Morandi, Signaling pathways regulating redox balance in cancer metabolism, Front. Oncol. 8 (2018) 126.
[18] V. Jendrossek, The intrinsic apoptosis pathways as a target in anticancer therapy, Curr. Pharmaceut. Biotechnol. 13 (2012) 1426–1438.
[19] M. Mari, A. Morales, A. Colell, C. García-Ruiz, N. Kaplowitz, J.C. Fernandez-Checa, Mitochondrial glutathione: features, regulation and role in disease, Biochim. Biophys. Acta 1830 (2013) 3317–3328.
[20] D.E. Handy, J. Loscalzo, Redox regulation of mitochondrial function, Antioxidants Redox Signal. 16 (2012) 1323–1367.
[21] G. Calabrese, B. Morgan, J. Riemer, Mitochondrial glutathione: regulation and functions, Antioxidants Redox Signal. 27 (2017) 1162–1177.
[22] A. Baulies, J. Montero, N. Matias, N. Insausti, O. Terrones, G. Basanez, C. Vallejo, L. Conde de La Rosa, L. Martinez, D. Robles, A. Morales, J. Abian, M. Carrascal, K. Machida, D.B.U. Kumar, H. Tsukamoto, N. Kaplowitz, C. Garcia-Ruiz, J.C. Fernandez-Checa, The 2-oxoglutarate Carrier promotes liver cancer by sustaining mitochondrial GSH despite cholesterol loading, Redox Biol. 14 (2018) 164–177.
[23] C. von Montfort, N. Matias, A. Fernandez, R. Fucho, L. Conde de la Rosa, M.L. Martinez-Chantar, J.M. Mato, K. Machida, H. Tsukamoto, M.P. Murphy, A. Mansouri, N. Kaplowitz, C. Garcia-Ruiz, J.C. Fernandez-Checa, Mitochondrial GSH determines the toxic or therapeutic potential of superoxide scavenging in steatohepatitis, J. Hepatol. 57 (2012) 852–859.
[24] S. Torres, N. Matias, A. Baulies, S. Nunez, C. Alarcon-Vila, L. Martinez, N. Nuno, A. Fernandez, J. Caballeria, T. Levade, A. Gonzalez-Franquesa, P. Garcia-Roves, E. Balboa, S. Zanlungo, G. Fabrias, J. Casas, C. Enrich, C. Garcia-Ruiz, J.C. Fernandez-Checa, Mitochondrial GSH replenishment as a potential therapeutic approach for Niemann Pick type C disease, Redox Biol. 11 (2017) 60–72.
[25] H.M. Wilkins, D. Kirchhof, E. Manning, J.W. Joseph, D.A. Linseman, Mitochondrial glutathione transport is a key determinant of neuronal susceptibility to oxidative and nitrosative stress, J. Biol. Chem. 288 (2013) 5091–5101.
[26] C.K. Kamga, S.X. Zhang, Y. Wang, Dicarboxylate Carrier-mediated glutathione transport is essential for reactive oxygen species homeostasis and normal respiration in rat brain mitochondria, Am. J. Physiol. Cell Physiol. 299 (2010) C497–C505.
[27] J. Matschke, E. Wiebeck, S. Hurst, J. Rudner, V. Jendrossek, Role of SGK1 for fatty acid uptake, cell survival and radioresistance of NCI-H460 lung cancer cells exposed to acute or chronic cycling severe hypoxia, Radiat. Oncol. 11 (2016) 75.
[28] B. Gyorffy, A. Lanczky, A.C. Eklund, C. Denkert, J. Budczies, Q. Li, Z. Szallasi, An online survival analysis tool to rapidly assess the effect of 22,277 genes on breast cancer prognosis using microarray data of 1,809 patients, Breast Canc. Res. Treat. 123 (2010) 725–731.
[29] B. Gyorffy, P. Surowiak, J. Budczies, A. Lanczky, Online survival analysis software to assess the prognostic value of biomarkers using transcriptomic data in non-small-cell lung cancer, PLoS One 8 (2013) e82241.
[30] J. Caradec, N. Sirab, C. Keumeugni, S. Moutereau, M. Chimingqi, C. Matar, D. Revaud, M. Bah, P. Manivet, M. Conti, S. Loric, 'Desperate house genes': the dramatic example of hypoxia, Br. J. Canc. 102 (2010) 1037–1043.
[31] M.W. Pfaffl, A new mathematical model for relative quantification in real-time RT–PCR, Nucleic Acids Res. 29 (2001) 00.
[32] J. Schindelin, I. Arganda-Carreras, E. Frise, V. Kaynig, M. Longair, T. Pietzsch, S. Preibisch, C. Rueden, S. Saalfeld, B. Schmid, J.Y. Tinevez, D.J. White, V. Hartenstein, K. Eliceiri, P. Tomancak, A. Cardona, Fiji: an open-source platform for biological-image analysis, Nat. Methods 9 (2012) 676–682.
[33] E.A.B. Glenn, C. Rice, Dennis C. Shrieve, William Lee, Mary Kovacs, Quantitative analysis of cellular glutathione by flow cytometry utilizing monochlorobimane: some applications to radiation and drug resistance in vitro and in vivo, Canc. Res. 46 (1986) 6105–6110.
[34] F.-C.J.K. N, The use of monochlorobimane to determine hepatic GSH levels and synthesis, Anal. Biochem. 190 (1990) 212–219.
[35] N.P. Visavadiya, S.P. Patel, J.L. VanRooyen, P.G. Sullivan, A.G. Rabchevsky, Cellular and subcellular oxidative stress parameters following severe spinal cord injury, Redox Biol. 8 (2016) 59–67.
[36] N.A. Franken, H.M. Rodermond, J. Stap, J. Haveman, C. van Bree, Clonogenic assay of cells in vitro, Nat. Protoc. 1 (2006) 2315–2319.
[37] I. Nicoletti, G. Migliorati, M.C. Pagliacci, F. Grignani, C. Riccardi, A rapid and simple method for measuring thymocyte apoptosis by propidium iodide staining and flow cytometry, J. Immunol. Meth. 139 (1991) 271–279.
[38] M. Weinmann, V. Jendrossek, D. Guner, B. Goecke, C. Belka, Cyclic exposure to hypoxia and reoxygenation selects for tumor cells with defects in mitochondrial apoptotic pathways, Faseb. J. 18 (2004) 1906–1908.
[39] F. Palmieri, The mitochondrial transporter family (SLC25): physiological and pathological implications, Pflügers Archiv. 447 (2004) 689–709.
[40] A. Patel, S. Sant, Hypoxic tumor microenvironment: opportunities to develop targeted therapies, Biotechnol. Adv. 34 (2016) 803–812.
[41] J.D. Martin, D. Fukumura, D.G. Duda, Y. Boucher, R.K. Jain, Reengineering the tumor microenvironment to alleviate hypoxia and overcome cancer heterogeneity, Cold Spring Harb Perspect. Med. 6 (2016).
[42] J.W. Ivey, M. Bonakdar, A. Kanitkar, R.V. Davalos, S.S. Verbridge, Improving cancer therapies by targeting the physical and chemical hallmarks of the tumor microenvironment, Canc. Lett. 380 (2016) 330–339.
[43] X. Zhou, J.A. Paredes, S. Krishnan, S. Curbo, A. Karlsson, The mitochondrial Carrier SLC25A10 regulates cancer cell growth, Oncotarget 6 (2015) 9271–9283.
[44] E. Motamedian, G. Ghavami, S. Sardari, Investigation on metabolism of cisplatin resistant ovarian cancer using a genome scale metabolic model and microarray data, Iran. J. Basic Med. Sci. 18 (2015) 267–276.
[45] H.J. Warnatz, D. Schmidt, T. Manke, I. Piccini, M. Sultan, T. Borodina, D. Balzereit, W. Wruck, A. Soldatov, M. Vingron, H. Lehrach, M.L. Yaspo, The BTB and CNC homology 1 (BACH1) target genes are involved in the oxidative stress response and in control of the cell cycle, J. Biol. Chem. 286 (2011) 23521–23532.
[46] S. Davudian, B. Mansoori, N. Shajari, A. Mohammadi, B. Baradaran, BACH1, the master regulator gene: a novel candidate target for cancer therapy, Gene 588 (2016) 30–37.
[47] S.C. Formenti, S. Demaria, Systemic effects of local radiotherapy, Lancet Oncol. 10 (2009) 718–726.
[48] L. Deloch, A. Derer, J. Hartmann, B. Frey, R. Fietkau, U.S. Gaipl, Modern radiotherapy concepts and the impact of radiation on immune activation, Front. Oncol. 6 (2016) 141.
[49] V. Ribas, C. Garcia-Ruiz, J.C. Fernandez-Checa, Glutathione and mitochondria, Front. Pharmacol. 5 (2014) 151.
[50] C.C. Wu, S.B. Bratton, Regulation of the intrinsic apoptosis pathway by reactive oxygen species, Antioxidants Redox Signal. 19 (2013) 546–558.
[51] A.L. Wadey, H. Muyderman, P.T. Kwek, N.R. Sims, Mitochondrial glutathione uptake: characterization in isolated brain mitochondria and astrocytes in culture, J. Neurochem. 109 (Suppl 1) (2009) 101–108.
[52] L.M. Booty, M.S. King, C. Thangaratnarajah, H. Majd, A.M. James, E.R. Kunji, M.P. Murphy, The mitochondrial dicarboxylate and 2-oxoglutarate carriers do not transport glutathione, FEBS Lett. 589 (2015) 621–628.
[53] G. Punzi, V. Porcelli, M. Ruggiu, M.F. Hossain, A. Menga, P. Scarcia, A. Castegna, R. Gorgoglione, C.L. Pierri, L. Laera, F.M. Lasorsa, E. Paradies, I. Pisano, C.M.T. Marobbio, E. Lamantea, D. Ghezzi, V. Tiranti, S. Giannattasio, M.A. Donati, R. Guerrini, L. Palmieri, F. Palmieri, A. De Grassi, SLC25A10 biallelic mutations in intractable epileptic encephalopathy with complex I deficiency, Hum. Mol. Genet. 27 (2018) 499–504.
[54] P.E. Barker, Cancer biomarker validation: standards and process: roles for the National Institute of Standards and Technology (NIST), Ann. N. Y. Acad. Sci. 983 (2003) 142–150.
[55] D.F. Hayes, Biomarker validation and testing, Mol. Oncol. 9 (2015) 960–966.
[56] O. Lytovchenko, E.R.S. Kunji, Expression and putative role of mitochondrial transport proteins in cancer, Biochim. Biophys. Acta 1858 (2017) 641–654.
[57] D.C. Wallace, Mitochondria and cancer, Nat. Rev. Canc. 12 (2012) 685–698.
[58] D.A. Patten, J. Wong, M. Khacho, V. Soubannier, R.J. Mailloux, K. Pilon-Larose, J.G. MacLaurin, D.S. Park, H.M. McBride, L. Trinkle-Mulcahy, M.E. Harper, M. Germain, R.S. Slack, OPA1-dependent cristae modulation is essential for cellular adaptation to metabolic demand, EMBO J. 33 (2014) 2676–2691.
[59] C. Canto, K.J. Menzies, J. Auwerx, NAD(+) metabolism and the control of energy homeostasis: a balancing act between mitochondria and the nucleus, Cell Metabol. 22 (2015) 31–53.
[60] E.E. Vincent, A. Sergushichev, T. Griss, M.C. Gingras, B. Samborska, T. Ntimbane, P.P. Coelho, J. Blagih, T.C. Raissi, L. Choiniere, G. Bridon, E. Loginicheva, B.R. Flynn, E.C. Thomas, J.M. Tavare, D. Avizonis, A. Pause, D.J. Elder, M.N. Artyomov, R.G. Jones, Mitochondrial phosphoenolpyruvate carboxykinase regulates metabolic adaptation and enables glucose-independent tumor growth, Mol. Cell. 60 (2015) 195–207.
[61] K. Leithner, A. Hrzenjak, M. Trotzmuller, T. Moustafa, H.C. Kofeler, C. Wohlkoenig, E. Stacher, J. Lindenmann, A.L. Harris, A. Olschewski, H. Olschewski, PCK2 activation mediates an adaptive response to glucose depletion in lung cancer, Oncogene 34 (2015) 1044–1050.

Diskussion

Insgesamt zeigten die Ergebnisse der beiden Publikationen, dass eine Exposition gegenüber akuter oder chronisch-zyklischer Hypoxie die Expression der mitochondrialen Carboxylat-Transporter SLC25A1 und SLC25A10 erhöht. Genetische und/oder pharmakologische Inhibition von SLC25A1, SLC25A10 und SLC25A11 steigerte die Zytotoxizität einer Bestrahlung. Jedoch führte nur die Inhibition von SLC25A1 und SLC25A10 zu einer Aufhebung der durch chronisch-zyklische Hypoxie induzierten, gesteigerten Strahlenresistenz. Hierbei bestand eine Assoziation zwischen verlangsamter Reparaturkinetik von strahleninduzierten DNA-Schäden und SLC25A1-Inhibition. Ferner beeinträchtigte die Inhibition von SLC25A1 und SLC25A10 sowohl die zelluläre und mitochondriale Redox-Homöostase als auch den mitochondrialen Metabolismus und metabolischen Bedarf, insbesondere in hypoxischen Tumorzellen. Überexpression von SLC25A1 und SLC25A10 war u.a. in Lungenkrebspatienten mit schlechterem Gesamtüberleben *in silico* assoziiert. Außerdem zeigten Xenograft-Tumoren der durch chronisch-zyklische Hypoxie selektionierten Tumorzellen hohe SLC25A10 Expression insbesondere in hypoxischen Tumorarealen sowie eine Aufhebung der durch chronisch-zyklische Hypoxie induzierten, gesteigerten Strahlenresistenz nach pharmakologischer Inhibition von SLC25A10 *in vivo*.

Die zuerst veröffentlichte Originalarbeit fokussiert dabei auf die Rolle des mitochondrialen Citrat-Carriers SLC25A1 für die Strahlenresistenz von humanen Lungentumorzellen (NCI-H460) mit Toleranz gegenüber chronisch-zyklischer Hypoxie (Hlouschek et al., 2018a). Bereits zuvor konnte in Lungentumorzellen die Abhängigkeit von SLC25A1 im Rahmen des Metastasierungsprozesses und der proliferationsabhängigen Fettsäuresyntese gezeigt werden (Jiang et al., 2017; Jiang et al., 2016). Im Rahmen der vorliegenden Originalarbeit konnte dagegen erstmals gezeigt werden, dass die Exposition von Lungentumorzellen gegenüber akuter und chronisch-zyklischer Hypoxie eine erhöhte Expression von SLC25A1 induzierte. Die pharmakologische Inhibition von SLC25A1 mit den Substanzen 1,2,3-Benzen-Tricarboxylat (BTA) sowie 4-Chlor-3-[[(3-Nitrophenyl)Amino]Sulfonyl]-Benzoesäure

(CNASB) depletierte die zelluläre Antioxidanskapazität, sorgte für vermehrte Bildung von mitochondrialen (m)ROS und wirkte der durch chronisch-zyklische Hypoxie induzierten erhöhten Strahlenresistenz effektiv entgegen. Des Weiteren war die pharmakologische Inhibition von SLC25A1 mit einer Herabsetzung des mitochondrialen Metabolismus und einer Akkumulierung des Onkometaboliten 2-Hydroxyglutarat (2-HG) assoziiert. Zudem zeigte sich nach Inhibition eine verschlechterte Reparatur strahleninduzierter DNA-Doppelstrangbrüche, gemessen durch zeitabhängige Induktion und Auflösung von Foci für das Histon H2A.X phosphoryliert an Serin 139 (γH2AX), welche einen Marker für DNA-Doppelstrangbrüche darstellen. Die strahlensensibilisierenden Effekte waren in den resistenten, gegenüber chronisch-zyklischer Hypoxie toleranten Zellen stärker ausgeprägt als in nicht adaptierten Kontroll-Tumorzellen.

Diese Resultate der Arbeit weisen damit erstmals auf eine bisher unbekannte Bedeutung von SLC25A1 für die zelluläre Strahlenresistenz hin, vermutlich durch verringerte NADPH-abhängige Regeneration von GSH zur ROS-Detoxifizierung sowie metabolische Beeinflussung der DNA-Reparaturkapazität. Außerdem liegt hierdurch für das klonogene Überleben von Tumorzellen eine Abhängigkeit von SLC25A1 im Rahmen der Adaptationsprozesse während Hypoxie und Reoxygenierungs-Stress vor. Die Beobachtung im Rahmen der Analyse von öffentlich verfügbaren Datenbanken (KM Plotter) *in silico* zeigte, dass erhöhte SLC25A1-Expressionen in Lungentumoren mit reduziertem Gesamtüberleben von Patienten assoziiert sind und stützt die mögliche klinische Bedeutung von SLC25A1 im Rahmen von Adaptationsprozessen, die zu Therapieversagen führen. Allerdings liegen noch keine prospektiven klinischen Daten bezüglich der Bedeutung einer erhöhten SLC25A1-Expression für ein schlechteres Ansprechen nach Strahlentherapie oder Therapieversagen im Allgemeinen vor. Dies wäre Voraussetzung für die Weiterentwicklung von SLC25A1 als Biomarker für eine erhöhte Strahlenresistenz bzw. als neue therapeutische Zielstruktur um potenziell eine neue Strategie zur Strahlensensibilisierung von Lungentumorzellen zu entwickeln.

Weitere Untersuchungen anderer Arbeitsgruppen nach Veröffentlichung der ersten Originalarbeit erweitern die Rolle von SLC25A1 für die maligne Progression und Therapieresistenz von Tumorzellen. Es konnte gezeigt werden, dass

Lungentumorstammzellen besonders abhängig von SLC25A1 sind und die Inhibition zu synthetischer Letalität mit Cisplatin oder einem Inhibitor des epidermalen Wachstumsfaktor Rezeptors (EGFR) führt (Fernandez et al., 2018). Die Entwicklung eines neuen, in deutlich geringeren Konzentrationen wirksamen Inhibitors für SLC25A1 und dessen Erprobung *in vivo* unterstreicht zudem das zukünftige Potenzial für eine mögliche klinische Translation (Fernandez et al., 2018). Hiermit erhöht sich die Evidenz für eine Rolle von SLC25A1 in Tumorzellen im Rahmen von Adaptationen an ein nachteiliges Tumormikromilieu neben chronisch-zyklischer Hypoxie auch durch Resistenzentwicklung von Tumorstammzellen gegenüber Chemotherapie (Cisplatin) und zielgerichteten Therapien (EGFR-Inhibitor). Zusätzlich wurden die antiproliferativen Eigenschaften einer Inhibition von SLC25A1 in Tumorzelllinien weiterer Entitäten (Papilläres Schilddrüsenkarzinom und Pankreaskarzinom) demonstriert (Liu et al., 2020a; Liu et al., 2020b). Des Weiteren wurde die Bedeutung von SLC25A1 im Rahmen der Pathogenese der nicht-alkoholischen Steatohepatitis (NASH) untersucht und gezeigt, dass eine Inhibition von SLC25A1 in präklinischen Modellen die Entstehungswahrscheinlichkeit einer NASH vermindert (Tan et al., 2020). Bemerkenswerterweise spielt sowohl bei der Entstehung einer NASH als auch bei der Tumorgenese der anhaltende Zustand chronischer Inflammation eine tragende Rolle. Die Funktion von SLC25A1 als Mediator zur Aufrechterhaltung proinflammatorischer Signaltransduktion durch den Transport von Citrat ins Zytosol könnte so in verschiedenen Krankheitsentitäten ein gemeinsamer therapeutischer Ansatzpunkt sein (Mosaoa et al., 2021). Insgesamt erhöhen diese Studien die Evidenz für eine funktionelle Rolle von SLC25A1 in Tumorzellen im Rahmen von Adaptationen an ein nachteiliges Tumormikromilieu in Assoziation mit Therapieresistenzen, die offenbar nicht nur eine Toleranz gegenüber Hypoxie und erhöhte Radioresistenz umfasst.

Erhöhte Spiegel des Onkometaboliten 2-HG beeinflussen die maligne Progression von Tumorzellen über verschiedene epigenetische Mechanismen, die eine genetische Instabilität begünstigen (Flavahan et al., 2017). Damit geht eine erhöhte Vulnerabilität von Tumorzellen mit hohen 2-HG Spiegeln gegenüber DNA-Schädigung einher (Gagne et al., 2017). Eine genauere mechanistische Untersuchung nach Veröffentlichung zeigte, dass die 2-HG induzierte Modulation von Lysin-Demethylasen der KDM-Familie durch Störung des Chromatinsignallings die homologe Rekombination (HR) der DNA-

Reparatur inhibieren kann (Sulkowski et al., 2017; Sulkowski et al., 2020; Sulkowski et al., 2018). Hierdurch bietet sich vermutlich durch die Erhöhung der 2-HG Spiegel durch SLC25A1-Inhibition ein potenzieller therapeutischer Ansatzpunkt zur indirekten Hemmung der HR. Die HR ist wiederum für eine möglichst fehlerfreie Reparatur komplexer DNA-Doppelstrangbrüche nach Exposition gegenüber IR notwendig (Schipler and Iliakis, 2013). Tumorzellen mit Fehlfunktionen in HR sind sensitiver gegenüber Inhibition weiterer DNA-Reparaturmechanismen, wie etwa durch Poly(ADP-Ribose)-Polymerasen (PARP)-Inhibitoren (Powell and Bindra, 2009). Hierdurch wäre es potenziell möglich, dass sich durch die Kombination von SLC25A1-Inhibtion mit beispielsweise PARP-Inhibitioren additive Effekte oder gar Induktion von synthetischer Letalität ergeben. Doch auch weitere Onkometabolite wie etwa Fumarat und Succinat zeigen Potenz zur Inhibition der Homologen Rekombination (Sulkowski et al., 2020; Sulkowski et al., 2018; Xiang et al., 2020).

Die in der vorliegenden Veröffentlichung gezeigte BTA-induzierte Erhöhung von 2-HG in Assoziation mit verringerter DNA-Reparaturkapazität zeigte noch keine direkte Evidenz für eine tatsächliche Relevanz des Ansatzes (Hlouschek et al., 2018a). Dagegen deuten neuere Untersuchungen auf eine breitere Bedeutung und neue Anwendungsmöglichkeiten hin, da sich die durch 2-HG induzierten vielfältigen Veränderungen des Epigenoms nicht nur auf den zuvor genannten Mechanismus beziehen (Sulkowski et al., 2020). Nicht nur SLC25A1 als Citrat-Transporter, sondern auch die ATP-Citrat-Lyase selbst kann inhibiert werden, um die Strahlenresistenz von Tumorzellen zu vermindern (Gottgens et al., 2019). Für beide Ansätze gilt, dass nach Inhibition weniger Acetyl-CoA als Acetylgruppendonor für epigenetische Modifikationen zur Verfügung stände (Flavahan et al., 2017). Des weiteren spielt 2-HG selbst eine Rolle für epigenetische Alterationen durch kompetitive Inhibition von α-Ketoglutarat-abhängigen Dioxygenasen, welche prinzipiell durch beide Enantiomere D-2-HG und L-2-HG erreicht werden kann (Xiang et al., 2020). Dennoch könnte in Zukunft die relative Bedeutung der beiden Enantiomere D-2-HG und L-2-HG für die Beeinflussung der HR noch genauer untersucht werden (Sulkowski et al., 2020; Xiang et al., 2020). Außerdem konnte nach Veröffentlichung eine neue mechanistische Hypothese zur Akkumulation von 2-HG nach SLC25A1-Inhibition entwickelt werden, da in *Drosophila melanogaster* gezeigt werden konnte, dass durch SLC25A1 kontrollierte

Citrat-Pools indirekt den 2-HG Abbau beeinflussen und somit ein negativer Feedback-Mechanismus besteht (Li et al., 2018). Ob dieser Mechanismus ebenfalls in menschlichen Tumorzellen vorhanden und funktionell relevant ist, konnte noch nicht gezeigt werden. Dafür spräche jedoch, dass das Fruchtfliegenhomolog von SLC25A1 neben seiner hohen Identität zu den Sequenzen von Mensch und Ratte zudem über hohe Übereinstimmungen mit deren Transportmerkmalen und kinetischen Parametern verfügt. Darüber hinaus haben in *Drosophila melanogaster* durchgeführte Studien gezeigt, dass SLC25A1 wichtige konservierte Funktionen von *Drosophila* bis zum Menschen bei der Aufrechterhaltung der Chromosomenstabilität hat (Curcio et al., 2020).

Die zweite anschließend veröffentlichte Originalarbeit untersucht die Bedeutung der mitochondrialen Carrier SLC25A10 und SLC25A11 für die erhöhte Antioxidanskapazität und Strahlenresistenz von humanen Tumorzellen verschiedener Entitäten mit Toleranz gegenüber chronisch-zyklischer Hypoxie (Hlouschek et al., 2018b). Die genetische oder pharmakologische Inhibition sowohl von SLC25A10 als auch von SLC25A11 induzierte vermehrt Zelltod, erhöhte ROS und mROS sowie die zytotoxische Potenz von IR. Jedoch war nur die Hemmung von SLC25A10 effektiv genug, um die durch chronisch-zyklische Hypoxie induzierte und damit erhöhte Therapieresistenz in Tumorzellen verschiedener Entitäten (NCI-H460, Lunge; DU-145, Prostata; T98G, Glioblastom) aufzuheben. Die antineoplastische Effektivität der pharmakologischen Inhibition von SLC25A10 mittels Butylmalonat (BMA) allein und in Kombination mit Radiotherapie konnte ebenfalls *in vivo* in ektopen Xenotransplantat-Tumoren der Hypoxie-resistenten Variante der Zelllinie NCI-H460 in athymischen Mäusen demonstriert werden. Außerdem zeigte sich immunhistochemisch in den Xenotransplantat-Tumoren eine Assoziation zwischen hypoxischen Arealen und erhöhter SLC25A10-Expression. Der Energiemetabolismus wurde durch die Behandlung mit BMA auf den Ebenen der Glykolyse, der mitochondrialen Atmung und der NADH-Homöostase gestört. Die Analysen *in silico* (KM Plotter) zeigten, dass eine erhöhte Expression von SLC25A10, nicht aber von SLC25A11, mit vermindertem Gesamtüberleben von Brust- und Lungentumorpatienten assoziiert ist. In Zusammenschau der genannten Ergebnisse zeigt sich, dass für SLC25A10 eine bisher unbekannte Doppel-Rolle in der Aufrechterhaltung von mitochondrialer Redox- und Energiehomöostase in Tumorzellen nachgewiesen werden

konnte. Diese scheint insbesondere im Rahmen der Adaptation von Tumorzellen an chronisch-zyklische Hypoxie wichtig zu sein, was eine neue Vulnerabilität therapieresistenter Tumorzellen darstellen würde. Eine potenzielle klinische Relevanz ergibt sich aus der demonstrierten Effektivität einer möglichen pharmakologischen Inhibition mittels BMA *in vivo* sowie der gezeigten Assoziation von erhöhter SLC25A10-Expression mit verringertem Gesamtüberleben von Tumorpatienten *in silico*.

Interessanterweise wurde nach Veröffentlichung der zweiten Originalarbeit eine weitere Strategie zur therapeutischen Beeinflussung von SLC25A10 in Tumorzellen beschrieben, da sich zeigte, dass das Biguanid Metformin die Expression von SLC25A10 in Tumorzellen negativ beeinflusst (Zhao et al., 2018). Die präklinischen Hinweise auf mögliche antineoplastische und sogar strahlensensibilisierende Effekte von Metformin, einem klinisch vielfach eingesetzten oralen Antidiabetikum, sind zahlreich. Die Ergebnisse werden allerdings in Bezug auf die klinische Bedeutsamkeit kontrovers diskutiert (Jeong et al., 2015; Najafi et al., 2018; Storozhuk et al., 2013; Sui et al., 2015). Durch den möglichen negativen Einfluss von Metformin auf die SLC25A10-Expression ließe sich in Zusammenschau mit der vorliegenden Arbeit ein Teil der antineoplastischen und insbesondere strahlensensibilisierenden Eigenschaften mechanistisch erklären. In diesem Fall käme die durch verminderte Expression herabgesetzte Transportaktivität von SLC25A10 dem Effekt einer direkten Inhibition gleich.

Außerdem konnte nach Veröffentlichung der zweiten Originalarbeit die onkogene Rolle von SLC25A10 erstmals auch in einer mesenchymalen Tumorentität demonstriert werden: Es zeigte sich eine erhöhte Expression von SLC25A10 in Gewebeproben von Osteosarkom-Patienten im Vergleich zu Normalgewebsproben, zudem war eine immunhistochemische SLC25A10-Positivität in Osteosarkomen mit einem signifikant vermindertem Gesamtüberleben der Patienten assoziiert (Wang et al., 2020). Auch diese neuen Erkenntnisse unterstreichen die Ergebnisse der vorliegenden Arbeit und deuten auch im Fall von SLC25A10 auf eine wichtige Rolle im Zusammenhang mit maligner Progression und Entstehung von Therapieresistenz über die hier untersuchten Fragestellungen mit Bezug auf Hypoxie-induzierte Strahlenresistenz hinaus.

Beide Originalarbeiten zeigen, dass Redoxhomöostase und mitochondrialer Energiemetabolismus Vulnerabilitäten Hypoxie-adaptierter Tumorzellen sind. Die Arbeiten zeigen außerdem, dass durch Inhibition Antioxidans-assoziierter mitochondrialer Transportsysteme diese beiden Faktoren über ein molekulares Ziel therapeutisch beeinflusst werden können. Dies stellt ein neuartiges, attraktives Konzept zur metabolischen Modulation der Strahlensensitivität dar.

Unklar ist sowohl für SLC25A1 als auch für SLC25A10 die bei Inhibition auftretende Normalgewebstoxizität, da insbesondere die Kombination von zielgerichteten Therapien mit weiteren Therapiemodalitäten wie Strahlentherapie zu kumulativer Toxizität führen kann (Wirsdorfer et al., 2018). Zwar zeigte die *in vivo*-Anwendung von BTA durch andere und BMA in der vorliegenden Arbeit keine Zeichen von Toxizität im Mausmodell, zur weiteren Translation wären jedoch umfassendere Untersuchungen notwendig (Catalina-Rodriguez et al., 2012; Hlouschek et al., 2018b; Kaelin, 2017). Bedeutsam zur weiteren präklinischen Validierung der Eignung von SLC25A1 oder SLC25A10 als therapeutische Angriffspunkte wäre außerdem die Überprüfung ihrer Effektivität in weiteren Tumormodellen *in vitro* oder *in vivo,* wie etwa 3D-Zellkulturen oder Chorionallantoismembran-Tests, auch in Verbindung mit Untersuchungen einer größeren Anzahl von Patientenproben (Dunker and Jendrossek, 2019; Eke and Cordes, 2011). Außerdem wäre, wie oben erwähnt, auch der Nachweis eines möglichen kausalen Zusammenhangs zwischen erhöhter Transporter-Expression und Therapieansprechen wichtig.

Unterschiedliche Effekte zwischen der Inhibition von SLC25A1 und SLC25A10 ergaben sich vor allem auf der mechanistischen Ebene. Die Inhibition von SLC25A1 mit BTA verlangsamte die DNA-Reparaturkinetik und verursacht zudem Residualschäden in Form von persistierenden γH2AX-Foci 24h nach Bestrahlung. Die Redox-Homöostase wird mit BTA insbesondere durch eine Verminderung der NADPH-Spiegel sowie eine Erhöhung des NADP+/NADPH Verhältnisses gestört. Als Konsequenz ergibt sich neben einer Verminderung des Fettsäurestoffwechsels eine Erhöhung von mROS und möglicherweise eine indirekte Verminderung von mGSH, vermittelt durch verminderte Regeneration von mGSSG durch mitochondrialen NADPH-Mangel (Hlouschek et al., 2018a). Die Inhibition von SLC25A10 mit BMA hingegen zeigte eine direkte

Verminderung von mGSH, gemessen in isolierten Mitochondrien mittels des Fluoreszenzfarbstoffs Monochlorobimane (Hlouschek et al., 2018b). Bedeutsam ist, dass die mROS-induzierenden Effekte von BMA durch artifizielle Erhöhung der zellulären und mitochondrialen GSH Spiegel oder aber durch vermehrte pharmakologische Detoxifizierung von mROS aufgehoben werden konnten. Dasselbe gilt für die Verminderung des klonogenen Zellüberlebens durch BMA-Behandlung, welches ebenfalls durch die genannten Verfahren wieder verbessert wurde.

Es liegt also nahe, dass unter den vorliegenden Modellbedingungen durch SLC25A10-Inhibition tatsächlich der mGSH-Import beeinflusst wird, wie es auch in weiteren Studien berichtet wurde (Calabrese et al., 2017; Mari et al., 2013). Dennoch gilt der mGSH-Import als nicht vollständig verstanden und scheint gewebespezifischen Unterschieden zu unterliegen, auch die Rolle von SLC25A10 wird in diesem Zusammenhang zumindest teilweise kontrovers diskutiert (Booty et al., 2015; Kamga et al., 2010; Punzi et al., 2018; Sreekumar et al., 2020; Wilkins et al., 2013). SLC25A1 und SLC25A10 fungieren in erster Linie als Antiporter für Tri- bzw. Dicarboxylate und versorgen somit unter anderem den Citratzyklus mit Substraten. Hierdurch erklären sich die vergleichbaren Effekte beider Ansätze bei Inhibition mit BTA bzw. BMA auf den mitochondrialen und zellulären Energiestoffwechsel. Zusammengefasst zeigen sich also vergleichbare Effekte beider Ansätze auf die Therapieresistenz von Tumorzellen mit Toleranz gegenüber chronisch-zyklischer Hypoxie mit geringfügigen mechanistischen Unterschieden (Abb. 1).

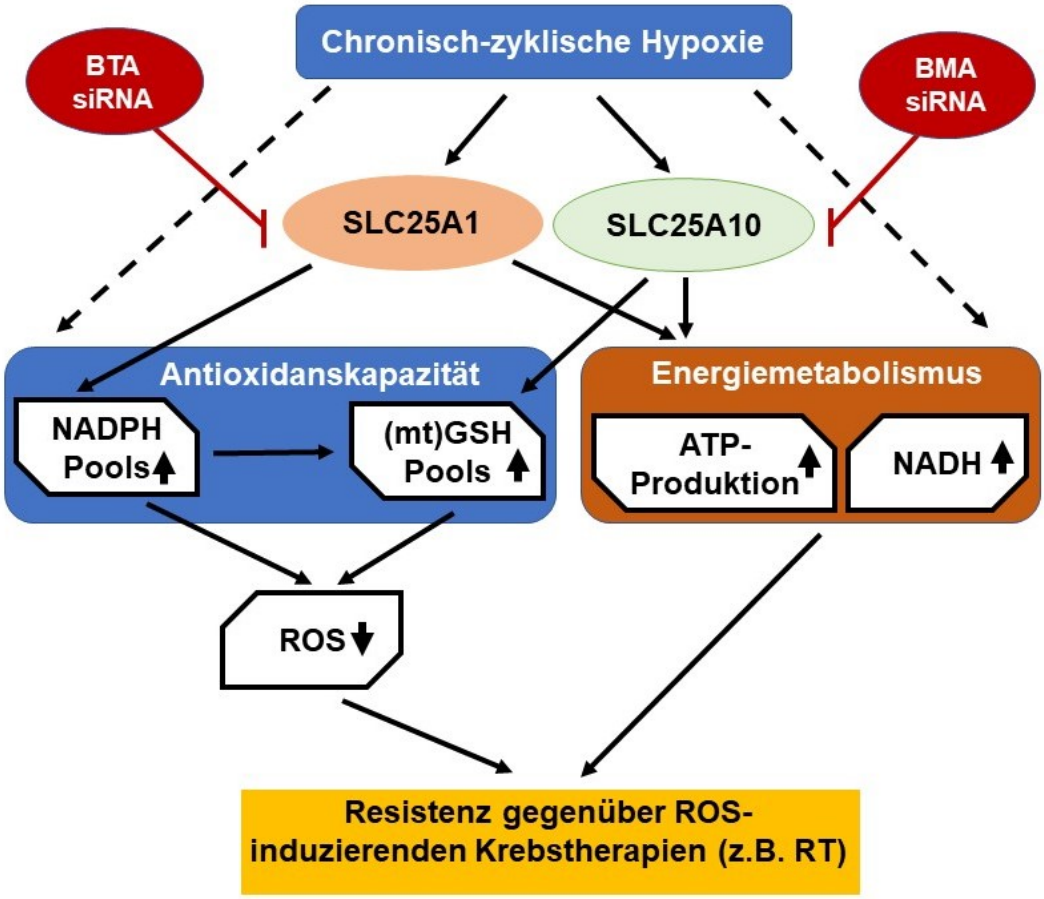

Abbildung 1: Schematische Darstellung der potenziellen Rollen von SLC25A1 und SLC25A10 im Rahmen der durch chronisch-zyklische Hypoxie induzierten Resistenzen gegenüber ROS-induzierenden Behandlungen. *Durchgezogene Linien repräsentieren direkte Effekte, gestrichelte Linien repräsentieren indirekte Effekte. BTA: 1,2,3-Benzen-Tricarboxylat; CNASB: 4-Chlor-3-[[(3-Nitrophenyl)Amino]Sulfonyl]-Benzoesäure BMA: Butylmalonat; siRNA: small interfering RNA; RT: Radiotherapie.*

Aufgrund der Tatsache, dass im Rahmen der Untersuchungen Möglichkeiten zur Überwindung der durch chronisch-zyklische Hypoxie induzierten Resistenzen geprüft werden sollten, kommt SLC25A11 eine untergeordnete Bedeutung zu. Die Hemmung von SLC25A11 war nicht effektiv genug, um die durch chronisch-zyklische Hypoxie induzierte Therapieresistenz in Tumorzellen aufzuheben und eine erhöhte Expression von SLC25A11 wirkte sich nicht signifikant auf das Gesamtüberleben von Brust- und Lungentumorpatienten aus (Hlouschek et al., 2018b). Dennoch deuten andere Untersuchungen in einem Modell des Hepatozellulären Karzinoms auf eine hohe

Relevanz von SLC25A11 als mögliches therapeutisches Ziel hin, während in diesem Kontext SLC25A10 eine geringere Rolle einzunehmen scheint (Baulies et al., 2018). Hierdurch ergeben sich Hinweise auf tumor- bzw. gewebsspezifische Unterschiede in Bezug auf die relative Bedeutung von SLC25A10 und SLC25A11 als therapeutische Ansatzpunkte zur Eradikation von Tumorzellen.

Um die Validierung der in dieser Arbeit untersuchten Carrier als potenzielle therapeutische Ansatzpunkte weiter voranzutreiben sind zukünftig weitere Untersuchungen nötig. Diese umfassen zum einen die genauere Evaluation der potenziellen Normalgewebstoxizität und zum anderen die Aufdeckung weiterer zellulärer Mechanismen infolge der Inhibition von SLC25A1 und SLC25A10, gegebenenfalls auch SLC25A11. Auch die Entwicklung spezifischerer niedermolekularer Inhibitoren stellt einen relevanten Faktor für die Weiterentwicklung dar.

Im Hinblick auf die rationale Kombination mit weiteren Therapiemodalitäten wie Strahlentherapie erscheint insbesondere die 2-HG vermittelte Inhibition der HR ein vielversprechender Ansatz, der über SLC25A1-Inhibition erreicht werden könnte (Jiang et al., 2016; Sulkowski et al., 2017; Sulkowski et al., 2020). In diesem Hinblick repräsentiert die gezielte Beeinflussung des Tumormetabolismus zur Entstehung therapiesensiblerer Phänotypen mit eingeschränkter DNA-Reparaturkapazität ein vielversprechendes Konzept zur Tumorzell-spezifischen Strahlensensibilisierung.

Insgesamt konnten durch die vorliegende Arbeit neue Ansatzpunkte zur Strahlensensibilisierung von Hypoxie-adaptierten, therapieresistenten Tumorzellen gefunden werden. Erstmals konnte gezeigt werden, dass die mitochondrialen Carrier SLC25A1 und SLC25A10 als Antioxidans-assoziierte Transportsysteme eine Rolle im Adaptationsprozess an chronisch-zyklische Hypoxie spielen und deren Inhibition die induzierten Therapieresistenzen überwinden kann. Hierbei wurde außerdem das Konzept einer Überwindung der Therapieresistenz durch duale Hemmung der Redox-Homöostase und dem Energiemetabolismus über einen einzelnen Ansatzpunkt als therapeutische Intervention an Hypoxie-resistenten Tumorzellen entwickelt. In Zukunft bedarf es weiterer Validierung der Carrier als mögliche therapeutische Ansatzpunkte, eventuell um existierende Krebstherapien für heterogene und hypoxische Tumore effektiver zu

gestalten und zusätzlich neue Therapiestrategien im fortlaufenden Kampf gegen den Krebs zu entwickeln.

Zusammenfassung (Deutsch)

Anpassungsprozesse an ein nachteiliges Tumormikromilieu treiben die Selektion chemo- und strahlenresistenter Krebszellen in soliden Tumoren voran. Daher ist die Untersuchung molekularer Determinanten, die Strahlenresistenz vermitteln und potenzielle therapeutische Schwachstellen aufdecken, eine vielversprechende Strategie zur Verbesserung der zukünftigen Krebstherapien. Frühere Ergebnisse deuteten darauf hin, dass Krebszellen, die chronisch-zyklischer Hypoxie ausgesetzt sind, aufgrund der metabolischen Reprogrammierung eine erhöhte Strahlenresistenz aufweisen, was eine Erhöhung der zellulären Antioxidans-Abwehr mit sich bringt.

In der vorliegenden Doktorarbeit wurde die Beteiligung von Antioxidans-assoziierten mitochondrialen Transportsystemen (Carrier der SLC25 Familie) an der Aufrechterhaltung der Redoxhomöostase während Adaptation von Krebszellen an akute oder chronisch-zyklische Hypoxie und damit assoziierte Strahlenresistenz untersucht.

Die Ergebnisse zeigten eine Doppelrolle von SLC25A1 und SLC25A10 bei der Unterstützung der Redoxhomöostase und des mitochondrialen Metabolismus von Krebszellen. Die Carrier unterstützten die erhöhte Strahlenresistenz von Krebszellen mit Toleranz gegenüber chronisch-zyklischer Hypoxie durch unterschiedliche Mechanismen. Während SLC25A1 das Redoxgleichgewicht durch Regulierung der mitochondrialen Glutathion (GSH)-Regeneration über NADPH aufrechterhielt, verlangsamte seine Hemmung zusätzlich die Reparatur von durch strahleninduzierten DNA-Schäden, die mit der Akkumulation des Onkometaboliten 2-Hydroxyglutarat (2HG) verbunden waren. Im Gegensatz dazu war SLC25A10 am Transport von GSH in die Mitochondrien beteiligt, und die Proteinexpression korrelierte mit hypoxischen Regionen innerhalb von Xenotransplantat-Tumoren in athymischen Mäusen. Die Hemmung von SLC25A10 induzierte zudem eine Wachstumsverzögerung von strahlenresistenten Xenotransplantat-Tumoren aus durch chronisch-zyklische Hypoxie selektionierten Zellen.

Insgesamt zeigen die Ergebnisse dieser Arbeit neue Mechanismen der Hypoxie-induzierten Therapieresistenz mit potenzieller klinischer Relevanz für das Patientenüberleben und deuten eine neue Strategie für therapeutische Interventionen in soliden Tumoren mit hypoxischen Zellfraktionen an.

Zusammenfassung (Englisch)

Adaptation processes to an adverse tumor microenvironment drive selection of chemo- and radioresistant cancer cells in solid tumors. Therefore, exploring molecular determinants which mediate radioresistance and uncovering potential therapeutic vulnerabilities represent a promising strategy to improve anticancer therapies in the future. Previous findings of our group suggested that cancer cells exposed to chronic-cycling hypoxia display increased radioresistance due to metabolic reprogramming, involving an increase of the cellular antioxidant defence.

In the present doctoral thesis, the involvement of antioxidant-associated mitochondrial transport systems (carriers of the SLC25 family) in maintenance of redox homeostasis during adaptation of cancer cells to acute or chronic-cycling hypoxia and associated radioresistance was examined.

These findings revealed a dual role of SLC25A1 as well as SLC25A10 in supporting both, redox homeostasis and mitochondrial metabolism of cancer cells. Of note, the carriers contributed to enhanced radioresistance of cancer cells with tolerance to chronic-cycling hypoxia by distinctive mechanisms. Whereas SLC25A1 sustained redox balance by regulating mitochondrial glutathione (GSH) regeneration via NADPH, its inhibition additionally slowed repair of DNA damage induced by ionizing radiation, which was associated with accumulation of the oncometabolite 2-hydroxyglutarate (2HG). In contrast, SLC25A10 was involved in the transport of GSH into the mitochondria and its protein expression correlated with hypoxic regions within xenograft tumors in athymic mice. Inhibition of SLC25A10 efficiently induced growth retardation of radioresistant xenograft tumors from chronic-cycling hypoxia-selected cells.

Taken together, the findings of this thesis reveal novel mechanisms of hypoxia-induced therapy resistance with potential clinical relevance regarding patient survival and propose a novel strategy for therapeutic interventions in solid tumors with hypoxic cell fractions.

Literaturverzeichnis

(Anmerkung: Weitere Literaturangaben finden sich in den jeweiligen Originalarbeiten)

1. Abrego, J., Gunda, V., Vernucci, E., Shukla, S.K., King, R.J., Dasgupta, A., Goode, G., Murthy, D., Yu, F., and Singh, P.K. (2017). GOT1-mediated anaplerotic glutamine metabolism regulates chronic acidosis stress in pancreatic cancer cells. Cancer Lett *400*, 37-46.
2. Bader, S.B., Dewhirst, M.W., and Hammond, E.M. (2020). Cyclic Hypoxia: An Update on Its Characteristics, Methods to Measure It and Biological Implications in Cancer. Cancers (Basel) *13*.
3. Baulies, A., Montero, J., Matias, N., Insausti, N., Terrones, O., Basanez, G., Vallejo, C., Conde de La Rosa, L., Martinez, L., Robles, D., Morales, A., Abian, J., Carrascal, M., Machida, K., Kumar, D.B.U., Tsukamoto, H., Kaplowitz, N., Garcia-Ruiz, C., and Fernandez-Checa, J.C. (2018). The 2-oxoglutarate carrier promotes liver cancer by sustaining mitochondrial GSH despite cholesterol loading. Redox Biol *14*, 164-177.
4. Begg, A.C., Stewart, F.A., and Vens, C. (2011). Strategies to improve radiotherapy with targeted drugs. Nat Rev Cancer *11*, 239-253.
5. Bock, F.J., and Tait, S.W.G. (2019). Mitochondria as multifaceted regulators of cell death. Nat Rev Mol Cell Biol.
6. Booty, L.M., King, M.S., Thangaratnarajah, C., Majd, H., James, A.M., Kunji, E.R., and Murphy, M.P. (2015). The mitochondrial dicarboxylate and 2-oxoglutarate carriers do not transport glutathione. FEBS Lett *589*, 621-628.
7. Bristow, R.G., and Hill, R.P. (2008). Hypoxia and metabolism. Hypoxia, DNA repair and genetic instability. Nat Rev Cancer *8*, 180-192.
8. Cairns, R.A., Harris, I.S., and Mak, T.W. (2011). Regulation of cancer cell metabolism. Nat Rev Cancer *11*, 85-95.
9. Calabrese, G., Morgan, B., and Riemer, J. (2017). Mitochondrial Glutathione: Regulation and Functions. Antioxid Redox Signal *27*, 1162-1177.
10. Catalina-Rodriguez, O., Kolukula, V.K., Tomita, Y., Preet, A., Palmieri, F., Wellstein, A., Byers, S., Giaccia, A.J., Glasgow, E., Albanese, C., and

Avantaggiati, M.L. (2012). The mitochondrial citrate transporter, CIC, is essential for mitochondrial homeostasis. Oncotarget *3*, 1220-1235.

11. Chandel, N.S. (2015). Evolution of Mitochondria as Signaling Organelles. Cell Metab *22*, 204-206.
12. Citrin, D.E. (2017). Recent Developments in Radiotherapy. N Engl J Med *377*, 1065-1075.
13. Curcio, R., Lunetti, P., Zara, V., Ferramosca, A., Marra, F., Fiermonte, G., Cappello, A.R., De Leonardis, F., Capobianco, L., and Dolce, V. (2020). Drosophila melanogaster Mitochondrial Carriers: Similarities and Differences with the Human Carriers. Int J Mol Sci *21*.
14. DeBerardinis, R.J., and Chandel, N.S. (2016). Fundamentals of cancer metabolism. Sci Adv *2*, e1600200.
15. Dewhirst, M.W., Cao, Y., and Moeller, B. (2008). Cycling hypoxia and free radicals regulate angiogenesis and radiotherapy response. Nat Rev Cancer *8*, 425-437.
16. Dunker, N., and Jendrossek, V. (2019). Implementation of the Chick Chorioallantoic Membrane (CAM) Model in Radiation Biology and Experimental Radiation Oncology Research. Cancers (Basel) *11*.
17. Eke, I., and Cordes, N. (2011). Radiobiology goes 3D: how ECM and cell morphology impact on cell survival after irradiation. Radiother Oncol *99*, 271-278.
18. Ferlay, J., Colombet, M., Soerjomataram, I., Dyba, T., Randi, G., Bettio, M., Gavin, A., Visser, O., and Bray, F. (2018). Cancer incidence and mortality patterns in Europe: Estimates for 40 countries and 25 major cancers in 2018. Eur J Cancer *103*, 356-387.
19. Fernandez, H.R., Gadre, S.M., Tan, M., Graham, G.T., Mosaoa, R., Ongkeko, M.S., Kim, K.A., Riggins, R.B., Parasido, E., Petrini, I., Pacini, S., Cheema, A., Varghese, R., Ressom, H.W., Zhang, Y., Albanese, C., Uren, A., Paige, M., Giaccone, G., and Avantaggiati, M.L. (2018). The mitochondrial citrate carrier, SLC25A1, drives stemness and therapy resistance in non-small cell lung cancer. Cell Death Differ.

20. Flavahan, W.A., Gaskell, E., and Bernstein, B.E. (2017). Epigenetic plasticity and the hallmarks of cancer. Science *357*.
21. Gagne, L.M., Boulay, K., Topisirovic, I., Huot, M.E., and Mallette, F.A. (2017). Oncogenic Activities of IDH1/2 Mutations: From Epigenetics to Cellular Signaling. Trends Cell Biol *27*, 738-752.
22. Gottgens, E.L., van den Heuvel, C.N., de Jong, M.C., Kaanders, J.H., Leenders, W.P., Ansems, M., Bussink, J., and Span, P.N. (2019). ACLY (ATP Citrate Lyase) Mediates Radioresistance in Head and Neck Squamous Cell Carcinomas and is a Novel Predictive Radiotherapy Biomarker. Cancers (Basel) *11*.
23. Hanahan, D., and Weinberg, R.A. (2011). Hallmarks of cancer: the next generation. Cell *144*, 646-674.
24. Handy, D.E., and Loscalzo, J. (2012). Redox regulation of mitochondrial function. Antioxid Redox Signal *16*, 1323-1367.
25. Harris, A.L. (2002). Hypoxia--a key regulatory factor in tumour growth. Nat Rev Cancer *2*, 38-47.
26. Hatem, E., El Banna, N., and Huang, M.E. (2017). Multifaceted Roles of Glutathione and Glutathione-Based Systems in Carcinogenesis and Anticancer Drug Resistance. Antioxid Redox Signal *27*, 1217-1234.
27. Hlouschek, J., Hansel, C., Jendrossek, V., and Matschke, J. (2018a). The Mitochondrial Citrate Carrier (SLC25A1) Sustains Redox Homeostasis and Mitochondrial Metabolism Supporting Radioresistance of Cancer Cells With Tolerance to Cycling Severe Hypoxia. Front Oncol *8*, 170.
28. Hlouschek, J., Ritter, V., Wirsdorfer, F., Klein, D., Jendrossek, V., and Matschke, J. (2018b). Targeting SLC25A10 alleviates improved antioxidant capacity and associated radioresistance of cancer cells induced by chronic-cycling hypoxia. Cancer Lett *439*, 24-38.
29. Hoeller, U., Borgmann, K., Oertel, M., Haverkamp, U., Budach, V., and Eich, H.T. (2021). Late sequelae of radiotherapy—the effect of technical and conceptual innovations in radiation oncology. Deutsches Aerzteblatt Online.
30. Horsman, M.R., Mortensen, L.S., Petersen, J.B., Busk, M., and Overgaard, J. (2012). Imaging hypoxia to improve radiotherapy outcome. Nat Rev Clin Oncol *9*, 674-687.

31. Jendrossek, V. (2012). The Intrinsic Apoptosis Pathways as a Target in Anticancer Therapy. Current Pharmaceutical Biotechnology *13*, 1426-1438.
32. Jeong, Y.K., Kim, M.S., Lee, J.Y., Kim, E.H., and Ha, H. (2015). Metformin Radiosensitizes p53-Deficient Colorectal Cancer Cells through Induction of G2/M Arrest and Inhibition of DNA Repair Proteins. PLoS One *10*, e0143596.
33. Jiang, H., Wang, H., and De Ridder, M. (2018). Targeting antioxidant enzymes as a radiosensitizing strategy. Cancer Lett *438*, 154-164.
34. Jiang, L., Boufersaoui, A., Yang, C., Ko, B., Rakheja, D., Guevara, G., Hu, Z., and DeBerardinis, R.J. (2017). Quantitative metabolic flux analysis reveals an unconventional pathway of fatty acid synthesis in cancer cells deficient for the mitochondrial citrate transport protein. Metab Eng *43*, 198-207.
35. Jiang, L., Shestov, A.A., Swain, P., Yang, C., Parker, S.J., Wang, Q.A., Terada, L.S., Adams, N.D., McCabe, M.T., Pietrak, B., Schmidt, S., Metallo, C.M., Dranka, B.P., Schwartz, B., and DeBerardinis, R.J. (2016). Reductive carboxylation supports redox homeostasis during anchorage-independent growth. Nature *532*, 255-258.
36. Kaelin, W.G., Jr. (2017). Common pitfalls in preclinical cancer target validation. Nat Rev Cancer *17*, 425-440.
37. Kamga, C.K., Zhang, S.X., and Wang, Y. (2010). Dicarboxylate carrier-mediated glutathione transport is essential for reactive oxygen species homeostasis and normal respiration in rat brain mitochondria. Am J Physiol Cell Physiol *299*, C497-505.
38. Kim, H., Lin, Q., and Yun, Z. (2018). The hypoxic tumor microenvironment in vivo selects tumor cells with increased survival against genotoxic stresses. Cancer Lett *431*, 142-149.
39. Kolukula, V.K., Sahu, G., Wellstein, A., Rodriguez, O.C., Preet, A., Iacobazzi, V., D'Orazi, G., Albanese, C., Palmieri, F., and Avantaggiati, M.L. (2014). SLC25A1, or CIC, is a novel transcriptional target of mutant p53 and a negative tumor prognostic marker. Oncotarget *5*.
40. Lee, C.T., Boss, M.K., and Dewhirst, M.W. (2014). Imaging tumor hypoxia to advance radiation oncology. Antioxid Redox Signal *21*, 313-337.

41. Li, H., Hurlburt, A.J., and Tennessen, J.M. (2018). A Drosophila model of combined D-2- and L-2-hydroxyglutaric aciduria reveals a mechanism linking mitochondrial citrate export with oncometabolite accumulation. Dis Model Mech.
42. Liauw, S.L., Connell, P.P., and Weichselbaum, R.R. (2013). New paradigms and future challenges in radiation oncology: an update of biological targets and technology. Sci Transl Med *5*, 173sr172.
43. Liu, J., Luo, X., Guo, R., Jing, W., and Lu, H. (2020a). Cell Metabolomics Reveals Berberine-Inhibited Pancreatic Cancer Cell Viability and Metastasis by Regulating Citrate Metabolism. J Proteome Res *19*, 3825-3836.
44. Liu, S., Zhang, D., Chen, L., Gao, S., and Huang, X. (2020b). Long non-coding RNA BRM promotes proliferation and invasion of papillary thyroid carcinoma by regulating the microRNA-331-3p/SLC25A1 axis. Oncol Lett *19*, 3071-3078.
45. Lytovchenko, O., and Kunji, E.R.S. (2017). Expression and putative role of mitochondrial transport proteins in cancer. Biochim Biophys Acta *1858*, 641-654.
46. Mari, M., Morales, A., Colell, A., Garcia-Ruiz, C., Kaplowitz, N., and Fernandez-Checa, J.C. (2013). Mitochondrial glutathione: features, regulation and role in disease. Biochim Biophys Acta *1830*, 3317-3328.
47. Matschke, J., Riffkin, H., Klein, D., Handrick, R., Ludemann, L., Metzen, E., Shlomi, T., Stuschke, M., and Jendrossek, V. (2016). Targeted Inhibition of Glutamine-Dependent Glutathione Metabolism Overcomes Death Resistance Induced by Chronic Cycling Hypoxia. Antioxid Redox Signal *25*, 89-107.
48. Matsumoto, S., Yasui, H., Mitchell, J.B., and Krishna, M.C. (2010). Imaging cycling tumor hypoxia. Cancer Res *70*, 10019-10023.
49. Missiroli, S., Perrone, M., Genovese, I., Pinton, P., and Giorgi, C. (2020). Cancer metabolism and mitochondria: Finding novel mechanisms to fight tumours. EBioMedicine *59*, 102943.
50. Mosaoa, R., Kasprzyk-Pawelec, A., Fernandez, H.R., and Avantaggiati, M.L. (2021). The Mitochondrial Citrate Carrier SLC25A1/CIC and the Fundamental Role of Citrate in Cancer, Inflammation and Beyond. Biomolecules *11*.

51. Najafi, M., Cheki, M., Rezapoor, S., Geraily, G., Motevaseli, E., Carnovale, C., Clementi, E., and Shirazi, A. (2018). Metformin: Prevention of genomic instability and cancer: A review. Mutat Res *827*, 1-8.
52. Nakashima, R., Goto, Y., Koyasu, S., Kobayashi, M., Morinibu, A., Yoshimura, M., Hiraoka, M., Hammond, E.M., and Harada, H. (2017). UCHL1-HIF-1 axis-mediated antioxidant property of cancer cells as a therapeutic target for radiosensitization. Sci Rep *7*, 6879.
53. Palmieri, F. (2014). Mitochondrial transporters of the SLC25 family and associated diseases: a review. J Inherit Metab Dis *37*, 565-575.
54. Powell, S.N., and Bindra, R.S. (2009). Targeting the DNA damage response for cancer therapy. DNA Repair (Amst) *8*, 1153-1165.
55. Punzi, G., Porcelli, V., Ruggiu, M., Hossain, M.F., Menga, A., Scarcia, P., Castegna, A., Gorgoglione, R., Pierri, C.L., Laera, L., Lasorsa, F.M., Paradies, E., Pisano, I., Marobbio, C.M.T., Lamantea, E., Ghezzi, D., Tiranti, V., Giannattasio, S., Donati, M.A., Guerrini, R., Palmieri, L., Palmieri, F., and De Grassi, A. (2018). SLC25A10 biallelic mutations in intractable epileptic encephalopathy with complex I deficiency. Hum Mol Genet *27*, 499-504.
56. Quante, A.S., Ming, C., Rottmann, M., Engel, J., Boeck, S., Heinemann, V., Westphalen, C.B., and Strauch, K. (2016). Projections of cancer incidence and cancer-related deaths in Germany by 2020 and 2030. Cancer Med *5*, 2649-2656.
57. Ribas, V., Garcia-Ruiz, C., and Fernandez-Checa, J.C. (2014). Glutathione and mitochondria. Front Pharmacol *5*, 151.
58. Rochette, L., Meloux, A., Zeller, M., Malka, G., Cottin, Y., and Vergely, C. (2020). Mitochondrial SLC25 Carriers: Novel Targets for Cancer Therapy. Molecules *25*.
59. Rouschop, K.M., Dubois, L.J., Keulers, T.G., van den Beucken, T., Lambin, P., Bussink, J., van der Kogel, A.J., Koritzinsky, M., and Wouters, B.G. (2013). PERK/eIF2alpha signaling protects therapy resistant hypoxic cells through induction of glutathione synthesis and protection against ROS. Proc Natl Acad Sci U S A *110*, 4622-4627.

60. Salem, A., Asselin, M.C., Reymen, B., Jackson, A., Lambin, P., West, C.M.L., O'Connor, J.P.B., and Faivre-Finn, C. (2018). Targeting Hypoxia to Improve Non-Small Cell Lung Cancer Outcome. J Natl Cancer Inst *110*.
61. Schipler, A., and Iliakis, G. (2013). DNA double-strand-break complexity levels and their possible contributions to the probability for error-prone processing and repair pathway choice. Nucleic Acids Res *41*, 7589-7605.
62. Siegel, R.L., Miller, K.D., and Jemal, A. (2018). Cancer statistics, 2018. CA Cancer J Clin *68*, 7-30.
63. Span, P.N., and Bussink, J. (2015). Biology of hypoxia. Semin Nucl Med *45*, 101-109.
64. Sreekumar, P.G., Wang, M., Spee, C., Sadda, S.R., and Kannan, R. (2020). Transporter-Mediated Mitochondrial GSH Depletion Leading to Mitochondrial Dysfunction and Rescue with alphaB Crystallin Peptide in RPE Cells. Antioxidants (Basel) *9*.
65. Storozhuk, Y., Hopmans, S.N., Sanli, T., Barron, C., Tsiani, E., Cutz, J.C., Pond, G., Wright, J., Singh, G., and Tsakiridis, T. (2013). Metformin inhibits growth and enhances radiation response of non-small cell lung cancer (NSCLC) through ATM and AMPK. Br J Cancer *108*, 2021-2032.
66. Sui, X., Xu, Y., Wang, X., Han, W., Pan, H., and Xiao, M. (2015). Metformin: A Novel but Controversial Drug in Cancer Prevention and Treatment. Mol Pharm *12*, 3783-3791.
67. Sulkowski, P.L., Corso, C.D., Robinson, N.D., Scanlon, S.E., Purshouse, K.R., Bai, H., Liu, Y., Sundaram, R.K., Hegan, D.C., Fons, N.R., Breuer, G.A., Song, Y., Mishra-Gorur, K., De Feyter, H.M., de Graaf, R.A., Surovtseva, Y.V., Kachman, M., Halene, S., Gunel, M., Glazer, P.M., and Bindra, R.S. (2017). 2-Hydroxyglutarate produced by neomorphic IDH mutations suppresses homologous recombination and induces PARP inhibitor sensitivity. Sci Transl Med *9*.
68. Sulkowski, P.L., Oeck, S., Dow, J., Economos, N.G., Mirfakhraie, L., Liu, Y., Noronha, K., Bao, X., Li, J., Shuch, B.M., King, M.C., Bindra, R.S., and Glazer, P.M. (2020). Oncometabolites suppress DNA repair by disrupting local chromatin signalling. Nature *582*, 586-591.

69. Sulkowski, P.L., Sundaram, R.K., Oeck, S., Corso, C.D., Liu, Y., Noorbakhsh, S., Niger, M., Boeke, M., Ueno, D., Kalathil, A.N., Bao, X., Li, J., Shuch, B., Bindra, R.S., and Glazer, P.M. (2018). Krebs-cycle-deficient hereditary cancer syndromes are defined by defects in homologous-recombination DNA repair. Nature Genetics.
70. Tan, M., Mosaoa, R., Graham, G.T., Kasprzyk-Pawelec, A., Gadre, S., Parasido, E., Catalina-Rodriguez, O., Foley, P., Giaccone, G., Cheema, A., Kallakury, B., Albanese, C., Yi, C., and Avantaggiati, M.L. (2020). Inhibition of the mitochondrial citrate carrier, Slc25a1, reverts steatosis, glucose intolerance, and inflammation in preclinical models of NAFLD/NASH. Cell Death & Differentiation.
71. Torre, L.A., Siegel, R.L., Ward, E.M., and Jemal, A. (2016). Global Cancer Incidence and Mortality Rates and Trends--An Update. Cancer Epidemiol Biomarkers Prev *25*, 16-27.
72. Torres, S., Matias, N., Baulies, A., Nunez, S., Alarcon-Vila, C., Martinez, L., Nuno, N., Fernandez, A., Caballeria, J., Levade, T., Gonzalez-Franquesa, A., Garcia-Roves, P., Balboa, E., Zanlungo, S., Fabrias, G., Casas, J., Enrich, C., Garcia-Ruiz, C., and Fernandez-Checa, J.C. (2017). Mitochondrial GSH replenishment as a potential therapeutic approach for Niemann Pick type C disease. Redox Biol *11*, 60-72.
73. van der Mijn, J.C., Panka, D.J., Geissler, A.K., Verheul, H.M., and Mier, J.W. (2016). Novel drugs that target the metabolic reprogramming in renal cell cancer. Cancer Metab *4*, 14.
74. Vasan, K., Werner, M., and Chandel, N.S. (2020). Mitochondrial Metabolism as a Target for Cancer Therapy. Cell Metab *32*, 341-352.
75. Vaupel, P. (2004). Tumor microenvironmental physiology and its implications for radiation oncology. Semin Radiat Oncol *14*, 198-206.
76. Vaupel, P., and Harrison, L. (2004). Tumor hypoxia: causative factors, compensatory mechanisms, and cellular response. Oncologist *9 Suppl 5*, 4-9.
77. von Montfort, C., Matias, N., Fernandez, A., Fucho, R., Conde de la Rosa, L., Martinez-Chantar, M.L., Mato, J.M., Machida, K., Tsukamoto, H., Murphy, M.P., Mansouri, A., Kaplowitz, N., Garcia-Ruiz, C., and Fernandez-Checa, J.C.

(2012). Mitochondrial GSH determines the toxic or therapeutic potential of superoxide scavenging in steatohepatitis. J Hepatol *57*, 852-859.

78. Wang, G., Xia, J., Chen, C., Qiu, J., Sun, P., Peng, Z., Chen, X., and Xu, B. (2020). SLC25A10 performs an oncogenic role in human osteosarcoma. Oncol Lett *20*, 2.
79. Wang, H., Jiang, H., Van De Gucht, M., and De Ridder, M. (2019). Hypoxic Radioresistance: Can ROS Be the Key to Overcome It? Cancers (Basel) *11*.
80. Weinmann, M., Belka, C., Guner, D., Goecke, B., Muller, I., Bamberg, M., and Jendrossek, V. (2005). Array-based comparative gene expression analysis of tumor cells with increased apoptosis resistance after hypoxic selection. Oncogene *24*, 5914-5922.
81. Weinmann, M., Jendrossek, V., Guner, D., Goecke, B., and Belka, C. (2004). Cyclic exposure to hypoxia and reoxygenation selects for tumor cells with defects in mitochondrial apoptotic pathways. FASEB J *18*, 1906-1908.
82. Wilkins, H.M., Kirchhof, D., Manning, E., Joseph, J.W., and Linseman, D.A. (2013). Mitochondrial glutathione transport is a key determinant of neuronal susceptibility to oxidative and nitrosative stress. J Biol Chem *288*, 5091-5101.
83. Wirsdorfer, F., de Leve, S., and Jendrossek, V. (2018). Combining Radiotherapy and Immunotherapy in Lung Cancer: Can We Expect Limitations Due to Altered Normal Tissue Toxicity? Int J Mol Sci *20*.
84. Xiang, K., Jendrossek, V., and Matschke, J. (2020). Oncometabolites and the response to radiotherapy. Radiat Oncol *15*, 197.
85. Zeng, W., Liu, P., Pan, W., Singh, S.R., and Wei, Y. (2015). Hypoxia and hypoxia inducible factors in tumor metabolism. Cancer Lett *356*, 263-267.
86. Zhao, Q., Zhou, X., Curbo, S., and Karlsson, A. (2018). Metformin downregulates the mitochondrial carrier SLC25A10 in a glucose dependent manner. Biochem Pharmacol *156*, 444-450.
87. Zhou, X., Paredes, J.A., Krishnan, S., Curbo, S., and Karlsson, A. (2015). The mitochondrial carrier SLC25A10 regulates cancer cell growth. Oncotarget *6*, 9271-9283.
88. Zong, W.X., Rabinowitz, J.D., and White, E. (2016). Mitochondria and Cancer. Mol Cell *61*, 667-676.

Anhang

Supplement Originalarbeit 1: Hlouschek et al. (2018) Front Oncol 8, 170.

frontiers

Supplementary Material

The mitochondrial citrate carrier (SLC25A1) sustains redox homeostasis and mitochondrial metabolism supporting radioresistance of cancer cells with tolerance to cycling severe hypoxia.

Julian Hlouschek, Christine Hansel, Verena Jendrossek, Johann Matschke

*** Correspondence:**

Dr. Johann Matschke, Institute of Cell Biology (Cancer Research), University of Duisburg-Essen, University Hospital Essen, Essen, Germany
johann.matschke@uk-essen.de

1.1 Supplementary Figures

Supplementary Material

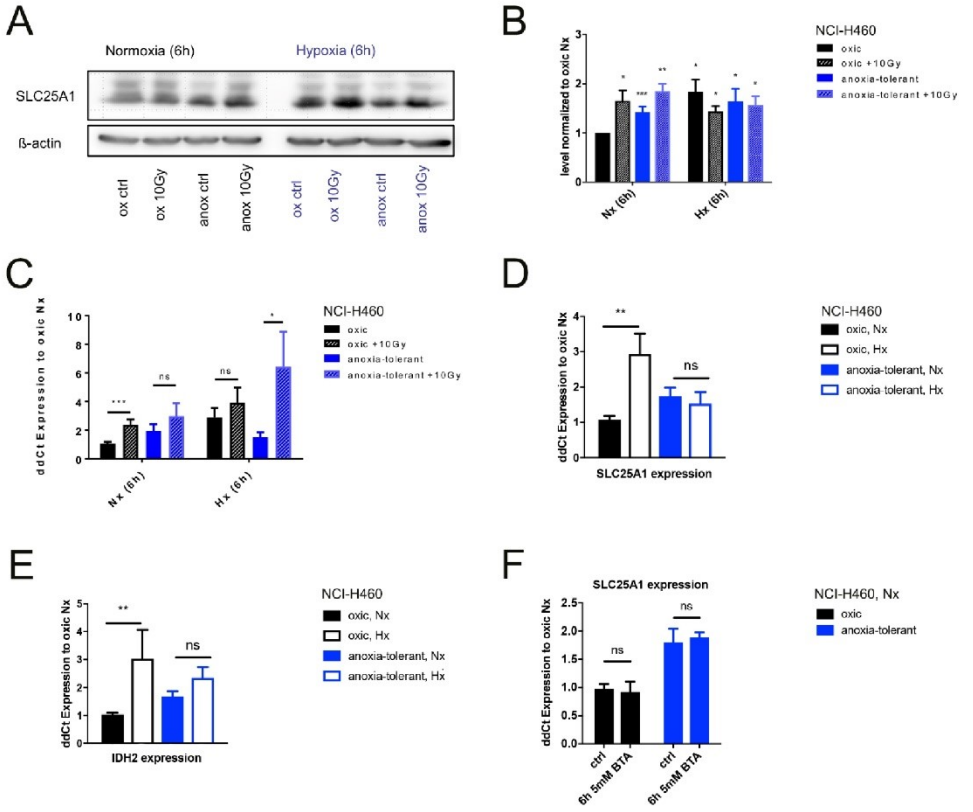

Supplementary Figure 1. Anoxia-tolerant NCI-H460 cells (anox) and oxic NCI-H460 control cells (ox) were cultured in normoxia (20% O_2) or severe hypoxia (0.2% O_2), irradiated and collected 6h after irradiation for the generation of cell lysates. A) Data show representative Western blots detecting the amount of SLC25A1 protein in lysates in cells cultured upon above mentioned conditions. B) Quantification of relative SLC25A1 protein expression detected by Western blot analyses. Comparisons to oxic Nx control are indicated above each bar. C) qRT-PCR validation of *SLC25A1* expression levels 6h after IR with 10Gy under normoxic (Nx, 20% O_2) and hypoxic (Hx, 0.2% O_2) conditions. D) Comparison of SLC25A1 expression upon 6h of exposure to hypoxia (Hx) compared to oxic Nx control determined by qRT-PCR. E) Comparison of IDH2 expression upon 24h of exposure to hypoxia (Hx) compared to oxic Nx control determined by qRT-PCR. F) Comparison of SLC25A1 expression upon 6h of treatment with 5mM BTA under normoxic (Nx) conditions compared to oxic Nx control determined by qRT-PCR. Mean values ±SEM are shown, n=3 (ns $p>0.05$, * $p\leq0.05$, ** $p < 0.01$, *** $p\leq0.001$; t-test).

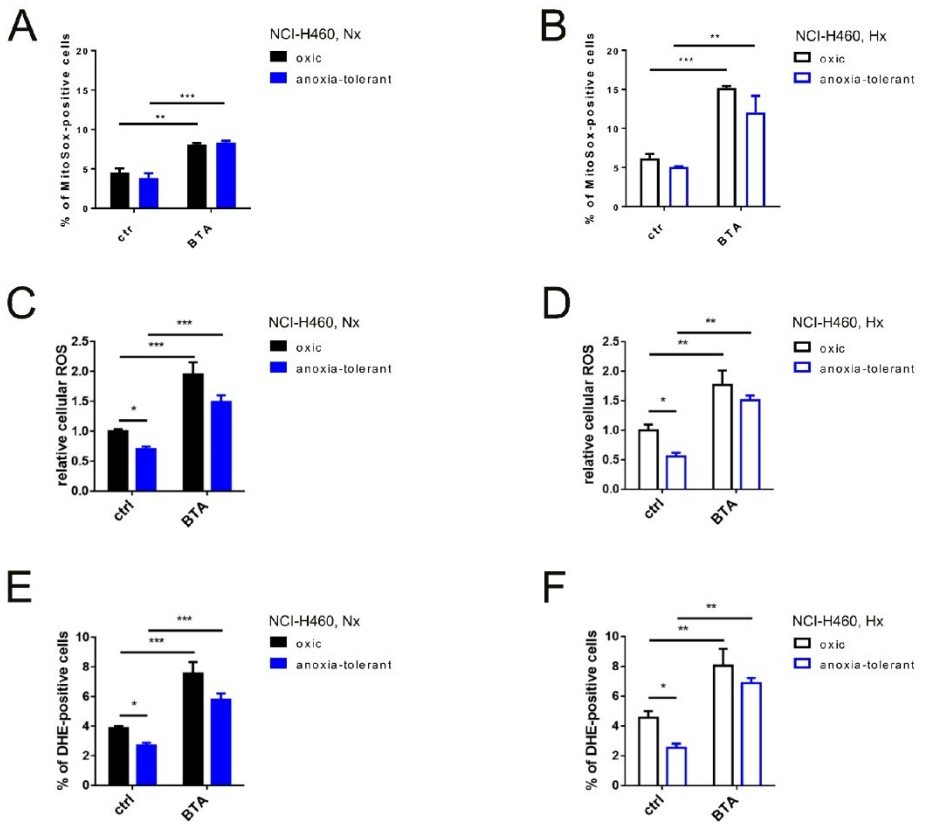

Supplementary Figure 2. NCI-H460 oxic and anoxia-tolerant cells were treated with 5mM BTA under normoxic (20% O_2) or hypoxic conditions (0.2% O_2), and mitochondrial superoxide reactive oxygen species (ROS) or cellular ROS were determined by flow cytometry upon cell staining with MitoSox or DHE. A) Mitochondrial ROS (Fraction (%) of gated MitoSox-positive cells) induced by 6h of BTA treatment in normoxia (Nx) B) Mitochondrial ROS (Fraction (%) of gated MitoSox-positive cells) induced by 6h of BTA treatment in hypoxia (Hx). C) Cellular ROS (relative to oxic control) induced by 24h of BTA treatment in normoxia (Nx) D) Cellular ROS (relative to oxic control) induced by 24h of BTA treatment in hypoxia (Hx). E) Cellular ROS (Fraction (%) of gated DHE-positive cells) induced by 24h of BTA treatment in normoxia (Nx) F) Cellular ROS (Fraction (%) of DHE-gated positive cells) induced by 24h of BTA treatment in hypoxia (Hx). Fraction (%) of gated positive cells (at least 10.000) are indicated. Mean values ±SEM are shown, n=3 (* $p \leq 0.05$, ** $p < 0.01$, *** $p \leq 0.001$; two-way ANOVA with Tukey post-test).

3

Supplementary Material

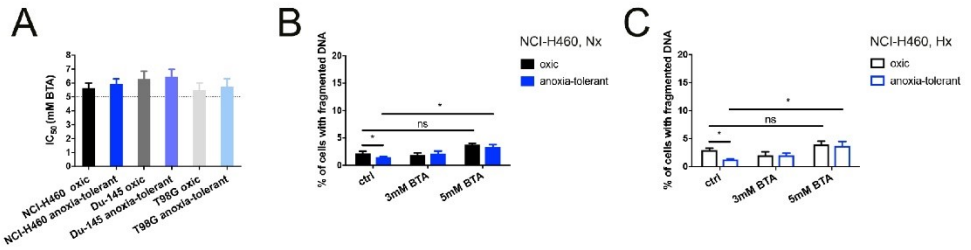

Supplementary Figure 3. Oxic and anoxia-tolerant cells were treated for 72h with different concentrations of BTA under normoxic (20% O_2) or hypoxic conditions (0.2% O_2). Apoptotic cells with fragmented DNA were determined by flow cytometry and proliferation or cell viability were determinded by crystal violet staining. A) Inhibitory concentrations of 50% proliferation reduction (IC_{50}) were determined by crystal violet staining under normoxia. B) NCI-H460 oxic and anoxia-tolerant cells with fragmented DNA upon BTA treatment in normoxia (Nx) were determined by flow cytometry. C) NCI-H460 oxic and anoxia-tolerant cells with fragmented DNA upon BTA treatment in hypoxia (Hx) were determined by flow cytometry. Fraction (%) of gated positive cells (at least 10.000) are indicated. Mean values ±SEM are shown, n=3 (* $p \leq 0.05$, ** $p < 0.01$, *** $p \leq 0.001$; two-way ANOVA with Tukey post-test).

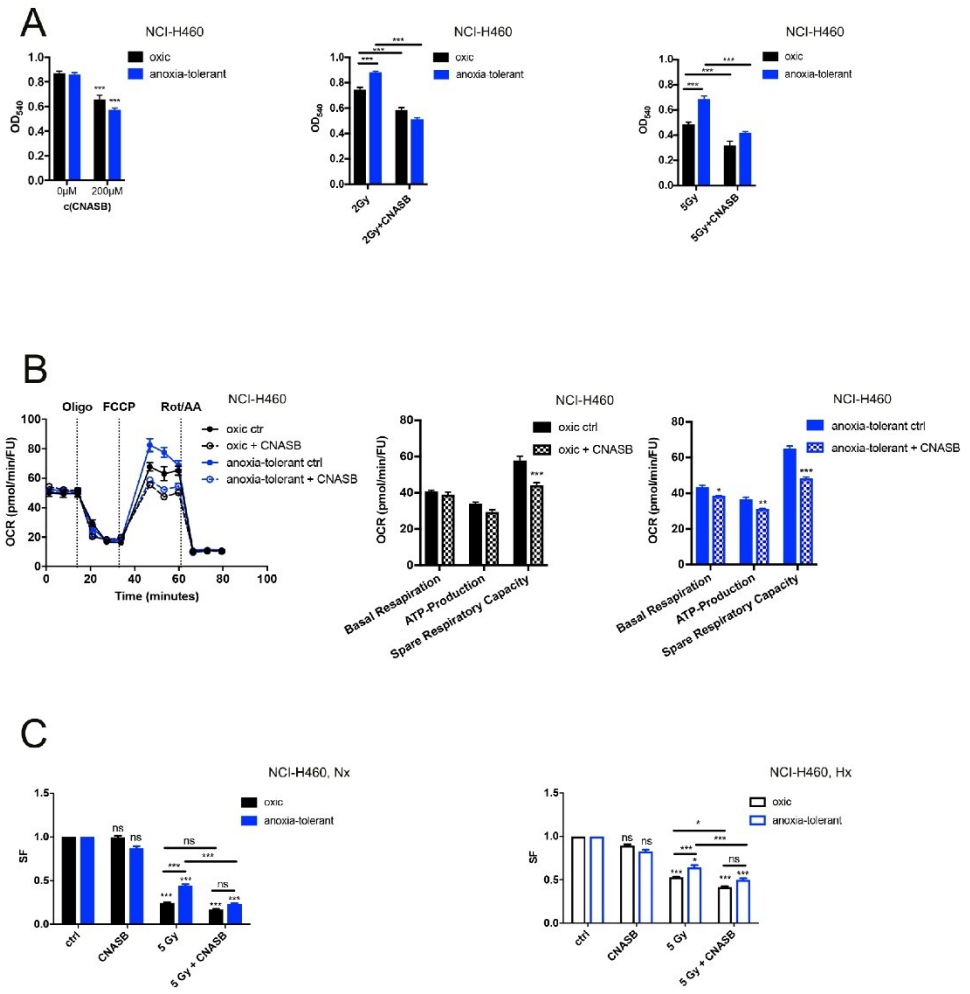

Supplementary Figure 4. NCI-H460 oxic and anoxia-tolerant cells were treated with 200µM of 4-Chloro-3-[[(3-nitrophenyl)amino]sulfonyl]-benzoic acid (CNASB), Inhibitor of SLC25A1 under normoxic (Nx, 20% O_2) or hypoxic conditions (Hx, 0.2% O_2)). In case of combined treatment with ionizing radiation (IR), 2h of pretreatment CNASB were performed. A) Influence of CNASB alone or in combination with IR on cell proliferation after 72h were determined by crystal violet staining and measurement of optic density at 540nm (OD_{540}) after cell-lysis. B) Oxygen consumption rate (OCR) normalized to Hoechst 33342 fluorescence units (FU) 24h after treatment with CNASB was measured using Seahorse XFe 96 analyzer and Mito Stress Test Kit. Real-time Injection of Oligomycin (Oligo, 1µM), Carbonyl cyanide-*4*-(trifluoromethoxy)phenylhydrazone (FCCP, 2µM), Rotenone (Rot, 0.5µM) and Antimycin A (AA, 0.5µM). Calculated parameters of the assay are indicated in bar graphs. C) Anoxia-tolerant NCI-H460 cells and the oxic NCI-H460 control cells were pretreated with 200µM

Supplementary Material

BTA (2h prior to IR) under normoxic condition (Nx, 20% O_2) or upon 2h pre-incubation in severe hypoxia (Hx, 0.2% O_2). 24h after treatment cells were collected, plated at different cell numbers (200-3200) in full medium without the inhibitor and grown under Nx for 9 days. Bars depict quantification of colony formation upon treatment with CNASB alone or in combination with IR in normoxia (Nx) and severe hypoxia (Hx). Colonies were scanned and counted using GelCount. Survival fractions (SF) were calculated to the plating efficiency of unirradiated cells under normoxic or hypoxic conditions. Mean values ±SEM are shown, n=3 (* $p \leq 0.05$, ** $p < 0.01$, *** $p \leq 0.001$; two-way ANOVA with Tukey post-test).

6

1.2 Supplementary Tables

Supplementary Table 1. Table showing the parameters for the *in silico* analysis of overall survival (OS) of cohort of patients with SLC25A1 up-regulation performed by KMPlotter.

Affy ID	210010_s_at (SLC25A1; CTP; SLC20A3)
Backward reference	CaArray
	GSE14814
	GSE19188
	GSE29013
	GSE30219
	GSE31210
	GSE3141
	GSE31908
	GSE37745
	GSE4573
	GSE50081
	TCGA
Survival	OS
Split patients by	median
Follow up threshold all	all
Censore at threshold	checked
Compute median over entire database	false
Cutoff value used in analysis	634
Expression range of the probe	21 - 4503
Probe set option	user selected probe set
Invert HR values below 1	not checked
Restrictions	
Histology	all
Grade	all
Stage	all
AJCC stage T	all
AJCC stage N	all
AJCC stage M	all
Gender	all
Smoking history	all
Surgery success	all
Chemotherapy	all
Radiotherapy	all
Dataset	all
Use earlier release of the database	2015 version (n=2437)
Array quality control	exclude biased arrays

Supplementary Table 2. Table showing the the parameters for the *in silico* analysis of overall survival (OS) of cohort of patients with SLC25A1 up-regulation and successful surgery with tumor-free margins (R0-resection) performed by KMPlotter.

Affy ID	210010_s_at (SLC25A1; CTP; SLC20A3)
Backward reference	CaArray
	GSE31210
	TCGA
Survival	OS
Split patients by	median
Follow up threshold	all
Censore at threshold	checked
Compute median over entire database	false
Cutoff value used in analysis	579
Expression range of the probe	93 - 4503
Probe set option	user selected probe set
Invert HR values below 1	not checked
Restrictions	
Histology	all
Grade	all
Stage	all
AJCC stage T	all
AJCC stage N	all
AJCC stage M	all
Gender	all
Smoking history	all
Surgery success	only surgical margins negative
Chemotherapy	all
Radiotherapy	all
Dataset	all
Use earlier release of the database	2015 version (n=2437)
Array quality control	exclude biased arrays

Supplement Originalarbeit 2: Hlouschek et al. (2018) Cancer Lett 439, 24-38.

Supplementary Material

Targeting SLC25A10 alleviates improved antioxidant capacity and associated radioresistance of cancer cells induced by chronic-cycling hypoxia.

Hlouschek Julian[1)], Ritter Violetta[1)], Wirsdörfer Florian[1)], Klein Diana[1)],Jendrossek Verena[1)], Matschke Johann[1)#]

[1)] Institute of Cell Biology (Cancer Research), University Hospital Essen, 45122 Essen, North Rhine-Westphalia, Germany;

[#] *corresponding author:*
Johann Matschke, Institute of Cell Biology (Cancer Research), University Hospital Essen, Virchowstrasse 173, 45122 Essen, Germany; Phone: +49-201-7232614; Fax: +49-201-7235904; E-mail: johann.matschke@uk-essen.de.

Supplementary Figures

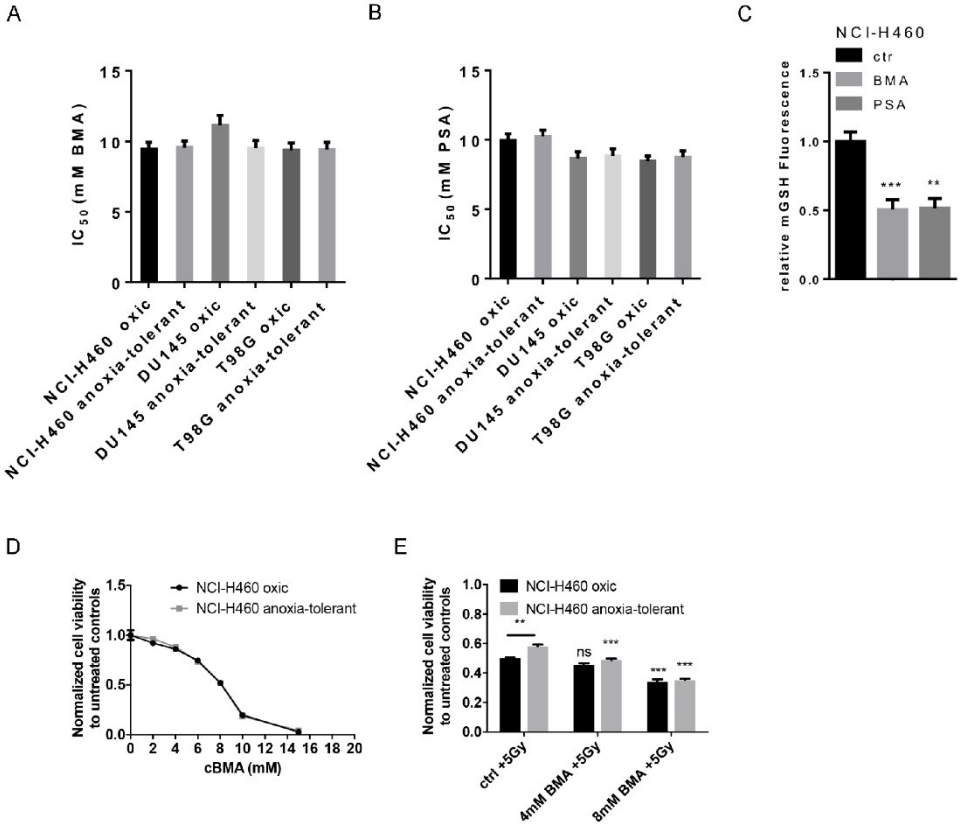

Supplementary Material

Supplementary Fig. 1: A) Inhibitory concentrations of 50% reduction in cell viablility/proliferation (IC_{50}) induced by BMA treatment for 72h were determined by crystal violet staining. **B)** Inhibitory concentrations of 50% reduction in cell viablility/proliferation (IC_{50}) induced by PSA treatment for 72h were determined by crystal violet staining. **C)** Levels of mitochondrial glutathione (mGSH) measured in isolated mitochondria by using monochlorbimane; isolation was performed 2h after pretreatment with 8mM BMA or 8mM PSA in NCI-H460 oxic cells. **D)** Concentration-dependent cell viability/proliferation inhibition after BMA-treatment alone for 48h determined by crystal violet staining. Measured OD values at 540nm were normalized to the untreated controls. **E)** Effect of BMA treatment for 48h on cell proliferation/viability in combination with ionizing radiation at 5Gy determined by crystal violet staining. Measured OD values at 540nm were normalized to the untreated controls. Mean values ±SEM are shown, n=3 (** $p \leq 0.01$, *** $p \leq 0.001$; 2-way ANOVA with Tukey post-test)

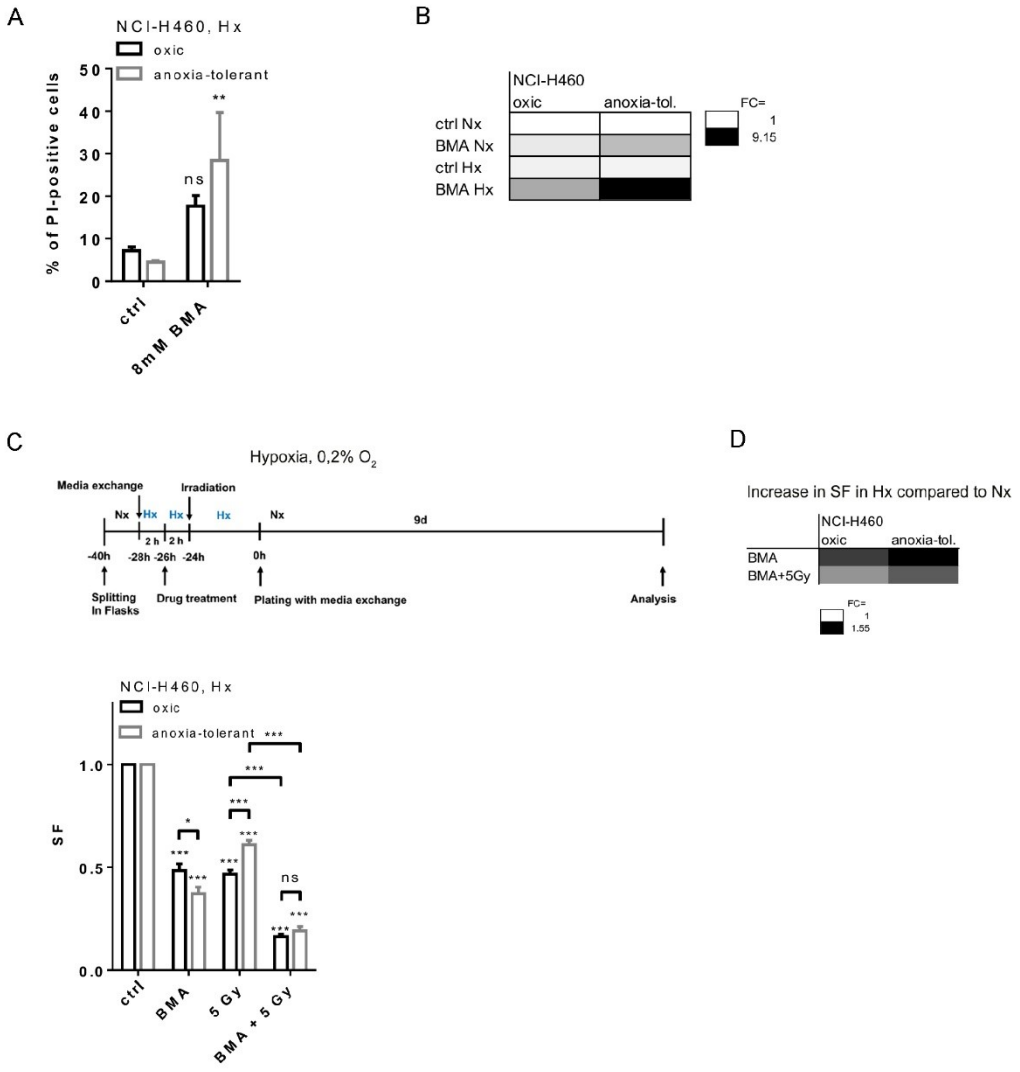

Supplementary Fig. 2: BMA-mediated cell death in acute hypoxia. **A)** Fraction of PI-positive cells determined by flow cytometry in NCI-H460 oxic and anoxia-tolerant cells 72h after BMA treatment in acute hypoxia (Hx, 0.2% O_2). **B)** Heat map representation of Fold change (FC) of BMA-mediated cell death induction in acute Hx compared to normoxia (Nx, 20% O_2) was calculated to the respective controls in Nx. **C)** Upper panel displays schematic representation of the experimental timeline in severe hypoxia (Hx, 0.2% O_2). Survival fraction (SF) of clonogenic survival of NCI-H460 oxic and anoxia-tolerant cells upon BMA-treatment and IR with 5Gy under severe hypoxic (Hx, 0.2% O_2) conditions is presented in a bar graph (lower panel). 24h after treatment cells

were collected and plated at different cell numbers in full medium without the inhibitor and grown under Nx for 9 days. **D)** Heat maps indicating fold changes (FC) of survival fraction (SF) when treated under hypoxic conditions in comparison to SF after treatment under normoxic conditions (as indicated in Fig. 2F) in NCI-H460 oxic and anoxia-tolerant cancer cells. Mean values ±SEM are shown, n=3 (** p≤0.01; 2-way ANOVA with Tukey post-test)

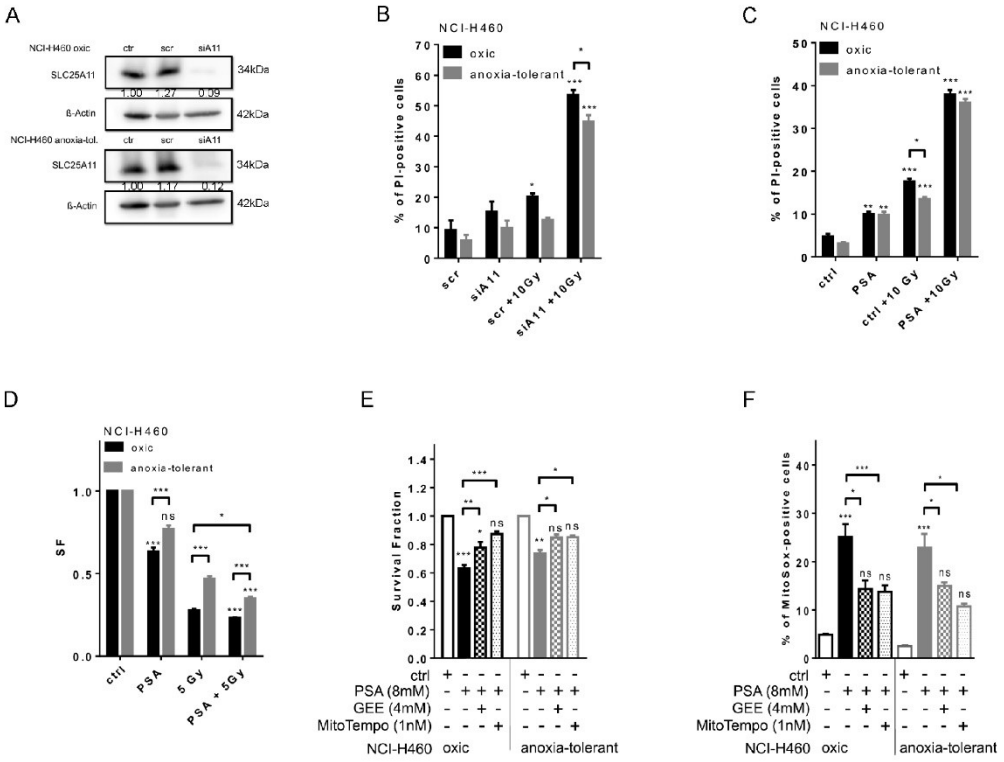

Supplementary Fig. 3: A) Western blots indicate SLC25A11 protein downregulation 48h after start of transfection at the timepoint of IR. Relative quantification is depicted with numbers under the appropriate protein band. **B)** Fraction of dead cells 72h after knockdown of SLC25A11 with or without IR determined by flow cytometry in NCI-H460 oxic and anoxia-tolerant cells. **C)** Fraction of dead cells 72h after 8mM PSA-mediated inhibition of SLC25A11 with or without IR determined by flow cytometry in NCI-H460 oxic and anoxia-tolerant cells. **D)** Survival fraction (SF) of clonogenic survival of NCI-H460 oxic and anoxia-tolerant cells upon 8mM PSA-treatment and IR with 5Gy. 24h after treatment cells were collected, plated at different cell numbers in full medium without the inhibitor and grown for 9 days. **E)** Rescue of PSA-mediated reduction of clonogenic survival fraction (SF) by 2h additional pretreatment with 4mM cell- and mitochondria-permeable glutathione-ethylester (GEE) or 1nM mitochondrial ROS scavenger MitoTempo (MT) in NCI-H460 oxic and anoxia-tolerant cells. 24h after treatment cells were collected, plated at different cell numbers in full medium without drugs and grown for 9 days. **F)** Rescue of PSA-mediated mROS-induction (fraction of MitoSox-positive cells determined by flow cytometry) after 24h by 2h additional pretreatment with 4mM cell- and mitochondria-

permeable glutathione-ethylester (GEE) or 1nM mitochondrial ROS scavenger MitoTempo (MT) in NCI-H460 oxic and anoxia-tolerant cells. Of note, treatment with GEE or MT alone did not alter mROS levels (data not shown). Mean values ±SEM are shown, n=3-5 (* p≤0.05, ** p≤0.01, *** p≤0.001; 2-way ANOVA with Tukey post-test)

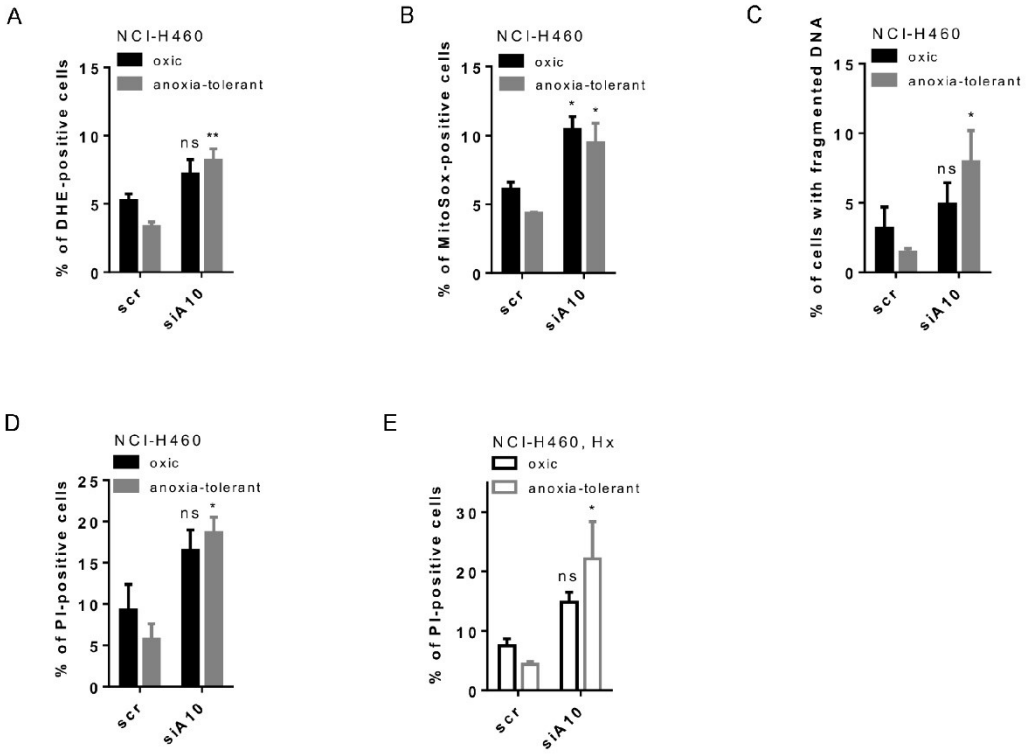

Supplementary Fig. 4: Functional flow cytometry assays after siRNA-mediated knockdown of SLC25A10. **A)** Fraction of DHE-positive cells stained for cellular ROS determined by flow cytometry in NCI-H460 oxic and anoxia-tolerant cells. **B)** Fraction of MitoSox-positive cells stained for mitochondrial ROS determined by flow cytometry in NCI-H460 oxic and anoxia-tolerant cells 24h after start of downregulation. **C)** Fraction of apoptotic cells with fragmented DNA (SubG1-fraction) determined by flow cytometry (PI staining in a hypotonic citrate buffer) in NCI-H460 oxic and anoxia-tolerant cells 72h after start of downregulation. **D)** Fraction of PI-positive cells determined by flow cytometry in NCI-H460 oxic and anoxia-tolerant cells 72h after start of downregulation under normoxic conditions. **E)** Fraction of PI-positive cells determined by flow cytometry in NCI-H460 oxic and anoxia-tolerant cells 72h after start of downregulation under hypoxic (Hx, 0.2% O_2) conditions. Mean values ±SEM are shown, n=3 (* p≤0.05, ** p≤0.01; 2-way ANOVA with Tukey post-test)

Supplementary Material

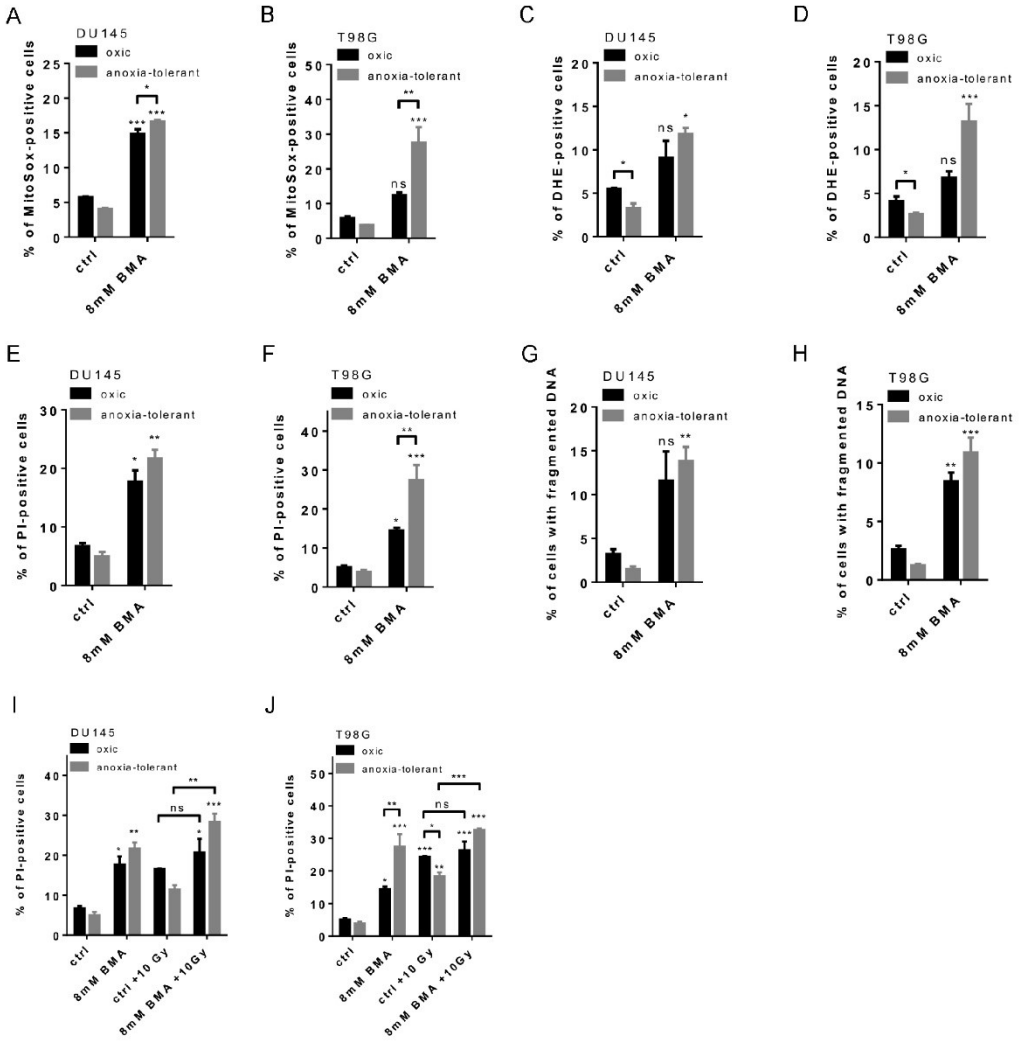

Supplementary Fig. 5: Raw data of fold changes presented in the manuscript in Fig. 2, 3, 4 of DU145 and T98G oxic and anoxia-tolerant cells in various parameters determined by flow cytometry (MitoSox, DHE, PI). **A)** Fraction of MitoSox-positive cells 24h after BMA treatment in DU145 oxic and anoxia-tolerant cells. **B)** Fraction of MitoSox-positive cells 24h after BMA treatment in T98G oxic and anoxia-tolerant cells. **C)** Fraction of DHE-positive cells 24h after BMA treatment in DU145 oxic and anoxia-tolerant cells. **D)** Fraction of DHE-positive cells 24h after BMA treatment in T98G oxic and anoxia-tolerant cells. **E)** Fraction of PI-positive cells 72h after BMA treatment in DU145 oxic and anoxia-tolerant cells. **F)** Fraction of PI-positive cells 72h after

BMA treatment in T98G oxic and anoxia-tolerant cells. **G)** Fraction of apoptotic cells with fragmented DNA in DU145 oxic and anoxia-tolerant cells after 72h of BMA treatment. **H)** Fraction of apoptotic cells with fragmented DNA in T98G oxic and anoxia-tolerant cells after 72h of BMA treatment. **I)** Fraction of dead cells 72h after BMA treatment with or without IR in DU145 oxic and anoxia-tolerant cells. **J)** Fraction of dead cells 72h after BMA treatment with or without IR in T98G oxic and anoxia-tolerant cells. Mean values ±SEM are shown, n=3 (* $p \leq 0.05$, ** $p \leq 0.01$, *** $p \leq 0.001$; 2-way ANOVA with Tukey post-test)

9

Supplementary Material

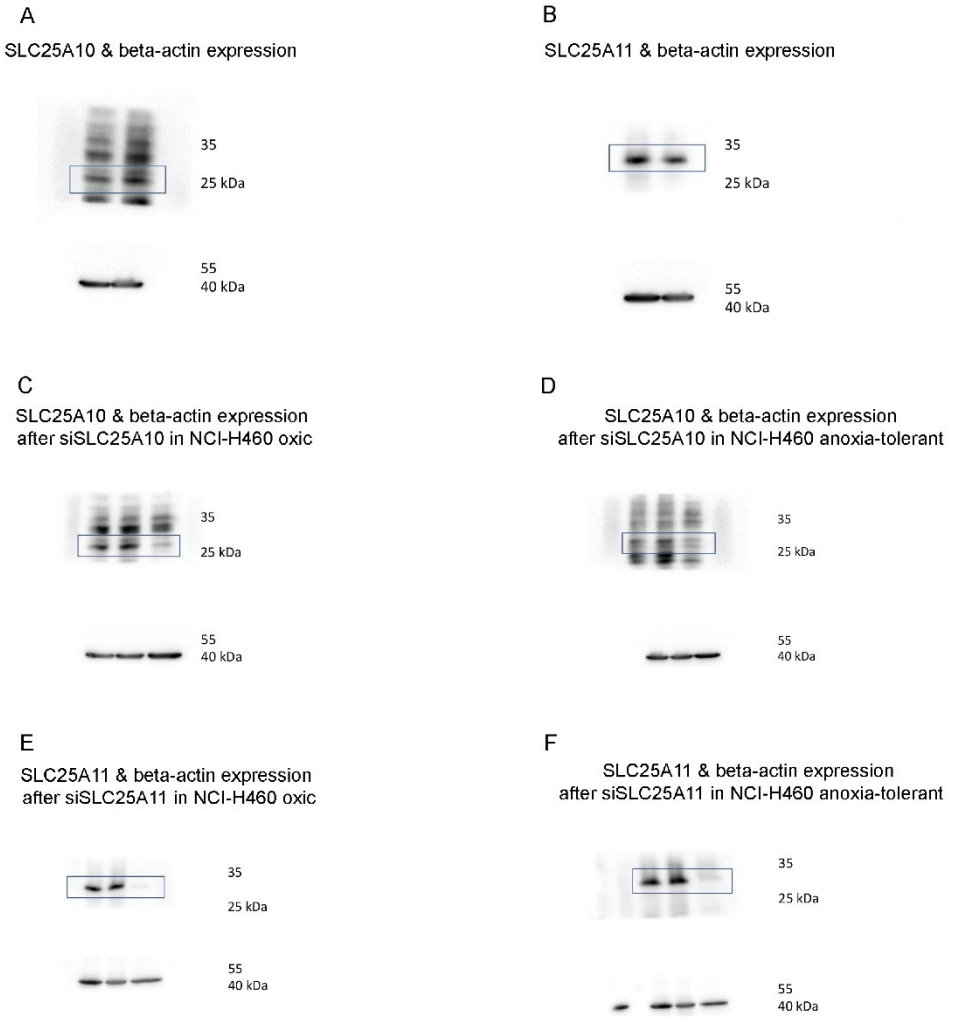

Supplementary Fig. 6: Protein expression determined by western blot shown as scans of whole membranes. **A)** SLC25A10 protein expression in NCI-H460 oxic and anoxia-tolerant cells with ß-actin as corresponding loading control (shown in Fig. 1). **B)** SLC25A11 protein expression in NCI-H460 oxic and anoxia-tolerant cells with ß-actin as corresponding loading control (shown in Fig. 1). **C)** SLC25A10 protein downregulation 48h after start of transfection with ß-actin as corresponding loading control in NCI-H460 oxic cells (shown in Fig. 2). **D)** SLC25A10 protein downregulation 48h after start of transfection with ß-actin as corresponding loading control

in NCI-H460 anoxia-tolerant cells (shown in Fig. 2). **E)** SLC25A11 protein downregulation 48h after start of transfection with ß-actin as corresponding loading control in NCI-H460 oxic cells (shown in Suppl. Fig. 3) **F)** SLC25A11 protein downregulation 48h after start of transfection with ß-actin as corresponding loading control in NCI-H460 anoxia-tolerant cells (shown in Suppl. Fig. 3).

Supplementary Material

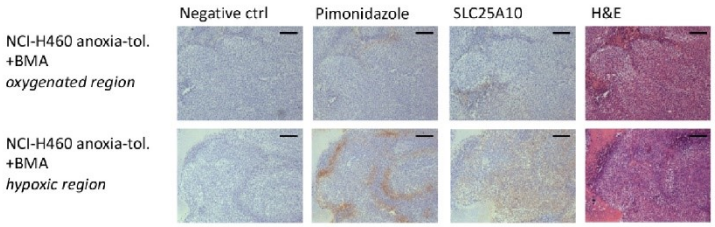

Supplementary Fig. 7: Xenograft tumors of BMA-treated (5x25mg/kg BMA every second day i.p.) NCI-H460 anoxia-tolerant cells were analyzed by immunohistochemistry (DAB-staining) for tumor hypoxia (pimonidazole-staining) and SLC25A10 levels. Representative pictures of corresponding regions (oxygenated and hypoxic) were taken with a 10x objective. Scale bar = 50µm.

Supplementary Tables

Supplementary Table 1: Table showing the parameters for the *in silico* analysis of overall survival (OS) of cohort of Lung cancer patients with SLC25A10 up-regulation performed by KMPlotter.

Affy ID	218275_at (SLC25A10, DIC)
Backward reference	CaArray
	GSE14814
	GSE19188
	GSE29013
	GSE30219
	GSE31210
	GSE3141
	GSE31908
	GSE37745
	GSE4573
	GSE50081
	TCGA
Survival	OS
Split patients by	median
Follow up threshold	all
Censore at threshold	not checked
Compute median over entire database	false
Cutoff value used in analysis	196
Expression range of the probe	5 - 1338
Probe set option	user selected probe set
Invert HR values below 1	not checked
Restrictions	
Histology	all
Grade	all
Stage	all
AJCC stage T	all
AJCC stage N	all
AJCC stage M	all
Gender	all
Smoking history	all
Surgery success	all
Chemotherapy	all
Radiotherapy	all
Dataset	all
Use earlier release of the database	all2015 version (n=2437)
Array quality control	exclude biased arrays
Multivariate analysis	
Not selected.	
Results	
P value	0.0001

Supplementary Material

Supplementary Table 2. Table showing the parameters for the *in silico* analysis of overall survival (OS) of cohort of Lung cancer patients with SLC25A11 up-regulation performed by KMPlotter.

Affy ID	209003_at (SLC25A11, OGC, SLC20A4)
Backward reference	CaArray
	GSE14814
	GSE19188
	GSE29013
	GSE30219
	GSE31210
	GSE3141
	GSE31908
	GSE37745
	GSE4573
	GSE50081
	TCGA
Survival	OS
Split patients by	median
Follow up threshold	all
Censore at threshold	not checked
Compute median over entire database	false
Cutoff value used in analysis	767
Expression range of the probe	147 - 3051
Probe set option	user selected probe set
Invert HR values below 1	not checked
Restrictions	
Histology	all
Grade	all
Stage	all
AJCC stage T	all
AJCC stage N	all
AJCC stage M	all
Gender	all
Smoking history	all
Surgery success	all
Chemotherapy	all
Radiotherapy	all
Dataset	all
Use earlier release of the database	all2015 version (n=2437)
Array quality control	exclude biased arrays
Multivariate analysis	
Not selected.	
Results	
P value	0.1412

Supplementary Table 3: Table showing the parameters for the *in silico* analysis of overall survival (OS) of cohort of Breast cancer patients with SLC25A10 up-regulation performed by KMPlotter.

Affy ID	218275_at (SLC25A10, DIC)
Backward reference	GSE1456
	GSE16446
	GSE16716
	GSE20271
	GSE20685
	GSE20711
	GSE3494
	GSE37946
	GSE42568
	GSE45255
	GSE7390
Survival	OS
Split patients by	median
Follow up threshold	all
Censore at threshold	checked
Compute median over entire database	false
Cutoff value used in analysis	259
Expression range of the probe	31 - 1449
Probe set option	user selected probe set
Invert HR values below 1	not checked
Restrictions	
ER status	all
derive ER status from gene expression data	not checked
PR status	all
HER2 status	all
Lymph node status	all
Intrinsic subtype	all
TP53 status	all
Pietenpol subtype	all
Grade	all
Use earlier release of the database	all
Use following dataset for the analysis	all
Quality control	
Remove redundant samples	checked
Array quality control	exclude biased arrays
Proportional hazards assumption	0
Not selected.	
Cohort	
Cohorts	not selected
Results	
P value	0.0071

15

Supplementary Table 4. Table showing the parameters for the *in silico* analysis of overall survival (OS) of cohort of Breast cancer patients with SLC25A11 up-regulation performed by KMPlotter.

Affy ID	209003_at (OGC, SLC20A4, SLC25A11)
Backward reference	GSE1456
	GSE16446
	GSE16716
	GSE20271
	GSE20685
	GSE20711
	GSE3494
	GSE37946
	GSE42568
	GSE45255
	GSE7390
Survival	OS
Split patients by	median
Follow up threshold	all
Censore at threshold	checked
Compute median over entire database	false
Cutoff value used in analysis	678
Expression range of the probe	169 - 8177
Probe set option	user selected probe set
Invert HR values below 1	not checked
Restrictions	
ER status	all
derive ER status from gene expression data	not checked
PR status	all
HER2 status	all
Lymph node status	all
Intrinsic subtype	all
TP53 status	all
Pietenpol subtype	all
Grade	all
Use earlier release of the database	all
Use following dataset for the analysis	all
Quality control	
Remove redundant samples	checked
Array quality control	exclude biased arrays
Proportional hazards assumption	0
Not selected.	
Cohort	
Cohorts	not selected
Results	
P value	0.5627

Abkürzungsverzeichnis

(Anmerkung: Weitere Abkürzungsverzeichnisse finden sich in den jeweiligen Originalarbeiten)

2-HG: 2-Hydroxyglutarat
BMA: Butylmalonat
BTA: 1,2,3-Benzen-Tricarboxylat
CNASB: 4-Chlor-3-[[(3-Nitrophenyl)Amino]Sulfonyl]-Benzoesäure
EGFR: epidermaler Wachstumsfaktor Rezeptor
GSH: reduziertes Glutathion
GSSG: oxidiertes Glutathion
HR: homologe Rekombination
IDH1: zytosolische Isocitrat-Dehydrogenase 1
IDH2: mitochondriale Isocitrat-Dehydrogenase 2
IR: Ionisierende Strahlung
mGSH: reduziertes mitochondriales Glutathion
mGSSG: oxidiertes mitochondriales Glutathion
mROS: mitochondriale reaktive Sauerstoffspezies
NADH: Nicotinamidadenindinukleotid
NADPH: Nicotinamidadenindinukleotidphosphat
NASH: nicht-alkoholische Steatohepatitis
PARP: Poly(ADP-Ribose)-Polymerasen
ROS: reaktive Sauerstoffspezies
SLC25A1: Citrat-Carrier
SLC25A10: Dicarboxylat-Carrier
SLC25A11: 2-Oxoglutarat-Carrier
γH2AX: Histon H2A.X phosphoryliert an Serin 139

Danksagung

Mein großer Dank gilt meiner Betreuerin Prof. Verena Jendrossek für die freundliche Überlassung des Themas, die fortwährende Unterstützung während des Promotionsprojektes und die großzügige Ermöglichung mehrerer prägender Kongressteilnahmen. Dr. Johann Matschke danke ich für die herausragende Einarbeitung und ein bis heute permanent offenes Ohr in allen Anliegen. Insbesondere euch beiden verdanke ich die hervorragende Vermittlung einer selbstständigen wissenschaftlichen Denk- und Arbeitsweise durch unzählige wissenschaftliche Diskussionen.

Auch die anderen aktuellen und ehemaligen Mitglieder der AG I (Molekulare Zellbiologie) am IFZ dürfen nicht unerwähnt bleiben – Ihr habt mir so manchen Labortag gerettet und verschönert. Danke für alles!

Dank gilt ebenfalls der Deutschen Forschungsgemeinschaft, durch deren Stipendienprogramm und die verbundene Teilnahme am Graduiertenkolleg GRK 1739 ich mich für ein gesamtes Jahr in Vollzeit dem Forschungsprojekt intensiviert widmen konnte und der Austausch mit Gleichgesinnten nicht zu kurz kam. Prof. Martin Schuler danke ich für die Übernahme des hochwertigen Mentorings im Rahmen des GRK. Außerdem danke ich der Stiftung Universitätsmedizin Essen für die jahrelange Unterstützung durch das Deutschland-Stipendium, welches mir die weitere Forschungstätigkeit parallel zum Medizinstudium deutlich erleichtert hat.

Zu guter Letzt möchte ich mich bei den wichtigsten Menschen in meinem Leben bedanken – bei meinen Eltern, meiner Freundin, meiner Familie, und meinen Freunden. Ihr habt das stetige Auf und Ab meines Promotionsprojektes und meine damit verbundenen Launen über einige Jahre mit ertragen müssen. Danke für eure Geduld und die großartige Unterstützung!

Lebenslauf

Der Lebenslauf ist in der Online-Version aus Gründen des Datenschutzes nicht enthalten.